I. PURIFICATION AND PARTIAL CHARACTERIZATION OF CHROMATIN SUBUNITS

II. STRUCTURAL STUDIES OF A MEMBRANE-BOUND ACETYLCHOLINE RECEPTOR

Thesis by

Michael J. Ross

In Partial Fulfillment of the Requirements

for the Degree of

Doctor of Philosophy

California Institute of Technology

Pasadena, California

1977

(Submitted July 9, 1976)

ACKNOWLEDGMENTS

I would like to thank my fellow graduate students as well as postdoctoral fellows for their counsel and support during my stay at Caltech. In addition to those collaborators whose names appear in the Appendices, they are Tony Kossiakoff, Steve Spencer, John Chambers, Diane Kent, Dick Vandlen and Steve Skedzelski.

The faculty at Caltech has been a wonderful source of knowledge and stimulation and, in addition to the kindness, attention and guidance given unceasingly by Bob Stroud, Drs. Sten Samson and Michael Raftery have been particularly helpful.

The excellent support facilities available in the division were invaluable in the design and construction of instrumentation used for this research. Bill Schuelke and members of the Instrument Shop--Jim Fetz, Guy Duremberg, Tony Stark and Delmer Dill--should be specially noted in this regard.

Dee Barr and Lillian Casler were of great assistance in typing and preparing figures for this thesis and the manuscripts in the Appendices; they both extended themselves far beyond what could have been expected to expedite the publication of these manuscripts.

My wife, Jenny, was a tireless proofreader, organizer, and supporter.

During my graduate career at Caltech I received support from the National Institutes of Health Training Grant No. GM-1262.

ABSTRACT

Investigations into the structural organization of integral membrane proteins and of protein-DNA complexes are reported. Purification and biochemical studies of chromatin subunits were carried out as preliminaries to structural studies. X-ray diffraction, electron microscopy and image processing techniques are applied to the study of membrane-bound acetylcholine receptor (AcChR) isolated from Torpedo californica.

Electrophoretic fractionation of monomer and oligomer chromatin subunits from rat liver and trout testes is reported. The nucleoprotein complexes do not dissociate or denature during electrophoresis. The bands seen in the gels contain both DNA and protein. The effects of DNA in homogeneity and histone degradation on the electrophoretic behavior of monomer subunit particles is discussed. Bands from the electrophoresis pattern of trout testes subunits were purified by preparative slab gel electrophoresis. These fractions remigrate as single peaks with unchanged mobility.

In the course of these investigations, DNAase II was studied as a possible probe of DNA-protein complexes. High concentrations of divalent cations inhibit enzymatic activity, and it is shown that the rate of catalyzed DNA hydrolysis decreases as a linear function of

divalent cation concentration. Calcium, magnesium and manganese have identical effects. No activity is measurable if the cation concentration is raised above 0.08 M.

The first structural studies of a eukaryotic cell surface protein are reported. Electron microscopy of negatively stained particles of AcChR-rich membranes reveal, for the first time, the presence of large, highly ordered lattices. These lattices are characterized and the surface structure of the molecules in them studied by image reconstruction techniques to a nominal resolution of 20 Å. Large and small angle x-ray diffraction patterns from pellets of AcChR-rich membranes are reported and analyzed. From these data, the electron density of this membrane-bound protein, perpendicular to the membrane sheet, is determined. Indications of three-dimensional ordering within the pellets are also found.

The errors inherent in the use of digitized film data for image reconstructions and for analysis of x-ray diffraction are studied. Instrumental errors in the Syntex AD-1 flatbed autodensitometer are also analyzed.

TABLE OF CONTENTS

I. Purification and Partial Characterization of Chromatin Subunits

Although the nature of DNA packaging in chromatin has been under investigation for many years, the initial evidence for a repeating particle structure came from Hewish and Burgoyne (1973), who found that endogeneous Ca^{++}/Mg^{++}-dependent nuclease would digest the DNA in chromatin at evenly spaced sites, leading to a distribution of digestion products which were multiples of one length. Noll (1974) extended these results using micrococcal nuclease digests of rat liver nuclei to find that the nuclease susceptible regions of chromatin were approximately 200 base-pairs apart. Concurrently, Olins and Olins (1973) had observed spherical particles spaced evenly along chromatin fibers using electron microscopy. The chromatin used in their experiments was prepared from swollen interphase nuclei. Van Holde et al. (1974) were able to obtain electron micrographs of isolated monomer and oligomer chromatin particles. These observations confirmed that the structures seen in electron micrographs of whole chromatin corresponded to alternating nuclease resistant chromatin subunits and nuclease susceptible spacer regions along the DNA.

Lacy and Axel (1975) digested rat liver nuclei with staphalococcal nuclease and found DNA lengths which were multiples of

185 base-pairs, which, on further digestion, yielded a reproducible pattern of fragments ranging in size from 160 to 60 base-pairs. The protein/DNA ratio in the particles remained the same as that in undigested chromatin (Lacy and Axel, 1975), suggesting that within each chromatin subunit there exists approximately 250,000 daltons of protein. This result along with the hypothesis of Kornberg (1974) concerning histone stoichiometry in chromatin led to the idea that a basic building block in chromatin might be made from two of each of the "core" histones (all but histone f1).

Several workers have used sucrose gradients to separate monomer chromatin subunits containing 140-200 base-pairs of DNA from the higher oligomers containing multiples of 200 base-pair lengths of DNA (Noll, 1974; Oosterhof et al., 1975; Honda et al., 1975). The analysis of each of these species by molecular weight or size fraction (recentrifugation or gel permeation chromatography, Honda et al., 1975) yielded only one major species, whereas analysis of the DNA in the particles revealed a family of species with slightly differing lengths (Noll, 1974; Sollner-Webb and Felsenfeld, 1975; Honda et al., 1975). Electron microscopy of the sucrose gradient isolated species of monomer, dimer, trimer, and tetramer (Finch et al., 1975) showed single beads for monomer, two for dimer, and so on, indicating that the bands seen in the centrifugation were due to

oligomers of these beads on a chromatin fiber.

As a prelude to low-angle x-ray studies and crystallization trials, DNAase II digests of rat chromatin (Gottesfeld et al., 1975) and staphylococcal nuclease digests of trout testes chromatin (provided by D. Baillie and B. Honda) were analyzed using gel electrophoresis. In both cases the monomer subunit fraction was resolved into multiple species (Ross and Stroud, 1976a). The monomer fractions were further purified by preparative gel electrophoresis but no further characterization of this highly purified material has yet been attempted.

As a corrolary to these studies, we investigated the usefulness of a nuclease (DNAase II) as a probe for coverage of DNA by histones. From these experiments we were able to determine conditions for precisely modulating the DNA hydrolysis by DNAase II as a function of varying concentrations of divalent cations (Ross and Stroud, 1976b).

References

Finch, J. T., Noll, M., and Kornberg, R. D. (1975) Proc. Nat. Acad. Sci. USA 72, 3320-3322.

Gottesfeld, J. M., Kent, D., Ross, M., and Bonner, J. (1975) in Florida Colloquium on Molecular Biology (G. Stern, Ed.), Academic Press, New York--in press.

Hewish, D. R., and Burgoyne, L. A. (1973) Biochem. Biophys. Res. Commun. 52, 504-510.

Honda, B. M., Baillie, D. L., and Candido, E. P. M. (1975) J. Biol. Chem. 250, 4643-4647.

Kornberg, R. D. (1974) Science 184, 868-871.

Lacy, E. and Axel, R. (1975) Proc. Nat. Acad. Sci. USA 72, 3978-3982.

Noll, M. (1974) Nature 251, 249-251.

Olins, A. L. and Olins, D. E. (1973) Science 183, 330-333.

Oosterhof, D. K., Hozier, J. C. and Rill, R. L. (1975) Proc. Nat. Acad. Sci. USA 72, 633-637.

Ross, M. J. and Stroud, R. M. (1976a)--submitted to J. Biol. Chem. Appendix A of this thesis.

Ross, M. J. and Stroud, R. M. (1976b)--submitted to J. Biol. Chem. Appendix B of this thesis.

Sollner-Webb, B. and Felsenfeld, G. (1975) Biochemistry 14, 2915-2920.

Van Holde, K. E., Sahasrabuddhe, C. G., Shaw, B. R., van Bruggen E. F. J., and Arnberg, A. C. (1974) Biochem. Biophys. Res. Commun. 60, 1365-1370.

II. Structural Studies of a Membrane-Bound Acetylcholine Receptor

Through the advances of x-ray crystallography, much is now known about the atomic structure of soluble proteins. Until recently, however, the large classes of integral membrane proteins (i.e. receptors, enzymes, structural proteins) have eluded high resolution structural analysis. Only one such protein, that from the purple membrane of Halobacterium halobium, has been studied to anything approaching atomic resolution (Henderson and Unwin, 1975). However, it was decided to try and study an active eukaryotic cell surface protein, and membrane-bound receptors presented themselves as an attractive subject.

We set out to study purified acetylcholine receptor (AcChR)-rich membranes from Torpedo californica using the techniques of x-ray diffraction and electron microscopy.

Acetylcholine receptor is one of several neural receptor proteins found in higher animals. It acts as a cation gate through the postsynaptic membrane causing membrane depolarization. Cations are allowed to pass only in the presence of transmitter molecules such as acetylcholine. AcChR is only one of many types of receptors found in membranes (Cuatrecasas, 1974), but, i) it can be isolated in large quantities from the electroplax of various species of Torpedo,

and ii) we would expect to derive significant findings from structural analysis of the membrane-bound protein at less than atomic resolution. For even at less than atomic resolution, structural changes due to addition of macromolecules such as α-Bungarotoxin, or conformational changes induced by ligand binding, could be observable using difference Fourier techniques.

Our investigations commenced with the studies of AcChR-rich membrane pellets by x-ray diffraction. A low-angle x-ray camera was designed and built to collect these data (Ross and Stroud, 1976). Two perpendicular silica mirrors (Franks, 1958) focused and collimated the x-ray beam from a rotating anode x-ray generator (Elliott Neutron Division of A. E. I.). The camera provided the capability for resolving structures as large as 1500 Å and as small as 2 Å. Membrane sample collectors were designed; these allowed samples of membrane fragments pelleted in an ultracentrifuge to be examined with the orientation of the bilayer planes either parallel or normal to the x-ray beam.

X-ray patterns of pelleted partically purified membrane fragments were obtained (Raftery et al. , 1974, 1975) at both low and high angles. From the high angle data, conclusions concerning the secondary structure present in both protein and lipid could be drawn

(Ross et al., 1976). The low-angle diffraction data from partially ordered pellets and from vesicles of AcChR-rich membranes were analyzed to extract the continuous diffraction pattern of one membrane sheet. This allowed determination of both the mean electron density through the bilayer and the overall thickness of the structure (Ross et al., 1976) using Fourier refinement techniques developed by Stroud and Agard (1976). Low-angle diffraction data also indicated the presence of three-dimensional ordering under certain pelleting conditions (Raftery et al., 1974, 1975; Ross et al., 1976).

Concurrent with these x-ray diffraction experiments, samples of AcChR membranes were examined in the electron microscope, and highly ordered lattices extending over > 10,000 Å were observed (Klymkowsky et al., 1976). The presence of these ordered structures allowed us to try image reconstruction techniques to improve the signal-to-noise ratio on the electron micrographs (Klug and DeRosier, 1966).

A set of image processing software was written for a minicomputer (Data General NOVA 800) based in part on the programs described by DeRosier and Moore (1970). Since the data were processed by digital computer, the electron micrographs of lattices had to be converted to digital form, and a flatbed autodensitometer (Syntex AD-1) was used to digitize the films. A study of the errors

involved in the use of this autodensitometer was undertaken to assess noise levels, possible artifacts, and overall system performance (Ross and Stroud, 1976b).

Image reconstruction of several micrographs was completed with considerable increase in the detail discernible in each micrograph (Ross et al., 1976). This technique was limited, however, to a nominal 20 Å resolution because of stain, and the images obtained were representative only of the surfaces of stained molecules. Nevertheless, these studies may allow identification of lattice changes (if any) with ligand binding, or α-Bungarotoxin binding sites. In addition, if attempts to increase the frequency with which lattice structures are observed are successful, images of unstained samples can be analyzed using the existing hardware and software (see above) to a resolution of better than 4 Å. Analysis of electron micrographs at this high resolution demands extreme accuracy in both microscope and film scanner (Unwin and Henderson, 1975) making the autodensitometer error analysis indispensable.

References

Cuatrecasas, P. (1974) Ann. Rev. Bioch. 43, 169-214.

DeRosier, D. J. and Moore, P. B. (1970) J. Mol. Biol. 52, 355-369.

Franks, A. (1958) Brit. J. Appl. Phys. 9, 349-352.

Henderson, R. and Unwin, P. N. T. (1975) Nature 257, 28-32.

Klug, A. and DeRosier, D. J. (1966) Nature 212, 29-32.

Klymkowsky, M. W., Ross, M. J. and Stroud, R. M. (1976)--submitted to J. Mol. Biol. Appendix D of this thesis.

Raftery, M. A., Bode, J., Vandlen, R., Michaelson, D., Deutsch, J., Moody, T., Ross, M. J., and Stroud, R. M. (1974) FEBS Meeting (Proc.), 9th 24, 9-23.

Raftery, M. A., Bode, J., Vandlen, R., Michaelson, D., Deutsch, J., Moody, T., Ross, M. J., and Stroud, R. M. (1975) in Protein-Ligand Interactions (H. Sund and G. Blaner, Eds.), pp. 328-352. Walter de Gruyter & Co., Berlin.

Ross, M. J., Klymkowsky, M. W., Agard, D. A., and Stroud, R. M. (1976)--submitted to J. Mol. Biol. Appendix C of this thesis.

Ross, M. J. and Stroud, R. M. (1976a)--manuscript in preparation.

Ross, M. J. and Stroud, R. M. (1976b)--submitted to Acta Crystallogr. Appendix E of this thesis.

Stroud, R. M., and Agard, D. A. (1976)--submitted to J. Mol. Biol.

Unwin, P. N. T., and Henderson, R. (1975) J. Mol. Biol. 94, 425-440.

APPENDIX A

Inhibition of DNAase II by Divalent Cations

M. J. Ross, and R. M. Stroud

Submitted to J. Biol. Chem.

MICHAEL J. ROSS† AND ROBERT M. STROUD

Norman W. Church Laboratory of Chemical Biology

California Institute of Technology

Pasadena, California 91125

SUMMARY

The activity of deoxyribonuclease II from hog spleen (DNAase II) at pH 5.0 has been studied as a function of EDTA and divalent cation concentrations. No inhibition nor activation of the enzyme by EDTA is noted. There is no divalent cation requirement for the enzyme at pH 5.0 in 0.2 M NaOAc. No change in enzyme activity occurs upon addition of less than 0.001 M quantities of divalent cations. Concentrations of divalent cations above 0.001 M inhibit enzymatic activity, with the rate of catalyzed DNA hydrolysis decreasing as a linear function of divalent cation concentration from 0 to 0.04 M. Mg^{++}, Ca^{++} and Mn^{++} behave identically under these conditions. No activity is observed at divalent cation concentrations greater than 0.1 M.

INTRODUCTION

Spleen deoxyribonuclease (DNAase II, deoxyribonucleate oligonucleotidohydrolase, EC 3.1.4.6) is a nuclease with a specificity for native double-stranded DNA, and it can cut either one or both of the strands of the nucleic acid (1, 2). During the initial stages of digestion, the double-stranded cuts outnumber the single-stranded nicks (3), but the predominance of cuts over nicks decreases with time of digestion (4).

The enzyme has been highly purified by several investigators and has been shown to be a single glycopeptide chain (5) of molecular weight 44,000 daltons (6). The fact that DNAase II could cleave both strands of duplex DNA at the same point on the double helix presented the possibility that the enzyme might consist of two identical subunits (7). The sulfate inhibition and iodoacetate inactivation studies of Oshima and Price (6, 8) instead suggested the presence of two closely related active sites in the single-chain molecule, one of which contained an essential histidine residue.

DNAase II does have some sequence specificity (9, 10), although the effects are exhibited as modulations on the rate rather than as absolute sequence requirements. Thus DNAase II can be a useful tool for the preparation of large quantities of heterodisperse DNA of a

given average size or as a probe of DNA availability in nucleoprotein complexes such as chromatin subunits, or repressor-operator complexes. Since it does have a propensity to make double-stranded cuts in the early stages of digestion, DNAase II would often be preferred instead of pancreatic DNAase I. It was with these applications in mind that we sought to better characterize conditions which would allow easy regulation of the enzyme.

Activities of many nucleic acid enzymes are modified by the presence of specific or general divalent cations. The activity of DNAase II is no exception. Investigations of partially purified enzyme indicated that the enzyme required either salt concentrations of 0.15 M or magnesium ion concentrations of 0.02 M for full activity at pH 4.5 (11). Shack (12) extended these results to show that the optimal Mg^{++} and Na^{+} (or K^{+}) concentrations at pH 7 were either ~0.008 M for Mg^{++} ($[Na^{+}]$ = 2.5 mM) or ~ 0.08 M for Na^{+} (no Mg^{++}). Slor and Lev (13) elucidated the complex interdependence of monovalent and divalent cation concentrations and pH on the rate of DNAase II. They found that while the enzyme had a pH optimum of 4.5 in 0.2 M $[Na^{+}]$, this optimum changed to 7.0 as the sodium ion concentration was reduced by an order of magnitude. Although low concentrations (< 3 mM) of Mg^{++} or Mn^{++} did not affect the enzymatic rate at pH 4.5 (0.2 M salt), a rate enhancement of 2-times was seen

when 0.8 mM Mg^{++} or Mn^{++} was added at pH 6.9 (0.02 M salt) (13).

In this work, measurements of the effect of divalent cations on the rate of DNAase II in 0.2 M NaOAc at pH 5.0 have been extended to 0.1 M concentrations of divalent cation where inhibition of all measurable enzymatic activity was achieved. Comparisons of the rate dependence on Mg^{++}, Ca^{++}, and Mn^{++} were undertaken to determine whether this inhibition could be effected by general divalent cations or whether a specific metal ion was needed.

MATERIALS AND METHODS

DNA Stock Solution--Calf thymus DNA (Sigma), repurified by the phenol technique of Mandell and Hershey (14) in sodium chloride-Tris-EDTA (STE) buffer (0.1 M NaCl, 0.01 M Tris-HCl, 0.005 M Na_2EDTA, pH 7.5), was dialyzed against five one-liter changes of STE buffer to remove most of the divalent cations, then ten one-liter changes of sodium chloride-Tris buffer (0.1 M NaCl, 0.01 M Tris-HCl, pH 7.5) to remove the EDTA. 100 ml aliquots of this solution (A_{260} = 25-35) were dialyzed against five one-liter changes of acetate buffer (NaOAc, 0.2 M, pH 5.0 at 37°C). DNA that was used in the assays was never stored for longer than one week after the pH was reduced from 7.5 to 5.0. The DNA solution was diluted to either an

OD_{260} of 6.25 or 1.6 with acetate buffer, and purged with helium to prevent bubble formation while heating to the assay temperature (37.5°C). The weight average molecular weight of the DNA was determined by band sedimentation velocity (15) in 0.1 M Na^+, and was 6.4×10^6 daltons.

Enzyme Stock Solution--1.66 mg of deoxyribonuclease II (Worthington Biochemicals, code HDAC) was dissolved in 6.33 ml of acetate buffer. In order to check for possible proteolytic degradation due to residual protease activity, or denaturation of the enzyme due to low overall protein concentration, bovine serum albumin (BSA, Pentex) was added (w/v = 0.05%) to an aliquot of the enzyme stock solution. The enzyme solution was stable (with a loss of < 10% activity) when stored for five days at 4°C. BSA did not affect enzyme activity or stability, and was not present in the solutions used for the kinetic assays.

DNAase II Activity Assays--Enzyme activity was measured using a modification of the hyperchromicity assay of Kunitz (16) in a Gilford Model 240 spectrophotometer with a jacketed cell compartment. The temperature in the cuvette was monitored by immersing a teflon-encased thermistor (Yellow Springs Instruments) in the

solution; the temperature was maintained at 37.5°C ±0.5°C. 50 µl of enzyme stock solution was diluted with 450 µl of acetate buffer at 37.5°C (with or without EDTA or divalent cation as required). 2.0 ml of DNA stock solution at 37.5°C was added to the diluted enzyme (time t = 0) and mixed thoroughly. These reactants were placed in a 0.1 cm pathlength silica cuvette (at 37.5°C). The first reading could be taken at t = 10 seconds. Tris was used as the free base (Sigma Trizma ® grade). All divalent cations were added as solutions of the acetate salts (Mallincrodt AR ® grade) which had been adjusted to pH 5.0.

RESULTS

When DNA digestions were carried out at pH 5.0 in 0.2 M NaOAc, the plots of hyperchromicity vs. time of digestion displayed the same characteristics described by Bernardi and Sadron (2), namely an initial slow induction phase followed by a linear phase and a final slow phase. This gave the curves sigmoidal shapes (see Figure 1). The increase in OD during the course of the measurements varied between 32% and 35% of the initial value indicating complete digestion of the native DNA substrate.

At pH 5.0 in 0.2 M NaOAc, the enzyme showed maximal

activity in the absence of divalent cations. Under these conditions, EDTA did not change the activity of the enzyme within the accuracy limits of our measurements (Figure 1). The reaction rate decreased linearly with increasing concentrations of divalent cation (Figure 2) until, at 0.06 M, the rate of hydrolysis was reduced sixtyfold, closely approaching that of hydrolysis in a control run without the enzyme. This nonenzymatic hydrolysis rate was characterized by a 10% increase in OD_{260} after 48 hours at 37.5°C (pH 5.0). At 0.1 M concentrations of divalent cation, no enzymatic catalysis could be measured, even with a fiftyfold increase in enzyme concentration.

Hydrolysis rate, as measured by the hyperchromicity assay, remained unchanged when the DNA concentration was reduced fourfold from OD_{260} of 6.0 to an OD_{260} of 1.5.

DISCUSSION

At pH 5.0 and at optimal ionic strength (0.2 M NaOAc), inhibition of DNAase II was linearly dependent on increasing concentrations of divalent cations (between 0 and 0.04 M). The effect was identical for each of the three cations tested. There was no evidence that divalent cations, bound to either substrate or enzyme, were necessary for catalysis. In contrast with this finding however, is the conclusion

drawn from the data of Slor and Lev (13) that DNA hydrolysis was enhanced by the addition of millimolar concentrations of magnesium at low ionic strength (0.02 M =[Na^+]). They observed this effect at both acidic and neutral pH.

One possible reason for this change in divalent cation dependence with ionic strength could be the requirement of the enzyme for a minimum concentration of cations which are not already strongly bound to DNA. An explanation of the complex relationship between salt concentration, pH, divalent cation and divalent anion concentration on the rate of DNAase II, is unlikely to be possible based on kinetic evidence alone.

In conclusion, several investigators have shown that DNAase II can be a useful probe of DNA-protein complexes (17, 18). We have shown that the action of DNAase II can be slowed, or stopped at will, by addition of appropriate concentrations of divalent cation, thereby enhancing its usefulness. DNAase II is a particularly attractive candidate for digestion of chromatin since the chromatin would remain soluble during the digestion (in the absence of divalent cations). The divalent cations added to quench the reaction would then precipitate the subunit particles (19) for easy harvesting. The precipitated reaction product, now free of nicked DNA, could then be resolubilized in EDTA (20).

REFERENCES

1. Oth, A., Fredericq, E., and Hacha, R. (1958) Biochim. Biophys. Acta 29, 287-296.
2. Bernardi, G., and Sadron, C. (1964) Biochemistry 3, 1411-1418.
3. Young, E. T. and Sinsheimer, R. L. (1965) J. Biol. Chem. 240, 1274-1280.
4. Soave, C., Thiery, J.-P., Ehrlich, S. D., and Bernardi, G. (1973) Eur. J. Bioch. 38, 423-433.
5. Bernardi, G. in The Enzymes (P. Boyer, Ed.), Vol. 4, pp. 271-287. Academic Press, New York, 1971.
6. Oshima, R. G. and Price, P. A. (1973) J. Biol. Chem. 248, 7522-7526.
7. Bernardi, G. (1965) J. Mol. Biol. 13, 603-605.
8. Oshima, R. G. and Price, P. A. (1974) J. Biol. Chem. 249, 4435-4438.
9. Thiery, J.-P., Ehrlich, S. D., Devillers-Thiery, A., and Bernardi, G. (1973) Eur. J. Bioch. 38, 434-442.
10. Bernardi, A., Gaillard, C., and Bernardi, G. (1975) Eur. J. Bioch. 52, 451-457.
11. Koerner, J. F. and Sinsheimer, R. L. (1957) J. Biol. Chem. 228, 1039-1048.

12. Shack, J. (1959) J. Biol. Chem. 234, 3003-3006.

13. Slor, H. and Lev, T. (1972) J. Biol. Chem. 247, 2926-2930.

14. Mandell, J. D. and Hershey, A. D. (1960) Anal. Bioch. 1, 66-77.

15. Studier, F. W. (1965) J. Mol. Biol. 11, 373-390.

16. Kunitz, M. (1950) J. Gen. Phys. 33, 349-362.

17. Oosterhof, D. K., Hozier, J. C., and Rill, R. L. (1975) Proc. Nat. Acad. Sci. USA 72, 633-637.

18. Gottesfeld, J. M., Murphy, R. F., and Bonner, J. (1975) Proc. Nat. Acad. Sci. USA 72, 4404-4408.

19. Honda, B. M., Baillie, D. L., and Candido, E. P. M. (1975) J. Biol. Chem. 250, 4643-4647.

20. Ross, M. J. and Stroud, R. M. (1976)--Submitted to J. Biol. Chem.

FOOTNOTES

*This work was performed with the support of National Institutes of Health grant GM-19984 and National Science Foundation grant BMS75-01405. One of us (RMS) is the recipient of a National Institutes of Health Career Development Award, and the other (MJR) is the recipient of a National Institutes of Health Predoctoral Traineeship. This paper is contribution No. 5356 from the Norman W. Church Laboratory of Chemical Biology, California Institute of Technology.

†Present address: Biological Laboratories, Harvard University, 12 Divinity Avenue, Cambridge, Massachusetts 02138.

FIGURE CAPTIONS

FIGURE 1. Hyperchromicity rate assay used for DNAase II at pH 5.0 in 0.2 M NaOAc. Relative absorbance ($OD_t/OD_{t=0}$) is plotted vs. time. A 35% increase in OD (rel. abs. = 1.35) is typical for complete digestion of native DNA. The results of the hyperchromic shift assay used here have been found identical to measurement of the release of acid soluble nucleotides (2). These data were collected at 37.5°C with a starting DNA OD_{260} of 6.0.

FIGURE 2. Inhibition of DNAase II activity by divalent cations. Assay conditions were the same as for Figure 1. The rate expressed here was measured from the slopes of the linear portion of the hyperchromicity assays. The starting OD_{260} for the DNA was 6.0.

Figure 1

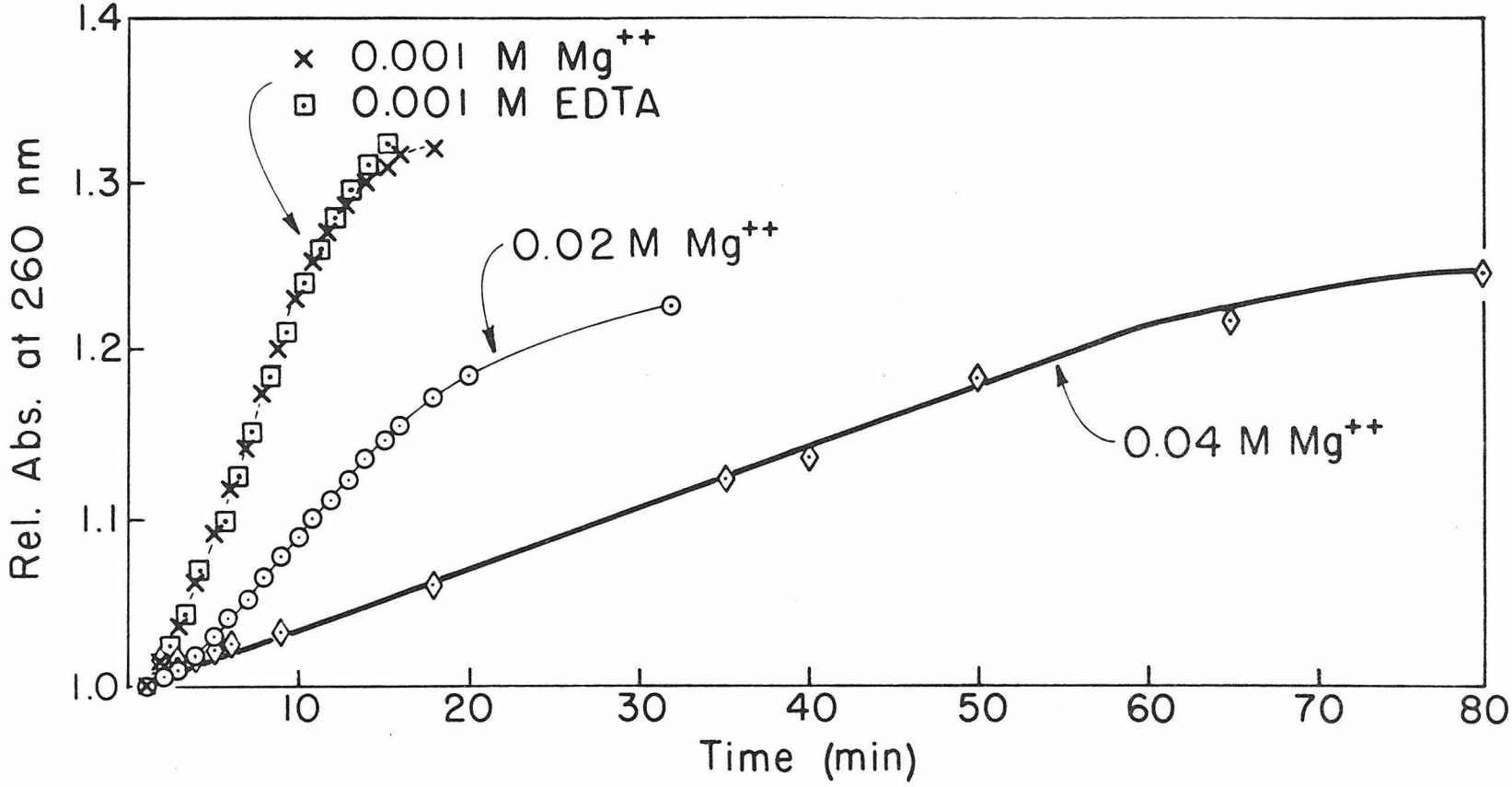
1.4
1.3
1.2
1.1
1.0
Rel. Abs. at 260 nm
× 0.001 M Mg++
⊡ 0.001 M EDTA
0.02 M Mg++
0.04 M Mg++
10
20
30
40
50
60
70
80
Time (min)

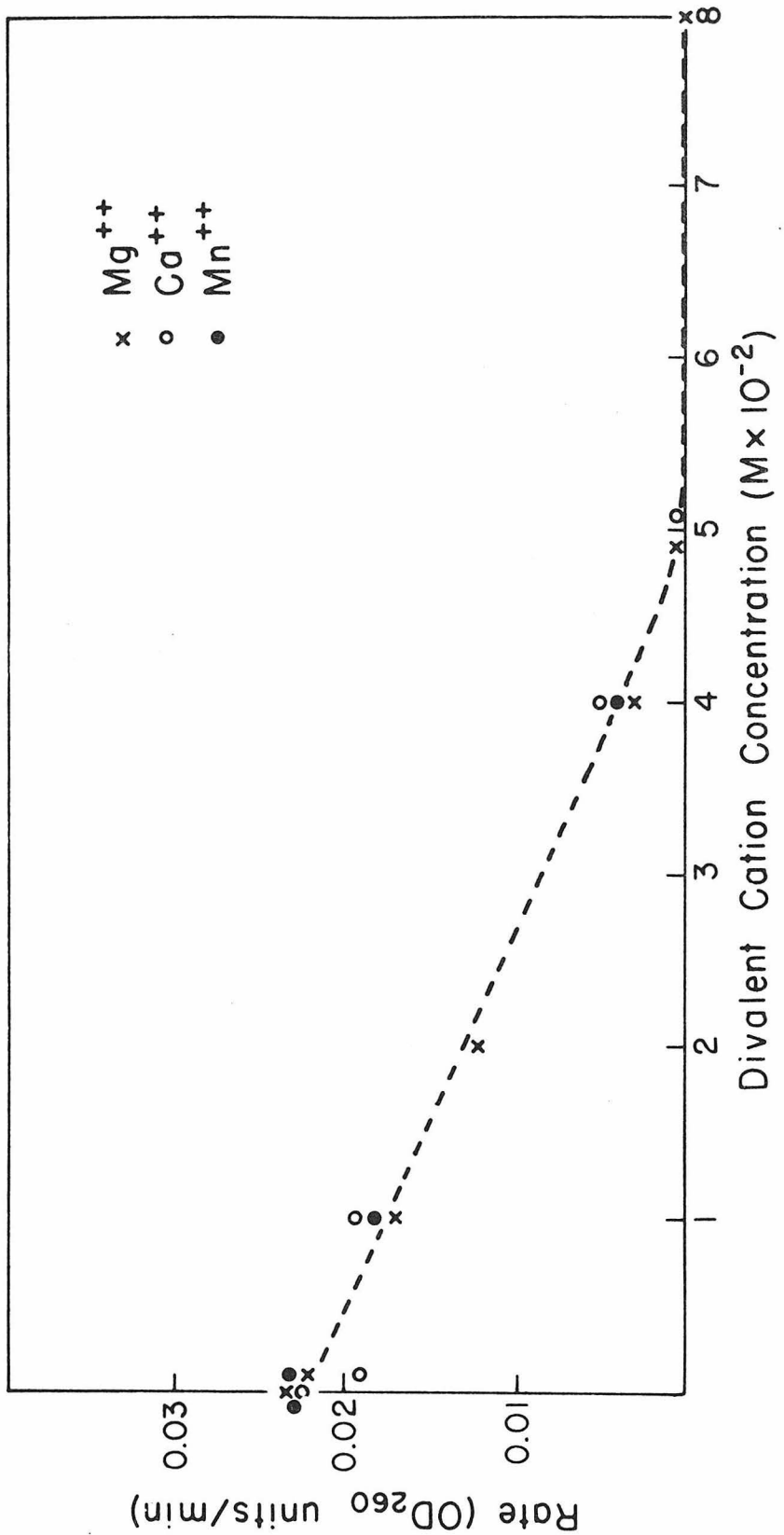
Rate (OD_{260} units/min)
0.03
0.02
0.01
Divalent Cation Concentration ($M \times 10^{-2}$)
1
2
3
4
5
x10
6
7
8
Mg^{++}
Ca^{++}
Mn^{++}

Figure 2

APPENDIX B

Analytical and Preparative Gel Electrophoresis of Chromatin Subunits

M. J. Ross, and R. M. Stroud

Submitted to J. Biol. Chem.

MICHAEL J. ROSS† AND ROBERT M. STROUD

Norman W. Church Laboratory of Chemical Biology

California Institute of Technology

Pasadena, California 91125

Running Title: Purification of Chromatin Subunits

SUMMARY

Chromatin subunits prepared from both trout testes and rat liver chromatin can be resolved into several distinct species using gel electrophoresis. Electrophoresis was carried out in the presence of both Mg^{++} (1 mM) and EDTA (2 mM) on 4% acrylamide gels. The gels were stained for both protein and DNA; no dissociation of the nucleoprotein was observed. DNA and histone content of the subunit fractions were analyzed. Rat liver chromatin subunits contained proteolytically degraded histones and highly nicked DNA; this caused the electrophoretic pattern to be smeared and indistinct. Monomer and oligomer subunit fractions isolated from sucrose gradients contained different bands when analyzed by electrophoresis.

A major narrow band in the electrophoresis pattern of trout testes monomer subunits was isolated from a slab gel and reanalyzed. This purified material remigrated as a single peak with unchanged mobility.

INTRODUCTION

It is now well established that chromatin can be digested into subunit particles by nucleases. The particles contain approximately 140 base pairs of DNA (1) and occur at 200 base-pair intervals along the DNA (2). Kornberg (3) hypothesized that the basic protein building blocks of these particles were two of each of the core histones (all but f1).

Sucrose density gradients have been used to separate monomer chromatin subunits from the higher oligomers (2, 4, 5). The analysis of each of these species by molecular weight or size (recentrifugation or gel permeation chromatography (5, 6)) yielded only one major species, whereas electrophoretic analysis of the DNA in the particles revealed broader bands than seen in restriction enzyme digests. This implied that the subunit fractions contained a family of species with slightly differing DNA lengths (5, 7, 8). Electron microscopy of the sucrose gradient isolated monomer, dimer, trimer, and tetramer subunits (9) showed single beads for monomer, two for dimer, and so on, indicating that the bands seen in the centrifugation were due to oligomers of these beads on a chromatin fiber.

In this communication we wish to present evidence that these seemingly homogeneous fractions are indeed heterogeneous and that

further purification of chromatin subunits can be effected by preparative gel electrophoresis. Our goal in preparing high purity monomers was to crystallize the subunits and further characterize their structure by electron and x-ray diffraction techniques.

MATERIALS AND METHODS

Electrophoresis of Chromatin Fragments--4% (in acrylamide with an acrylamide/bis ratio of 20:1) gels were prepared from recrystallized acrylamide and bis acrylamide (Biorad). Two different buffer systems were used; Tris-acetate buffer: 0.02 M NaOAc, 0.04 M Tris (Sigma Trizma ® grade)-OAc, 2 mM EDTA, 1 mM $Mg(OAc)_2$, pH 8.0, and MES buffer: 0.02 M NaOAc, 0.01 M 2-(N-morpholino)ethane sulfonic acid (10) (MES, Calbiochem), 2 mM EDTA, 1 mM $Mg(OAc)_2$. All salts used were reagent grade. All analytical gels were cast in 0.6 mm I.D. glass tubes and prerun for six hours at 3 ma/tube before use. This system is a modification of that described by Loening (11) for use with RNA. Electrophoresis was carried out in the cold with a current of 2 ma/tube. Migration was from negative to positive. Samples were diluted or dialyzed into buffer (8 mM Tris-OAc, 1 mM $Mg(OAc)_2$, 2 mM EDTA, pH 8.0) containing 20% sucrose and bromphenol blue marker dye. Between

10 µl and 50 µl of sample was layered on the gels. In order to achieve equivalent stain density, gels which were to be stained for protein needed approximately five times more material (100 µg) than those to be stained for DNA (20 µg).

Staining and Densitometry of Gels--Gels were removed from the tubes after running, and stained for either DNA or protein. For DNA staining, the gels were soaked in 1 µg/ml ethidium bromide (EtBr) solution for one hour at 4°C. They were placed on a short wavelength UV light source and photographed through a 23 A red filter on Kodak Royal Pan sheet film (12). The film was developed in D-11 for five minutes at 20°C. Gels were stained for protein with either 0.025% Coomassie brilliant blue (Schwarz Mann) in 10% acetic acid, 20% isopropanol (13), 1% amide black (MC/B) in 20% acetic acid, 20% ethanol (a modification of the technique of Fambrough and Bonner (14)), or 1% fast green FCF (Eastman Organic Chemicals) in 10% acetic acid (15).

Destaining was accomplished by diffusion in 10% acetic acid for Coomassie brilliant blue or fast green, and electrophoretically in 20% ethanol, 20% acetic acid for amide black. The destained protein gels were photographed by transmitted light on Kodak Plus-x Pan sheet film, and the films were developed in D-11 for four minutes at 20°C.

The films obtained from both ethidium fluorescence and protein stain were scanned on a flatbed autodensitometer (Syntex AD-1) with a 109 μ x 219 μ aperture spot. The digitized images were integrated across the width of each gel and displayed as either optical density or the negative of optical density versus distance of migration on a matrix printer/plotter (Versatec model 1100A). Integrals of each peak were used to estimate peak ratios.

Preparative Electrophoresis of Chromatin Fragments--A 4% slab gel (16) (15 cm x 10 cm x 0.4 cm) was cast with Tris-acetate buffer (see above) diluted 1:5 with water (EDTA and Mg^{++} concentrations were kept constant). The salt concentration was reduced to decrease the current through the gel and reduce ohmic heating. The result was slightly broadened bands with run-times decreased from over 24 hours to six hours. 1 ml of sample was layered on the gel after prerunning it with 120 mA current for ten hours. The sample was run at 60 mA for about six hours at 4°C. During both the prerun and electrophoresis, the tray buffers were changed every four hours. The slab was removed and soaked in 1 μg/ml EtBr for four hours at 4°C, and the bands were viewed under short wavelength UV light and excised with a scalpel. The resulting strips of acrylamide were chopped and Dounce homogenized in 1 mM Tris, 0.2 mM EDTA

buffer, pH 7.6. The gel slurries were stirred in 100 ml aliquots of buffer for one day, filtered and concentrated by dialysis against high molecular weight polyethylene glycol (Calbiochem Aquacide ®). Recovery of sample was estimated to be ~ 60% by OD_{260} measurements. Removal of soluble acrylamide from the gel (when desired) was accomplished either by velocity centrifugation in sucrose gradients, or precipitation by 5 mM Mg^{++} and resolubilization in 10 mM EDTA.

Extraction and Electrophoresis of DNA--Chromatin fragments were precipitated with 10 mM Mg^{++} and extracted twice with distilled phenol buffered at pH 7.6 with 0.01 mM Tris-HCl. The aqueous phase was then extracted with chloroform and ether to remove excess phenol and dialyzed against Tris-acetate buffer diluted 1:5. The resulting DNA was analyzed on 4% gels (11). The gels were stained with EtBr and photographed under shortwave UV light as described above.

Electrophoresis of Histones--Chromatin subunit fractions were precipitated with 10 mM Mg^{++} and resuspended in 0.9 M HOAc, 10 M urea and heated at 37°C for thirty minutes to dissolve the histones. The electrophoresis of these samples was performed as described by

Panyim and Chalkley (17) in the absence of urea.

Preparation of Chromatin Fragments--Trout testes chromatin fragments prepared by micrococcal nuclease digestion were a gift from D. Baillie, B. Honda, and P. Candido. The digests were either fractionated on a linear 10%-30% sucrose gradient by Honda et al. (5) or by us on a 12-ml isokinetic 15%-30% sucrose gradient in 0.2 mM EDTA, 1 mM Tris-HCl buffer, pH 7.6 run for twelve hours at 36,000 rpm in a Beckman SW-41-Ti rotor.

Rat liver chromatin subunits were a gift of J. Gottesfeld. They were prepared by DNAase II digestion of rat liver chromatin and isolated on a 15%-26% isokinetic sucrose gradient (18). We reran the monomer fraction on the 15%-30% sucrose gradient described above and 95% of the material resedimented as a single peak. This peak was collected and used as monomer.

RESULTS

Chromatin subunits prepared as described above were fractionated by velocity centrifugation in sucrose gradients. The 11 S peak was collected as the monomer peak--the higher molecular weight species were pooled as oligomer. The monomer fractions of both rat

and trout subunits were rerun on 15%-30% isokinetic sucrose gradients and they sedimented as single bands. Monomer, oligomer, and unfractionated digests of rat liver and trout testes chromatin were analyzed on 4% acrylamide gels (Figure 1).

The gels were stained for either DNA with EtBr or protein with either amide black, fast green FCF, or Coomassie brilliant blue. All of the observed bands stained for both protein and DNA. Cross-reactivity of the protein stains with DNA and EtBr with histones was tested by staining histone-containing gels with EtBr and DNA-containing gels with the protein stains. No bands were visible on the gels and none could be resolved in the autodensitometer analysis of the gel photographs. Error analysis of our densitometer techniques (19) indicated that peaks as small as 0.03 OD should be detectable; none were found. Typical peaks for the sample sizes we customarily used were ~ 1.5 OD in height. The staining patterns of the three protein stains used were superimposable to better than 2% (Figure 2). Considerable differences in ratios of peak heights and peak shapes could be seen between DNA-stained and protein-stained gels (Figures 3 and 4). Such differences could be attributed to varying protein/DNA ratios, however differences in accessibility of the DNA and protein to the stains, DNA conformation, and nonlinearity of fluorescence staining (20) should all affect these patterns. The ratios of these

peak areas change by 40% at most between protein- and DNA-stained gels of the same sample.

Trout monomer subunits were separated into several peaks by gel electrophoresis (Figures 1 and 3). A single narrow band contained approximately 40%-50% of the nucleoprotein; this amount (determined by staining) depended on the digest analyzed. This peak was designated Fraction I (Figure 3). The broader and lower peaks of higher mobility disappeared with shorter nuclease digestion (see Figure 2), but became the dominant peaks after extensive nuclease digestion. The peaks trailing Fraction I were not fully resolved under our conditions and were collectively labeled Fraction II. The ratios of the stain densities of Fractions I and II varied across the 11 S band from the sucrose gradient. Fraction II was at a minimum at the lower molecular weight side of the peak. The trout oligomer fraction was contaminated with ~ 20% Fraction I, but with less than 5% Fraction II. The rest of the oligomer ran in a complex manifold of bands (Fraction III) which fell behind almost all of the monomer (Figure 3).

Electrophoretic patterns from monomer and oligomer fractions of rat liver digests indicated greater heterogeneity in the sample than found in the comparable trout fractions. The monomer fraction did however contain broad peaks equal in mobility to Fractions I and II from trout. The gel scans (Figure 3) showed that the rat oligomer

fraction was heavily (~ 30%) contaminated with Fraction I and contained a low mobility peak similar to the Fraction III seen in the scans of trout oligomer subunit gels. The material from rat oligomer, however, showed none of the fine structure in Fraction III that was seen in the trout oligomer gels.

Nuclease digests of trout chromatin were run on a preparative slab gel and each of the bands was isolated and rerun on an analytical tube gel (Figure 5). Fraction I reran as a completely homogeneous band. Fraction II and the other bands reran as peaks with exactly the same peak shape as the band which was isolated. At the top of the gel there was a large peak which appeared in all trout oligomer fractions and all trout digests not fractionated by centrifugation (see Figure 1). When isolated and rerun, this peak separated into a pattern almost identical to that of the oligomer subunits. This suggested that the material at the top of the gel was a noncovalent aggregate which could be dissociated under the proper conditions.

The histones from the chromatin subunits were analyzed to test for possible heterogeneity and proteolysis. The electrophoretic patterns of the histones (Figure 6) from monomer, oligomer and unfractionated trout digests were compared with the pattern from undigested chromatin. They were identical, with the exception that the size of the f1 peak (lowest mobility) was reduced in the monomer

fraction (5). Assignment of peaks in the pattern to individual histones was described by Panyim and Chalkley (17). The histones from rat liver subunits showed increased mobility and broadening of the peaks (Figure 5). It can be seen that histone f2a1 (IV) has been almost completely degraded to lower molecular weight products in this preparation. Panyim and Chalkley (17) described similar electrophoretic behavior in histone preparations degraded by proteolysis.

The DNA extracted from monomer and oligomer fractions of trout testes chromatin digests was analyzed by gel electrophoresis. Results were identical to those already published by Honda et al. (5): the oligomer fraction contained bands which were integer multiples of 190-200 base pairs and the monomer fraction contained most of the DNA in bands corresponding to 140-145 base pairs (7). Our gels were calibrated with eco R1 restriction fragments of Φx - 174 DNA. The DNA extracted from oligomer rat liver subunits was heterogeneous and showed no sharp bands. DNA from rat monomer showed one band corresponding to 140 base pair length DNA with very high backgrounds obscuring all other peaks.

DISCUSSION

Several investigators have reported electrophoretic separations of complex nucleoproteins such as ribosomes and their subunits (21, 22). If dissociation or denaturation could be prevented, electrophoresis seemed well suited to the problem of analysis and purification of chromatin subunits. Weintraub (23) had reported a gel electrophoresis system for analysis of the trypsin digests of chromatin subunits; however, the intact subunits did not enter the gels. When we carried out electrophoresis of nuclease digests of chromatin in the presence of EDTA,[1] dissociation of the DNA and histone occurred and much of the nucleoprotein denatured under the electric field. Most of the sample remained at the top of the gel, although some free DNA and some nucleoprotein complex did enter the gel and migrate.[2]

Dahlberg et al. (21) reported that during electrophoresis ribosomal subunits did dissociate in the presence of EDTA but did not when Mg^{++} was present. Addition of even small concentrations of Mg^{++} to the chromatin subunits was found to cause aggregation and precipitation (5). We found that buffering the Mg^{++} concentration by adding the divalent cation and a twofold molar excess of EDTA eliminated all tendencies toward aggregation. Under these conditions,

electrophoretic analysis of the nuclease digests was accomplished without denaturation. Presumably Mg^{++} bound to high affinity sites on the chromatin subunits must confer additional stability to these particles.

It has been demonstrated here that monomer subunit particles, even when composed of degraded DNA and histones (as in the rat liver preparations), sediment as a single band in the ultracentrifuge. However, these particles, when analyzed by native gel electrophoresis, show a high degree of heterogeneity. Monomer and oligomer subunit particles from trout testes chromatin can also be resolved into several distinct species by gel electrophoresis. This fractionation is probably based on the variable histone f1 content (5) of the subunits and the heterogeneity of the lengths of the DNA in them.

The techniques described in this paper can be used to prepare milligram quantities of electrophoretically pure monomer chromatin from one slab gel.

ACKNOWLEDGMENTS

We wish to thank Barry Honda, Dave Baillie and Peter Candido for providing the trout testes chromatin digests, and Joel Gottesfeld and James Bonner for the preparations of rat liver chromatin subunits. Without their help, this work would have been impossible.

REFERENCES

1. Sahasrabuddhe, C.G. and Van Holde, K.E. (1974) J. Biol. Chem. 249, 152-156.
2. Noll, M. (1974) Nature 251, 249-251.
3. Kornberg, R.D. (1974) Science 184, 868-871.
4. Oosterhof, D.K., Hozier, J.C., and Rill, R.L. (1975) Proc. Nat. Acad. Sci. USA 72, 633-637.
5. Honda, B.M., Baillie, D.L., and Candido, E.P.M. (1975) J. Biol. Chem. 250, 4643-4647.
6. Shaw, B.R., Corden, J.L., Sahasrabuddhe, C.G., and Van Holde, K.E. (1974) Biochem. Biophys. Res. Commun. 61, 1193-1198.
7. Rill, R.L., Oosterhof, D.K., Hozier, J.C., and Nelson, D.A. (1975) Nucl. Acid Res. 2, 1525-1538.

8. Sollner-Webb, B. and Felsenfeld, G. (1975) Biochemistry 14, 2915-2920.

9. Finch, J. T., Noll, M., and Kornberg, R. D. (1975) Proc. Nat. Acad. Sci. USA 72, 3320-3322.

10. Good, N. E., Winget, G. D., Winter, W., Connolly, T. N., Izawa, S., and Singh, R. M. M. (1966) Biochemistry 5, 467-477.

11. Loening, U. E. (1967) Biochem. J. 102, 251-257.

12. Sharp, P. A., Sugden, B., and Sambrook, J. (1973) Biochemistry 12, 3055-3063.

13. Chrambach, A., Reisfeld, R. A., Wyckoff, M., and Zaccari, J. (1967) Anal. Bioch. 20, 150-154.

14. Fambrough, D. M. and Bonner, J. (1966) Biochemistry 5, 2563-2570.

15. Gorovsky, M. A., Carlson, K., and Rosenbaum, J. L. (1970) Anal. Bioch. 35, 359-370.

16. Studier, F. W. (1973) J. Mol. Biol. 79, 237-248.

17. Panyim, S. and Chalkley, R. (1969) Arch. Biochem. Biophys. 130, 337-346.

18. Gottesfeld, J. M., Murphy, R. F., and Bonner, J. (1975) Proc. Nat. Acad. Sci. USA 72, 4404-4408.

19. Ross, M. J. and Stroud, R. M. (1976). Submitted to Acta Cryst.

20. Pulleyblank, D. E., Shure, M., Tang, D., Vinograd, J., and Vosberg, H.-P. (1975) Proc. Nat. Acad. Sci. USA 72, 4280-4284.

21. Dahlberg, A. E., Dingman, C. W., and Peacock, A. C. (1969) J. Mol. Biol. 41, 139-147.

22. Szer, W., and Leffler, S. (1974) Proc. Nat. Acad. Sci. USA 71, 3611-3615.

23. Weintraub, H. (1975) Proc. Nat. Acad. Sci. USA 72, 1212-1216.

FOOTNOTES

*This work was performed with the support of National Institutes of Health grant GM-19984 and National Science Foundation grant BMS75-01405. One author (RMS) is the recipient of a National Institutes of Health Career Development Award, and the other (MJR) held a National Institutes of Health Predoctoral Traineeship. This paper is contribution No. 5353 from the Norman W. Church Laboratory of Chemical Biology, California Institute of Technology.

†Present address: The Biological Laboratories, Harvard University, 12 Divinity Avenue, Cambridge, Massachusetts 02138.

[1] M. J. Ross and R. M. Stroud (1974), unpublished results.

[2] While preparing this manuscript, a preliminary report of the analysis of chromatin subunits by gel electrophoresis was published by A. J. Varshavsky, V. V. Bakayev and G. P. Georgiev (1976) Nucl. Acid Res. 3, 477-492. EDTA was used in their buffer system with no Mg^{++} added.

FIGURE CAPTIONS

FIGURE 1. Ethidium bromide stained gels of chromatin subunit fractions. The gels were run as described in Materials and Methods, using Tris-acetate buffer; the direction of electrophoresis was top to bottom. The samples shown are (from left to right) rat liver monomer, trout testes oligomer, trout monomer, and unfractionated trout chromatin subunits. The oligomer and monomer fractions were prepared by velocity sedimentation. High molecular weight aggregate can be seen on the top of the unfractionated digest and oligomer gels.

FIGURE 2. Autodensitometer traces of protein stained gels of unfractionated trout testes chromatin subunits. These subunits were prepared with a shorter digestion time than that used to prepare the monomer fraction analyzed in Figures 1, 3 and 4. Reading from top to bottom, the gels were stained with fast green FCF, amide black and Coomassie brilliant blue. The gels were run in Tris-acetate buffer.

FIGURE 3. Autodensitometer traces of ethidium bromide stained chromatin subunit gels. These data were taken from the photograph shown in Figure 1. Direction of electrophoresis was left

to right. Fractions I and II can be seen on the scans of the monomer gels and Fraction III on the scans of the oligomer gels.

FIGURE 4. Autodensitometer analysis of Coomassie brilliant blue stained chromatin subunit gels. The ethidium bromide stained gels from Figures 1 and 2 were washed and fixed in two one-liter changes of 10% acetic acid then stained for protein as described in Materials and Methods. The direction of electrophoresis was left to right. The quantity of nucleoprotein in these gels is 5x less than usually used in gels which were to be stained for protein.

FIGURE 5. Autodensitometer analysis of trout chromatin subunits purified by preparative slab gel electrophoresis. These analytical gels were run from left to right in MES buffer. The three tracings correspond to unfractionated chromatin subunits before preparative electrophoresis (top), Fraction I monomer subunits (middle), and high molecular weight aggregate isolated from the very top of the slab gel (bottom). The Fraction I monomer subunits re-electrophoresed with unchanged mobility.

FIGURE 6. Autodensitometer tracings of the gel electrophoresis pattern of histones isolated from rat liver and trout testes

monomer fraction chromatin subunits. Direction of electrophoresis was left to right. The histones were stained with amide black.

Figure 1

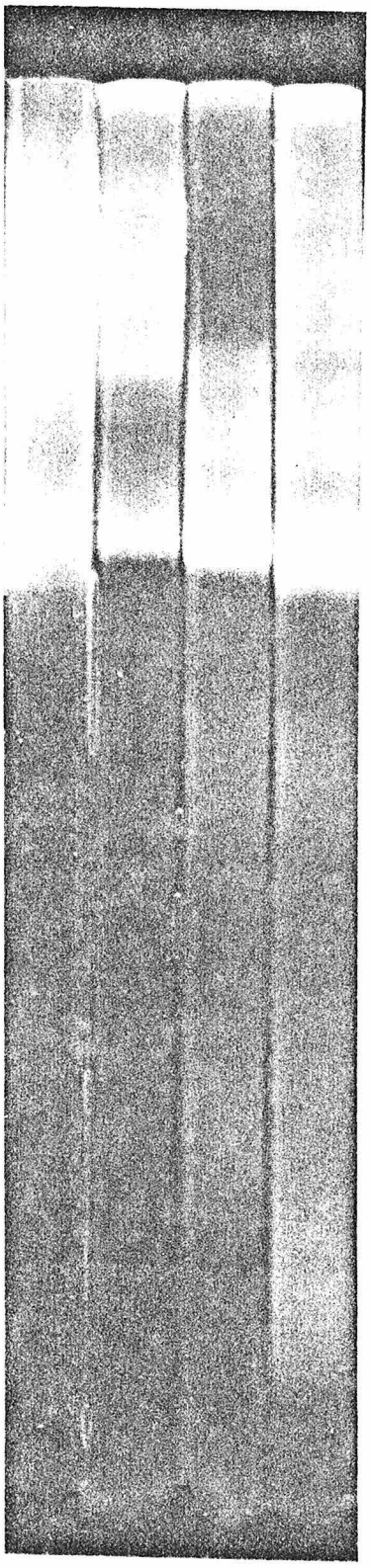

Figure 2

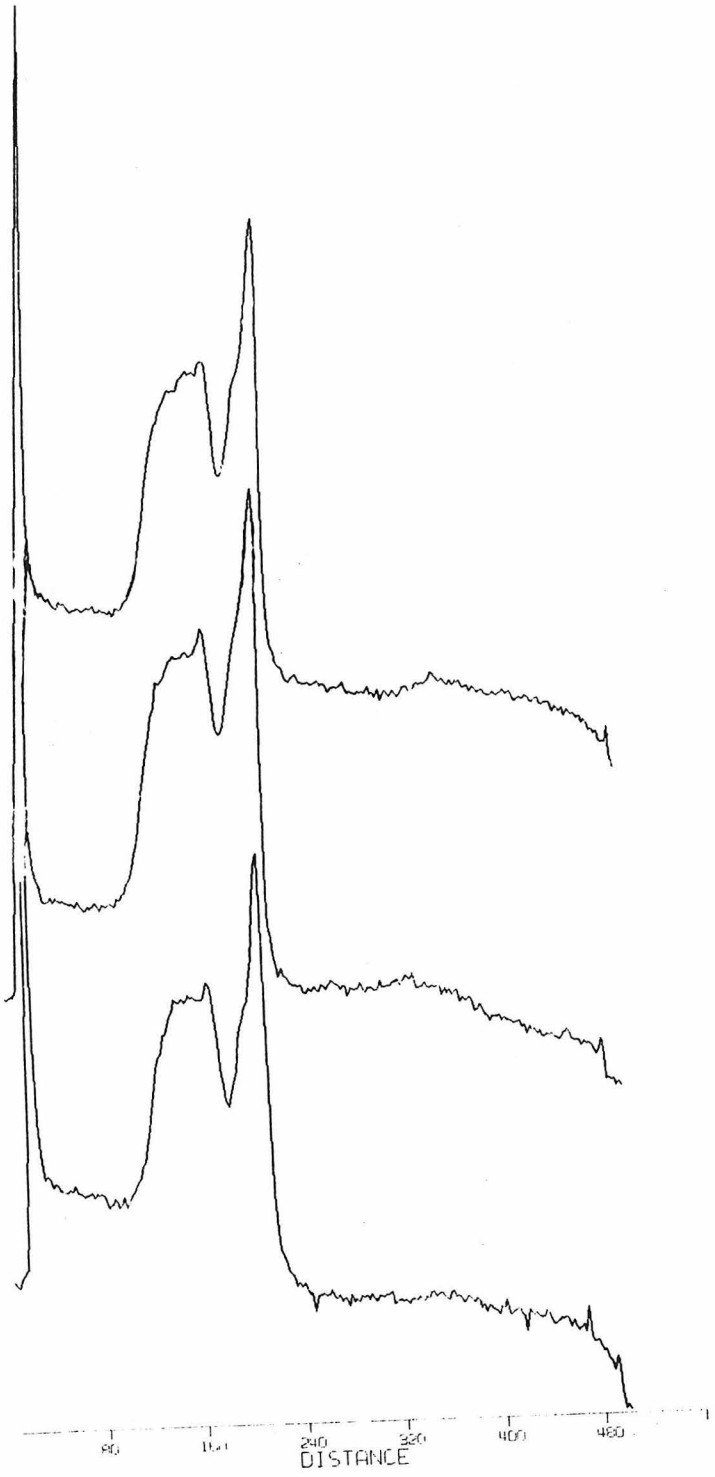

Figure 3

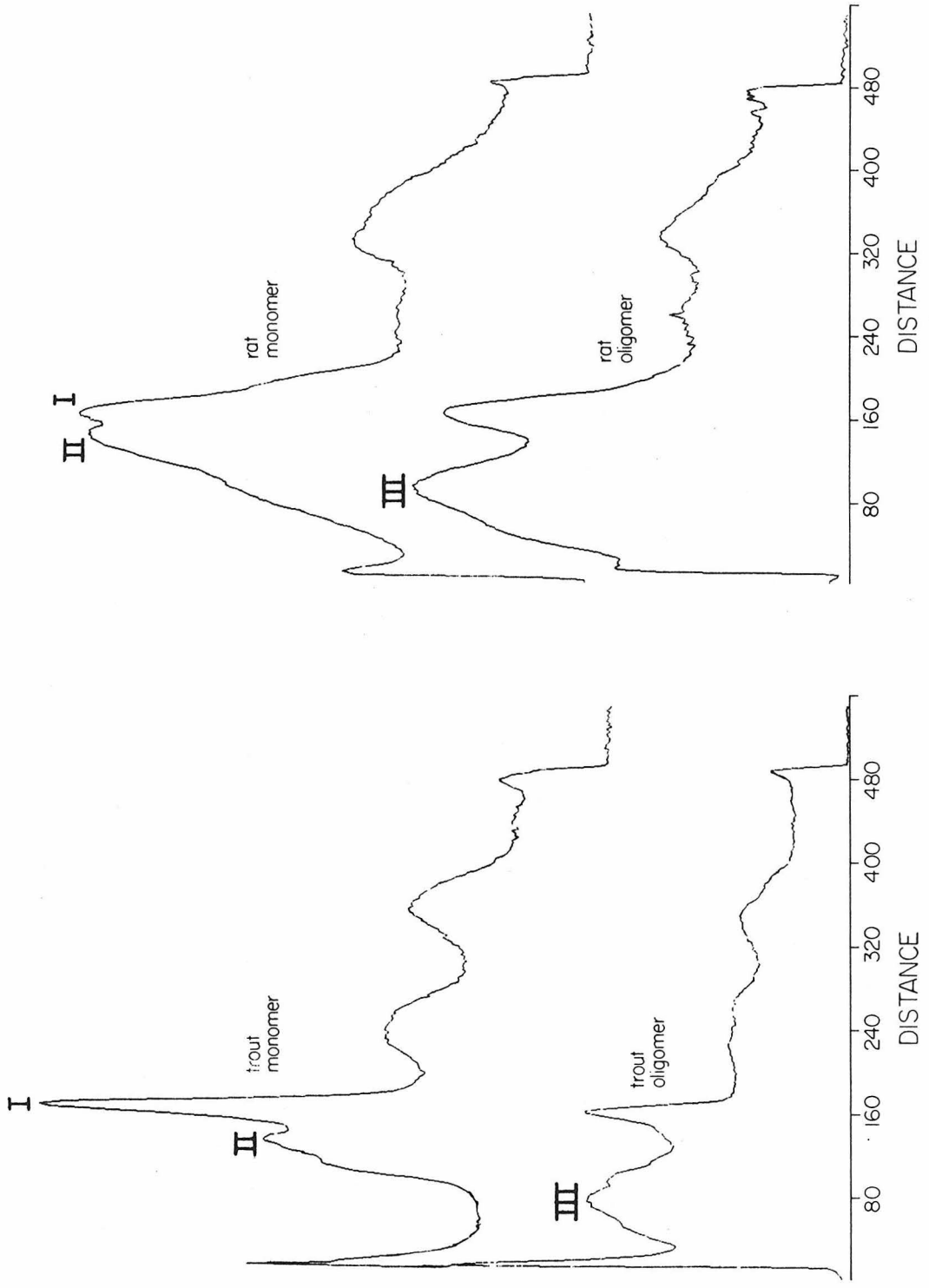
I
II
III
trout
monomer
trout
oligomer
80
160
240
320
400
480
DISTANCE
I
II
III
rat
monomer
rat
oligomer
80
160
240
320
400
480
DISTANCE

Figure 4

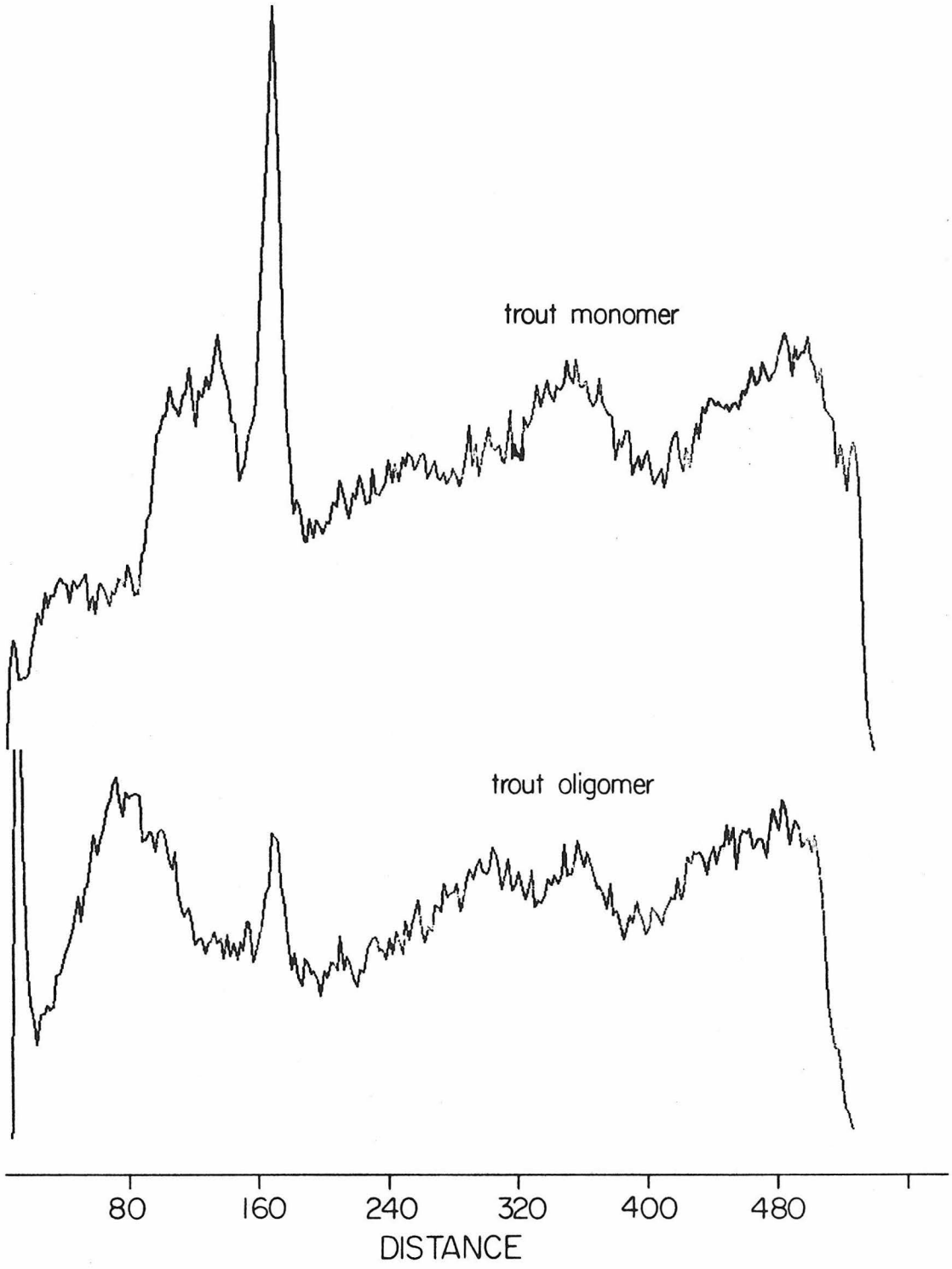
trout monomer
trout oligomer
80
160
240
320
400
480
DISTANCE

Figure 5

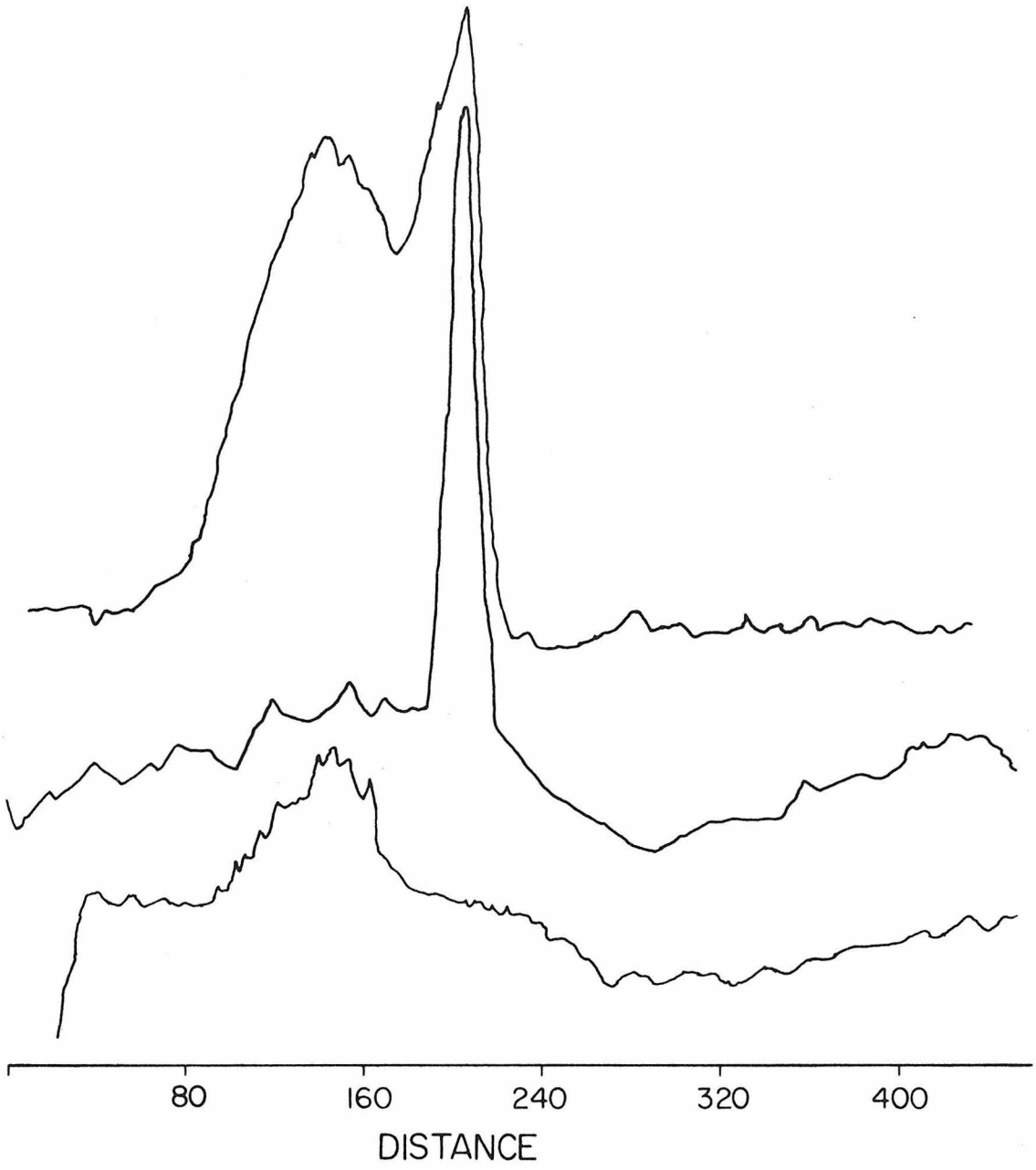

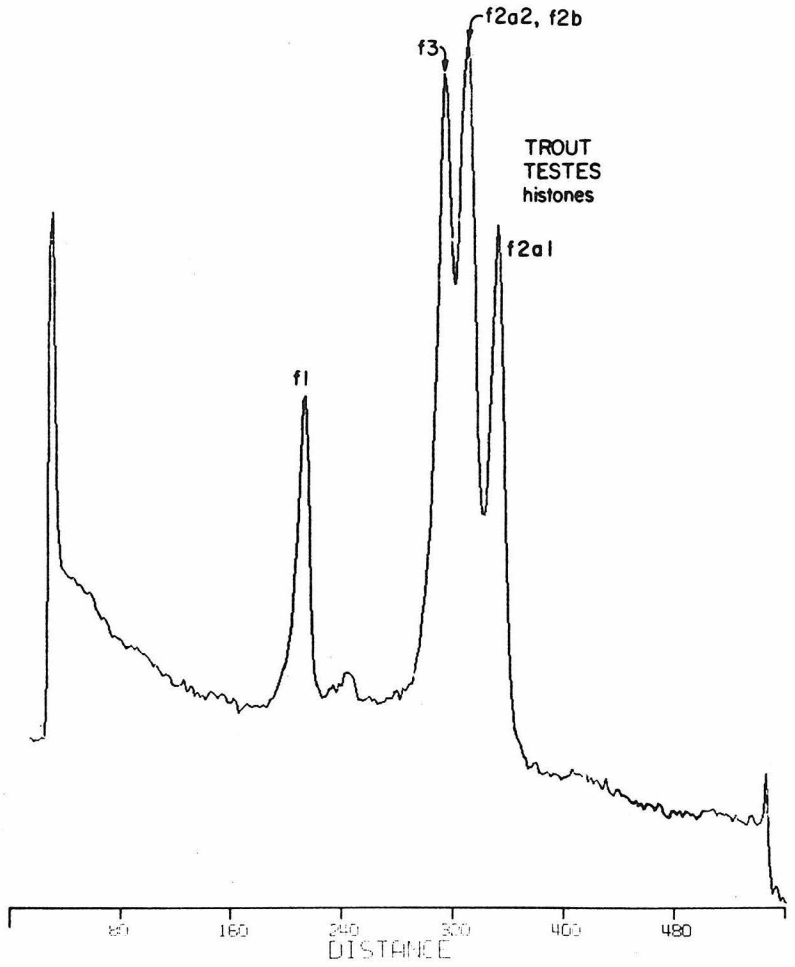
f2a2, f2b
f3
TROUT
TESTES
histones
f2a1
f1
80
160
240
320
400
480
DISTANCE

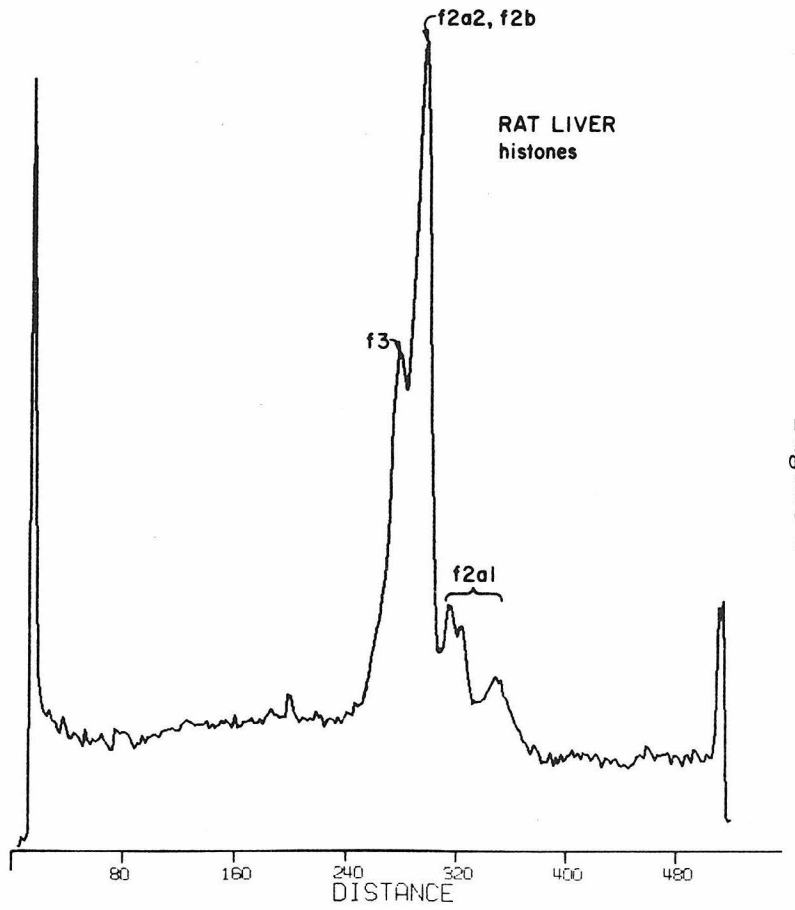
f2a2, f2b
RAT LIVER
histones
f3
f2a1
80
160
240
320
400
480
DISTANCE

Figure 6

APPENDIX C

Error Analysis in the Biophysical Applications of a Flatbed Autodensitometer

M. J. Ross, and R. M. Stroud

Submitted to Acta Crystallogr.

Error Analysis in the Biophysical Applications of a Flatbed Autodensitometer*

BY

MICHAEL J. ROSS† AND ROBERT M. STROUD‡

Norman W. Church Laboratory of Chemical Biology

California Institute of Technology

Pasadena, California 91125, U.S.A.

Running Title: Error Analysis of an Autodensitometer.

---

*Contribution No. 5360. Supported by National Institutes of Health Grant GM-19984 and National Science Foundation Grants BMS75-01405 and GB-34881.

†National Institutes of Health Predoctoral Trainee. Present address: The Biological Laboratories, Harvard University, Cambridge, Massachusetts 02138.

‡National Institutes of Health Career Development Awardee, U.S. Public Health Service Grant GM-70469.

Abstract

The positional, electronic, and density accuracy of the Syntex AD-1 flatbed autodensitometer is discussed. The standard deviation of optical density measurements due to electronic noise is ±0.001 optical density units at an optical density of 0, rising to ±0.04 at an optical density of 2. No deviation from linearity in optical density measurements could be measured. During scanning, the standard deviation in position is less than 1.5 μ. Film grain noise for various films is compared and the effects of signal averaging on this noise is studied. This scanner is compared with other scanners available for accuracy of data collection from precession films.

Introduction

Many physical and biophysical techniques now in common use depend upon film methods for data collection, and to an increasing extent the analysis of these data is enhanced by, or dependent on, digital computers. The applications of computer-controlled microdensitometers to the field of x-ray diffraction have ranged from digitization of single crystal x-ray films (Arndt, Crowther and Mallet, 1968; Xuong, 1969; Nockolds and Kretsinger, 1970; Werner, 1970;

and Matthews, Klopfenstein and Colman, 1972) to treatment of small angle or large angle x-ray scattering data from less well-ordered samples (Wooster and Fasham, 1958). The scanners are necessary for computer aided image processing (Nathan, 1971) and image reconstruction from electron micrographs (DeRosier and Moore, 1970; Unwin and Henderson, 1975; Ross, Klymkowsky, Agard and Stroud, 1976). Additional uses are analysis of data from ultracentrifugation, electrophoretic gels, and chromatograms. These applications have generally been the province of analog microdensitometers; however, as data analysis in these fields becomes more sophisticated, the availability of computers and digitized data becomes more important.

The features of two types of computer-controlled microdensitometers have already been described in the literature. The flying spot or cathode ray tube (CRT)-type scanner (Arndt et al., 1968; Billingsley, 1971) has very high speed and flexibility, but it has a limited optical density (OD) range, relatively low positional accuracy and a high cost. The rotating drum scanner (Abrahamsson, 1966; Xuong, 1969; Nockolds and Kretsinger, 1970; and Matthews et al., 1972) has relatively high speed, relatively good positional accuracy and good OD linearity. However, only flexible films with certain specific size limitations can be used, and the x and y axes of the scanner are not independently controllable.

A third type of scanner available is the flatbed scanner (Drenth, Kloosterman, van der Woude, Croon, and van Zwet, 1965). This design offers excellent positional accuracy, the ability to scan any specified area of a flat object (such as electron microscope (EM) glass plates), and good OD linearity. The one drawback for protein crystallographers alone, is the lower speed of data collection.

In this paper we describe a systematic analysis of the errors inherent in data collection with a moving stage flatbed microdensitometer manufactured by Syntex Analytical Instruments. In order to set limits on expected errors which may be encountered when using this microdensitometer for the above mentioned applications, we have tested some of the basic instrument parameters, specifically, positional accuracy, OD linearity, spatial resolution, stability and absolute OD accuracy. Since the accuracy of single-crystal data collection is a combination of many of the above mentioned factors (Wooster, 1964), the overall scanner performance was evaluated by analysis of x-ray precession films.

Film methods as a whole have many drawbacks. The first and most obvious is the inherent trade-off between film grain (noise) and film efficiency. Others are the lack of linearity, dynamic range, and sensitivity of films compared with electronic counting systems. Nevertheless, film is used for many experiments because; 1) there

may be no alternatives, as in the cases of electron microscopy and electron diffraction where no digital electron microscope is widely available; 2) film methods often require far less capital investment than the competing methods; and 3) film offers the advantages of spatial resolution which can lead to more efficient data collection than obtainable with present day counting systems (Arndt, Champness, Phizackerley, and Wonnacott, 1973).

Experimental

Instrument Description

All data were collected on a Syntex Analytical Instruments AD-1 flatbed autodensitometer interfaced to a Data General NOVA 1200 computer with 20K words of core and a 9-track magnetic tape unit. The scanner has a useful scanning area of 15 cm x 15 cm, with the item to be scanned supported on a glass plate. The scanner electronics consist of computer-controlled independent x and y drive screws which drive the stage at rates up to 9.8 mm/sec. during data collection. Light amplification and digitization is accomplished with a photomultiplier, preamplifier and 10-bit analog to digital (A/D) converter which is linear in transmittance; conversion to optical density is carried out digitally in the computer.

The source is a tungsten filament bulb*. Light is focused through microscope objective optics, and a rectangular defining aperture. Light transmitted through the sample is focused through a round receiving aperture of diameter approximately equal to 2.5 times the diagonal dimension of the source aperture. This arrangement allows a measurement of the specular density of the specimen. Four source aperture sizes are available: 10 μ x 10 μ, 32 μ x 32 μ, 55 μ x 109 μ, and 109 μ x 219 μ. The overall gain of the optical train is adjusted by varying the high voltage on the photomultiplier. A shutter and optical fiber light pipe are used to record the photomultiplier dark current and light source intensity at each reversal of the stage direction. The scanner is capable of taking data at 6 μ intervals (1.63 kHz)†.

Film Processing

Kodak no-screen x-ray film was developed in Kodak liquid x-ray developer for five minutes at 20°C with nitrogen burst agitation every twenty seconds. Electron microscope film was developed

*The power supply for the light bulb was modified to allow operation at either an increased voltage of 6.3V or at the standard 5V; this increase in light intensity was useful when the 10 μ spot was used.

†A modification of the frequency response characteristics of the preamplifier was implemented in order to change the roll-off frequency from 400 Hz to 2000 Hz.

in Kodak D-19 at 20°C for five minutes with continuous agitation. All other films were developed using Kodak D-11 developer with continuous agitation. All films were rinsed in distilled water and treated with a wetting agent (Kodak Photoflow 200).

Scanning Algorithms

Data were collected using either the assembly language programs or FORTRAN programs provided by Syntex (the FORTRAN programs are modifications of the original versions written by one of us (MJR)). This software calculates optical density as $OD = -\log [(C-D)/(R-D)]$, where C is the observed photomultiplier output at a given position, and D and R are the dark and reference values from the previous light pipe reading, respectively. At the start of each area-scan, the stage is moved to the starting x, y position at slow speed and the nonscanning-axis position (x)* is then corrected to its final value using a three step process. The starting position in the scanning-axis (y)* is chosen to allow the scanning speed to stabilize before the initiation of data collection; this startup distance is about 0.8 mm.

---

*Although for most applications x (left to right, facing the instrument) is chosen as the nonscanning-axis and y as the scanning-axis, the FORTRAN software allows the user to change this, if desired. In this paper, the nonscanning-axis will be referred to as the x-axis and the scanning-axis as the y-axis.

Positional accuracy in the y-axis is maintained by collecting data at constant speed and by correcting for backlash using software. Areas on films are digitized by alternately moving the stage back and forth in y, taking a reference (light pipe) reading and a single step in x between each scan. The three step algorithm for x-axis positioning is not carried out in between each scan.

Single crystal reflections from precession films were densitometered using the FORTRAN software which consists of a centering routine, a least-squares subroutine, and a data collection routine. The centering algorithm consists of manual "joystick" movement of the film to superimpose the light spot on three axial reflections, followed by a rough calculation of an orientation matrix. This matrix is used to calculate the position of six to fifteen check-reflections and each of these is scanned using the reflection scanning (spot-scan) algorithm described in Figure 1. The centers of these reflections are calculated and then a least-squares coordinate transform matrix is computed for use by the data collection subroutine. Individual spot-scans centered about each calculated reciprocal lattice point on the film are carried out and from these individual scans, backgrounds and integrated intensities for each reflection are calculated (Figure 1). If Laue streaks are present, the program allows the option of collecting backgrounds only on those sides of the reflection through

which the streaks do not pass. The film OD's are corrected for non-linearity effects by using the logarithmic correction determined by Morimoto and Uyeda (1963): for Kodak no-screen film the equation is

$$OD_{corr} = -7.823 \log_e ((8.333 - OD_{obs})/8.333)$$

where OD_{corr} is the corrected OD. This correction was chosen as an alternative to the parabolic correction used by Matthews et al. (1972) because it could be used for data collected with only one film per pack, whereas the parabolic correction is based on scaling two or more films together. Parameter data files containing the indices of check-reflections, information on space group and other data collection parameters, are stored on disk or tape and need be generated only once for each crystal structure being studied.

Data Reduction

Data reduction was carried out on a Data General NOVA 800 computer with 32K words of core, a 2.4 M byte disk, a Syntex Analytical Instruments floating point processor, two magnetic tape units and a Versatec 1100A matrix printer/plotter. Data from area scans were treated in several ways: 1) a gray-level histogram (Billingsley, 1971), displaying the number of pixels (digital picture elements) present in the image at each optical density, was calculated

(for example, see Figure 2a); 2) the image was linearly integrated over either x or y with the resultant average OD plotted vs. position along the other axis (for example, see Figure 2b); 3) the digitized data were displayed as a halftoned image on the matrix plotter (for example, see Figure 2c).

From the histogram, the minimum, maximum, mean, mode, and median OD's were calculated as were the OD's between which 95.4% of the observations occurred. The latter would represent two standard deviations from the mean, if the data obeyed a Gaussian distribution and will be referred to in this paper as 2σ levels, even when applied to non-Gaussian distributions.

Precession film data were corrected for both Lorentz and polarization factors (Waser, 1951); all symmetry equivalent reflections were averaged, and those with large standard deviations were flagged; first, second and third films from the same pack (when available) were scaled linearly together on medium strength reflections. Reflections with OD's greater than 2.3 were not used.

Positional Accuracy

A razor blade (Wilkinson platinum) was set on the glass stage with the edge perpendicular to the scan axis. The razor blade was scanned using a scanner step size of 10 μ and the 219 μ length of the

219 μ x 109 μ spot size. The transmittance (counts) was plotted vs. position for each scan. The counts should decrease linearly as the spot is slowly eclipsed with any positional errors reflected as deviations from linearity. The very beginning and end of the graphs curve, because of the diffraction limits of the optics, to give an overall sigmoidal shape to the plot. The central portion of each plot (from 20% to 80% transmittance) was fitted to a least-squares line and the deviation from linearity was used as a measure of positional accuracy along the scanning-axis.

The nonscanning-axis positioning was checked using a similar technique. In this case, the razor blade edge was placed parallel to the scanning-axis and the stage was iteratively moved (10 μ steps in the nonscanning-axis direction) so as to eclipse the light spot. The transmittance readings were plotted and subjected to least-squares analysis as above. The nonscanning-axis positioning was tested using the two different algorithms supplied by Syntex: 1) slewing to position followed by a three-step positional adjustment; and 2) stepping the nonscanning-axis between successive scans. The long dimension of the 219 μ x 109 μ spot was used for these tests since it allows data collection over longer distances in the region of the edge.

Spatial Resolution

The projected light spot size, although a major factor, is not the only parameter affecting scanner resolution. In the AD-1, lens imperfections, the frequency response of the detection and digitizing circuitry, and the absolute diffraction limitations of the optics (Billingsley, 1968) could lead to resolution lower than that theoretically obtainable for a given spot size. Instead of trying to measure or calculate each of these individual parameters and risk overlooking others, it was decided to simply measure the sine-wave response function of the optical system (Perrin, 1960). In this test, parallel Ronchi rulings (engine enscribed 50% black, 50% clear glass rulings, Edumund Scientific, 50, 100, 200, and 300 cycles/inch) were scanned* with each of the four spot sizes; they were scanned with the direction of the ruled lines either parallel or perpendicular to the scanning-axis. At some low ruling frequency where the light spot is much smaller than the objects (i. e. rulings) to be resolved, an essentially perfect rendition of the pattern would be realized; however, as the ruling frequency approaches the resolution limits of the densitometer, the scanner response decreases, and at some limiting high spatial frequency no response at all should be detectable.

*Sine-wave patterns should ideally be used, but are difficult to manufacture. Perrin (1960) points out that square waves, i. e., alternating light and dark bars are a satisfactory substitute.

Electronic Noise

The glass plate was removed from the scanner stage and the optics were refocused. An area containing 200 x 200 OD measurements (pixels) was densitometered and recorded on magnetic tape using the area collection algorithm. Total noise was measured as a function of: 1) spot size; 2) photomultiplier voltage, and 3) readings from the photomultiplier (ψOD)*.

Total Scanner Noise

In order to assay for increased noise caused by dust or small scratches on the glass, an area (200 x 200 pixels) of the glass plate was scanned using the area collection algorithm for each of the four spot sizes and a statistical analysis of the scanner noise was carried out as described above. Since image reconstructions of electron micrographs are done using the Fourier transform of digitized images, the Fourier components of the scanner noise were calculated using a two-dimensional fast Fourier algorithm (Ross et al., 1976).

---

*ψOD is the calculated OD corresponding to the digital output of the AD-1 electronics. It is not necessarily the same as the true OD of the sample being densitometered. The ψOD can be manipulated by changing the gain of the photomultiplier, changing the lamp power supply voltage, or by changing the scanner apertures.

Long Term Stability

The dark current, light pipe reference reading, and light through the optical system were sampled every eight hours for three days. The test was carried out using the 109 μ x 55 μ spot with a clean glass stage and no stage movement. During this period of three days, the room temperature was allowed to vary from 20°C to 30°C. The filament in the source was left on continuously.

Photomultiplier Fatigue

The scanner was designed such that the photomultiplier would be kept in a state of constant fatigue (low sensitivity) by "flashing" it with the bright reference beam at the conclusion of each y-scan. A "worst case" test of the effectiveness of this procedure was designed: long (longer than two seconds) scans of high ψOD were digitized to see whether photomultiplier sensitivity changed within a given y-scan.

This test was carried out by scanning seven-centimeter-long sections (y-scan time of about seven seconds) of a glass optical wedge (absolute OD 0.5 to 3.0; total length was 22.5 cm; manufactured by Joyce-Loebl). Scans up the wedge started at low relative optical density and ended at higher relative optical density. The reverse was true for scans down the wedge. The integrals of the OD's on the scans up and the scans down the wedge were compared. If the

photomultiplier were to change in sensitivity during the y-scans, we would expect the integral of the OD's on the scans up the wedge to be larger than the integral of the OD's on the scans down the wedge; a dark (high OD) section of the scan at the scan start would presumably cause the OD measurements for the rest of the scan to be anomalously low (photomultiplier too sensitive).

Absolute OD Accuracy

Gelatin neutral density filters of OD 0.10, OD 0.50, and OD 0.90 (Eastman Kodak) were scanned both separately and in pairs. The average measured density of each filter was corrected to an absolute OD value by subtracting the measured OD of the glass plate.

OD Linearity

Two independent tests for OD linearity were employed. In the first test a razor blade (Wilkinson platinum) was placed at an angle of approximately 0.5° to the y-axis. The scanner was positioned such that the light spot did not intersect the razor blade at the start of a y-scan and had completely disappeared by the end of it; the razor blade was so scanned for each of the four spot sizes. The razor blade was examined microscopically and found to have an edge roughness of about 0.5 μ rms. The scans were displayed as counts

(transmittance) versus position; these plots bore a strong resemblance to the sigmoidal plots described under Positional Accuracy above. The central portions of the curves (from 20% to 80% transmittance) were fitted to a least-squares line and the deviations from linearity were measured.

The second test involved use of a linear glass density wedge (see above). Although care had to be taken that defects in the wedge were not being measured, this test was used to extend the results of the razor blade test to the full range of densities measurable by the scanner. The glass wedge was placed on the densitometer bed and scanned using all four spot sizes and the full range of photomultiplier voltage settings.

Two different seven-centimeter sections of the wedge were used for all tests to estimate the contributions due to nonlinearity in the wedge. For each test, data from twenty scans were averaged to reduce the noise.

Film Noise

Unexposed samples of each film type were processed, areas of each film were digitized using the area-scan algorithm for various spot sizes, and the OD's in the digitized area were statistically analyzed. The scanned area was then further processed by averaging

integral numbers of rows and/or columns of pixels to test the effect of signal averaging on film grain noise.

Results

Positional Accuracy

The maximum deviation in scanning-axis position was 4.6 μ. The standard deviation was ±1.5 μ from the calculated position. Since the x-axis positioning between scans was handled differently than the x-axis positioning at the start of a scan sequence (see Experimental Section), the errors in these two processes were measured separately. The maximum deviation found in the x-axis positioning algorithm used at the start of spot- or area-scans was 2.2 μ. The standard deviation of positioning was ±1.4 μ. Between y-scans, the x positioning was found to have a maximum deviation of 2.9 μ and a standard deviation of ±0.9 μ.

Spatial Resolution

The scans of the glass rulings were analyzed with gray-level histograms (Figure 2a). The ΔOD between the 2σ levels in the histograms were normalized (ΔOD = 3 was deemed to be 100% response), and displayed as a function of ruling frequency for each

spot size (Figure 3). Substantial loss (> 30%) of the high spatial frequency content of the image occurred whenever the scanner spot was larger than one third the size of the object to be resolved. This falloff can be corrected by real space or Fourier space filtering of the digitized image.

Since the normalized ΔOD never fell below 5% even when the spot size exceeded the ruling spacing by several times, we examined both halftoned (Figure 2c) and linearly integrated images (Figure 2b) of each digitization. In all cases, image contrast reversal* (Andrews, 1970) started to appear in these images as the normalized ΔOD fell below 20%. Thus, when the scanner is to be used for image analysis, care should be taken not to densitometer images with high amplitude features smaller than the spot size, even if their resolution is not desired, because the appearance of false features in the digital image will be the result.

---

*Image contrast reversal is a condition which occurs during digitization of images in which black areas appear white and white areas appear black. It is a result of the sampling of the densitometer and is also called "false resolution" since features appear resolvable but are not accurate representations of the object being densitometered.

Noise

The noise level of the densitometer was measured by the standard deviation of the densitometer readings from the median OD with the glass stage removed, and characterized as a function of several variables. There was no change in the noise level as the photomultiplier voltage was changed from 400 V to 1100 V (ψOD was kept constant), nor was there any detectable dependence on spot size (ψOD also constant). In both of these cases, the noise level (ψOD = 0) was found to have standard deviations of from ±0.0015 OD to ±0.0025 OD. However, as might be expected in a system which is digitized as a linear function of transmittance, the noise level increased exponentially with increasing ψOD (see Figure 4). The scanner exhibited a very low noise level at low optical densities, increasing to one with a standard deviation of ±0.066 OD (±3%) for measurements at OD 2.2.

When the glass plate used for supporting films was replaced in the scanner and these measurements repeated, no change in the standard deviations of the measurements from the median were observed, although the maximum deviations from the median OD increased to a value of 0.02 OD (ψOD = 0) for all spot sizes. This represented increases in maximum deviations from the median of up to five times at low optical densities.

Fourier analysis of this densitometer noise yielded two interesting results. First, with all apertures, one feature appeared in transformations: a strip of higher magnitude Fourier coefficients which were zero order in x appeared. These higher magnitude terms seemed evenly distributed along y (see Figure 5). This effect was traced to the method by which the densitometer calculated OD (see Experimental Section): the OD's within each y-scan were being calculated relative to the light pipe (reference) reading for that scan. Therefore the noise from the statistical variations in the reference readings appeared as zero order Fourier terms along the y axis. To correct for this, the area-scan algorithm was changed to allow calculation of OD assuming a constant reference and dark current for all y-scans; these values were determined at the start of the scan of the entire area. This procedure eliminated the strip of larger Fourier coefficients (Figure 5) but had one potential drawback: long-term drift in OD readings could result from thermal or light bulb drift. These errors would, however, be automatically filtered out if a Fourier space masking procedure such as that used in image reconstructure were carried out.

The second phenomenon observed from Fourier analysis of the noise became most obvious when using the 10 μ x 10 μ source aperture. Relatively strong repetitive noise (thirty times that seen using

the 32 μ x 32 μ spot) was observed with the smaller spot (Figure 5a) and traced to mechanical vibration of the DC pulse motors used to drive the stage. The noise terms were large enough to interfere with image reconstructions of electron micrographs scanned with the 10 μ x 10 μ spot. We found that they could be almost eliminated (reduced seventyfold) by using a larger receiving aperture than usual. When the receiving aperture normally used with the 32 μ x 32 μ spot was used with the 10 μ square light spot, only a 5% reduction in resolution could be measured (Figure 3), implying that the reduction in noise was not coupled with a substantial decrease in performance. A similar reduction in the systematic noise level found with the 32 μ x 32 μ source spot was achieved by use of a larger receiving aperture (that normally used with the 109 μ x 55 μ spot).

Stability and Hysteresis

The long-term stability of the scanner was tested to determine the efficacy of the pseudo-double beam optics used. Over a period of four days with ambient temperatures of 20°C to 30°C, the drift in transmittance was 5.8%, but the corrected optical densities varied by only 0.01 OD. The photomultiplier sensitivity was found to increase during long (longer than two seconds) scans of high ψ OD (i.e., low photomultiplier current). This led to an observed

hysteresis in the scans of the optical wedge (see Figure 6). This effect was found to be a function of the average ψOD during a scan, but not a function of the photomultiplier voltage. A large increase in photomultiplier sensitivity during the scans was noted as the average ψOD rose above 1.6 (Figure 6).

OD Accuracy and Linearity

The measured OD of calibrated neutral density filters varied linearly with OD rating of the filters such that the measured OD was approximately 4.5% high. This is not surprising since the filters are calibrated on a densitometer which measures transmitted light over a 180 degree angle of acceptance (diffuse density) whereas the AD-1 measures transmitted light scattered over an angle of about four degrees (specular density). This specular density is always greater than or equal to the diffuse density since any light scattered at an angle of greater than four degrees cannot be recorded.

The deviations from optical linearity as measured by the oblique scan of the razor blade was ±3 counts for the largest spot size (Figure 7a). (Transmittance was digitized in the range of 0-1023 counts.) The measured errors increased with decreasing spot size to ±13 counts for the 10 μ x 10 μ spot. Visual inspection of the difference plots (deviation from least-squares line, Figure 7b)

showed that most of the measured deviation was due to high frequency noise which was traced to roughness in the razor blade edge.

An inherently less noisy test of linearity was carried out using a glass OD wedge. The results were analyzed as a function of ψOD, spot size, and photomultiplier voltage (Figure 8a, c). Root mean-square (standard) deviations of the difference curve (deviations from the least-squares line) were the same as measured in the electronic noise test for any ψOD range from 0 to 2.8 (Figure 8b, d). At low average optical densities, nonlinearities of 0.005 OD should have been detectable but were not seen.

Small low frequency variations in the difference curve were observable even though they were too small to affect the statistical analysis of the noise (Figure 8b, d). These features were traced to imperfections in the wedge rather than to nonlinearities in the optical system. This follows from the observations that the low frequency variations remained invariant as ψOD, spot size, or photomultiplier voltage were changed but moved in position when different areas of the wedge were analyzed.

Film Noise

A table of maximum and standard deviations (from the median OD) for processed unexposed films was compiled to act as a reference

for noise estimation in images recorded on these films (Table I).

The results for signal-to-noise enhancement by averaging neighboring picture elements are shown in Figure 9. The higher spatial frequency components of the film grain noise would be expected to be reduced by this averaging while the longer range components of the noise would remain. The noise level (especially as measured by the maximum deviation) is seen to drop with averaging, but a surprising amount of grain noise is not eliminated. Although the standard deviations for electron microscope film (about ± 0. 004 OD) are much lower than for x-ray film (about ± 0. 03 OD) when no averaging has been performed, the relative improvement in the noise level after averaging is similar for the two films. The implication of this result is that superposition techniques used in image enhancement and radial integration techniques used in processing low-angle x-ray films have limited effectiveness in reducing noise.

Single Crystal X-ray Data Collection

The setup, centering, and least-squares process can be accomplished in less than five minutes using the software provided by Syntex. The rate at which individual reflections could be densitometered varied from two to seven seconds per reflection. Sixteen spots of four different average OD's were measured 100 times each using

the same orientation matrix. (The matrix was calculated once at the start of the test using the software described in the Experimental Section.) The individual calculated intensities ($I_j(k)$) for each reflection were compared with the average intensity for that reflection ($\bar{I}(k)$) as a residual R_1:

$$R_1 = \frac{\sum_{j=1}^{100} |I_j(k) - \bar{I}(k)|}{\sum_{j=1}^{100} |I_j(k)|}$$

R_1 was then averaged over the four reflections of similar intensity. The results are summarized in Table II. The reproducibility varied from 0.45% to 0.8% for reflections with average OD's greater than 0.2 OD above backgrounds and rose to 4% when an equivalent area of the film containing a systematically absent reflection was similarly treated. This increase in percent error can be ascribed to film grain noise since the film grains being measured are on the order of 0.1 μ and are much smaller than either the positional precision of the scanner or the spot size.

Symmetry related reflections on the same film were compared using R_{sym} (Arndt et al., 1968):

$$R_{sym} = \frac{\sum_{i}^{sym} |I_i(h) - \bar{I}(h)|}{\sum_{i}^{sym} |I_i(h)|}$$

The results of the best film and of typical films are compared with published results derived from precession data collected on other scanners (see Table III).

Discussion

The Syntex AD-1 has been found to have an average error in position of less than 1.5 μ in each dimension. It has a spatial resolution limited only by the light spot chosen (as small as 10 μ x 10 μ). No nonlinearity of the light sensing circuitry could be measured above the electronic noise level,and the variations in OD due to electronic noise increased logarithmically with OD as would be expected since the digital electronics were linear in transmittance. The 2σ noise level was ±0.002 OD at a measured OD of 0 increasing to only ±0.04 OD at OD 2. With appropriate precautions, there were no limitations placed on the use of the scanner for Fourier image analysis using any spot size.

The instrument exhibited excellent long-term (hours to days) stability even with wide temperature fluctuations. The one notable problem with the scanner occurred only when scanning long stretches of high optical density film (ψ OD > 2). Under these conditions the

photomultiplier sensitivity changed as much as 5% during the scan.

The noise properties of the films examined (Table I) varied widely. The higher sensitivity films such as Royal Pan and x-ray film had far higher film grain noise than the lower sensitivity films such as Type 4127 or electron microscope film. The measured film noise can be used to set reliability limits on digitized data collected using these films.

The measurement of intensities from single crystal x-ray films requires both accuracy in positional and density measurements. Several researchers (Arndt et al., 1968; Xuong, 1969; Matthews et al., 1972; Nockolds and Kretsinger, 1970) have described results from both flying spot and drum autodensitometers when used for this purpose. These instruments collect data at the rate of about 0.5 to 0.6 seconds per reflection. Peak OD's of reflections of up to 1.2 (Arndt et al., 1968) can be used with the flying spot densitometer; Matthews et al. (1972) found that OD's of up to 2.5 could be accommodated with application of appropriate corrections for film non-linearity. Data collected on the AD-1 scanner had equivalent or better precision than the above mentioned instruments (see Tables II and III) with a data collection speed of two to seven seconds per reflection and a setup time of less than five minutes per film.

In conclusion, the AD-1 proved to be a satisfactory instrument

for use in collecting single crystal data from x-ray films. It is also capable of the positional and electronic precision necessary in more exacting applications such as digitizing electron micrographs.

References

Abrahamsson , S. (1966). J. Sci. Instr. 43, 931-933.

Andrews, H. C., Computer Techniques in Image Processing, p. 37. Academic Press, New York, 1970.

Arndt, U. W., Champness, J. N., Phizackerley, R. P., and Wonnacott, A. J. (1973). J. App. Crystallogr. 6, 457-463.

Arndt, U. W., Crowther, R. A., and Mallet, J. F. W. (1968). J. Phys. E. 1, 510-517.

Billingsley, F. C. (1971). Adv. in Opt. and Elect. Micros. 4, 127-159.

DeRosier, D. J. and Moore, P. B. (1970). J. Mol. Biol. 52, 355-369.

Drenth, J., Kloosterman, D., van der Woude, J., Croon, H. C., and van Zwet, L. C. M. (1965). J. Sci. Instr. 42, 222-224.

Matthews, B. W., Klopfenstein, C. E. and Colman, P. M. (1972). J. Phys. E. 5, 353-359.

Morimoto, H. and Uyeda, R. (1963). Acta Crystallogr. 16, 1107-1119.

Nathan, R. (1971). Adv. in Opt. and Elect. Micros. 4, 85-126.

Nockolds, C.E. and Kretsinger, R.H. (1970). J. Phys. E. 3, 842-846.

Perrin, F.H. (1960). J. of the SMPTE 69, 239-249.

Ross, M.J., Klymkowsky, M.W., Agard, D.A., and Stroud, R.M. (1976)--submitted to J. Mol. Biol.

Unwin, P.N.T. and Henderson, R. (1975). J. Mol. Biol. 94, 425-440.

Waser, J. (1951). Rev. Sci. Instru. 22, 563-568.

Werner, P.E. (1970). Acta Crystallogr. A26, 489-491.

Wooster, W.A. (1964). Acta Crystallogr. 17, 878-882.

Wooster, W.A. and Fasham, F.A.L. (1958). J. Sci. Instr. 35, 153-156.

Xuong, Ng.-H. (1969). J. Phys. E. 2, 485-489.

TABLE I

Film Grain Noise

Film	Deviation (OD) Maximum	Standard
High Contrast Lantern Slide Plates[*a]	0.15	0.0011
Electron Microscope Film[*a]	0.08 - 0.26	0.0056
Electron Microscope Film[*d]	0.07 - 0.31	0.0056
Type 4127 Commercial Film[*a]	0.14	0.010
Type 4125 Copy Film[*a]	0.069	0.014
Plus-X Pan[*a]	0.11	0.019
Royal Pan[*a]	0.17	0.025
Cronex X-ray Film[†a]	0.39	0.040
No-Screen X-ray Film[*a]	0.29	0.044
No-Screen X-ray Film[*b]	0.17	0.013
No-Screen X-ray Film[*c]	0.078	0.012

---

[*] Eastman Kodak

[†] E. I. DuPont

[a] 32 μ x 32 μ spot

[b] 109 μ x 55 μ spot

[c] 219 μ x 109 μ spot

[d] 10 μ x 10 μ spot

TABLE II

Reproducibility of the measurement of single crystal diffraction data from the same film.

Reflection Strength	R_1*
Weak† (0.2 OD)	0.8 %
Intermediate† (0.8 OD)	0.45%
Strong† (2.0 OD)	0.5 %
No reflection† (0 OD)	4.0 %
Entire film‡ (All reflections >2σ above noise)	3.2 %

*R_1 as defined in the text.

†Same orientation matrix.

‡New orientation matrices calculated for each of five measurements of the same film.

TABLE III

Comparison of symmetry-related reflections

R_{sym}*	Maximum OD	Scanner Type
5.1%	1.2	Flying spot[a]
6.0%	2.0	Rotating drum[b]
4.4% (typical film)	2.5	Rotating drum[c]
3.6% (best film)	2.5	Rotating drum[c]
4.3% (typical film)	2.3	Flatbed[d]
2.0% (best film)	2.3	Flatbed[d]

*R_{sym} as defined in the text.

[a]Arndt et al. (1968).

[b]Xuong (1969).

[c]Matthews et al. (1972).

[d]This work.

Figure Captions

FIGURE 1. Single crystal spot scan. The figure shows the positions of the optical densities (X10,000) which were collected around a typical strong reflection. The interior of the circled area was used for intensity integration and the surrounding area for background estimation. Data are from a scan of a 17° precession (h0ℓ layer) x-ray diffraction photograph of trypsinogen. This scan was collected using the assembly language software.

FIGURE 2. Analysis of the area-scans of rulings (black-white) at various spatial frequencies. The scanner light spot size was 32 μ x 32 μ. A decrease in scanner response can be noted as the ruling spatial frequency is increased.

a) Gray-level histograms show the number of pixels (OD measurements) present in the image at each optical density. 1σ and 2σ levels are noted on the histograms.

b) Linear integrations of the digitized images show image degradation as the frequency is increased.

c) Halftoned images are examined to check for fidelity of the digitized image.

FIGURE 3. Sine-wave response test. Normalized 2σ deviations from gray-level histograms (Figure 2a) are plotted as a function of the ruling frequency in cycles/mm. The width of each stripe (black or clear) on the rulings is half of the spatial frequency of the rulings. The data for resolution in both the horizontal (x-axis) and vertical (y-axis) direction are plotted for each of the spot sizes. The following symbols are used: □ = 219 μ x 219 μ spot; + = 109 μ x 55 μ spot; ○ = 32 μ x 32 μ spot; ● = 10 μ x 10 μ spot. The scanner response was also measured with the 10 μ x 10 μ light spot using the receiving aperture normally used with the 32 μ x 32 μ spot (△).

FIGURE 4. Electronic noise. Deviations from the median ψOD are plotted as a function of ψOD: ○ = maximum deviation from the median; □ = 2 standard deviations from the median; ● = 1 standard deviation from the median.

FIGURE 5. Halftoned two-dimensional Fourier transform scanner noise displayed 100x normal image intensity to accentuate the pattern. The vertical axes on these plots correspond to the transformed x-axis of the scanner, and the horizontal axis to the y-axis. Frequency in $[\text{scan area}]^{-1}$ is noted in the Figure.

a) The 10 μ light spot and receiving aperture was used. The

horizontal line at zero frequency is due to variations of the average OD of each scan from changes in the reference reading; other lines are due to vibration resonances and only appear when the smallest aperture is used.

b) 10 μ light spot, 32 μ receiving aperture. Reference and dark current readings were held constant for the OD calculations. Note the disappearance of most of the lines caused by vibration and also the zero order term in x.

FIGURE 6. Photomultiplier fatigue. The average OD for scans down a glass OD wedge (higher to lower OD) were subtracted from the average OD for scans up the same wedge. The resulting hysteresis is plotted vs. the average ψ OD of the wedge. The photomultiplier sensitivity is shown to change during the y-scans.

FIGURE 7. Linearity: oblique scan of a razor blade. The razor blade was placed at an angle of ~ 0.5° to the y-axis.

a) The resulting scan was plotted as counts (transmittance) vs. position.

b) The linear portion of a) was fitted to a least-squares line and the difference between the observed data and the line was plotted.

FIGURE 8. Linearity: scan of an OD wedge. The wedge was scanned with different starting ψ OD's. Twenty scans were averaged for each graph. All graphs are of the same section of wedge using the 219 μ x 109 μ spot.

a) Low average OD. Note the low overall noise level.

b) Same as a) with least-squares line subtracted.

c) High average OD. Note the higher average noise level.

d) Same as c) with least-squares line subtracted.

FIGURE 9. Effect of data averaging on film noise. Unexposed films and the resulting density array reduced in size by averaging neighboring pixels. Noise (deviation from median OD of the film) is plotted as a function of $\sqrt{\text{reduction ratio}}$ where reduction ratio = image area before averaging/image area after averaging. ● = maximum deviation for Kodak no-screen x-ray film; ○ = standard deviation for Kodak no-screen x-ray film; + = maximum deviation for Kodak electron micrograph film; vertical scale is at the left of the figure. □ = standard deviation for electron microscope film; vertical scale is at the left of the figure for these data only. Spot size was 32 μ x 32 μ for all data.

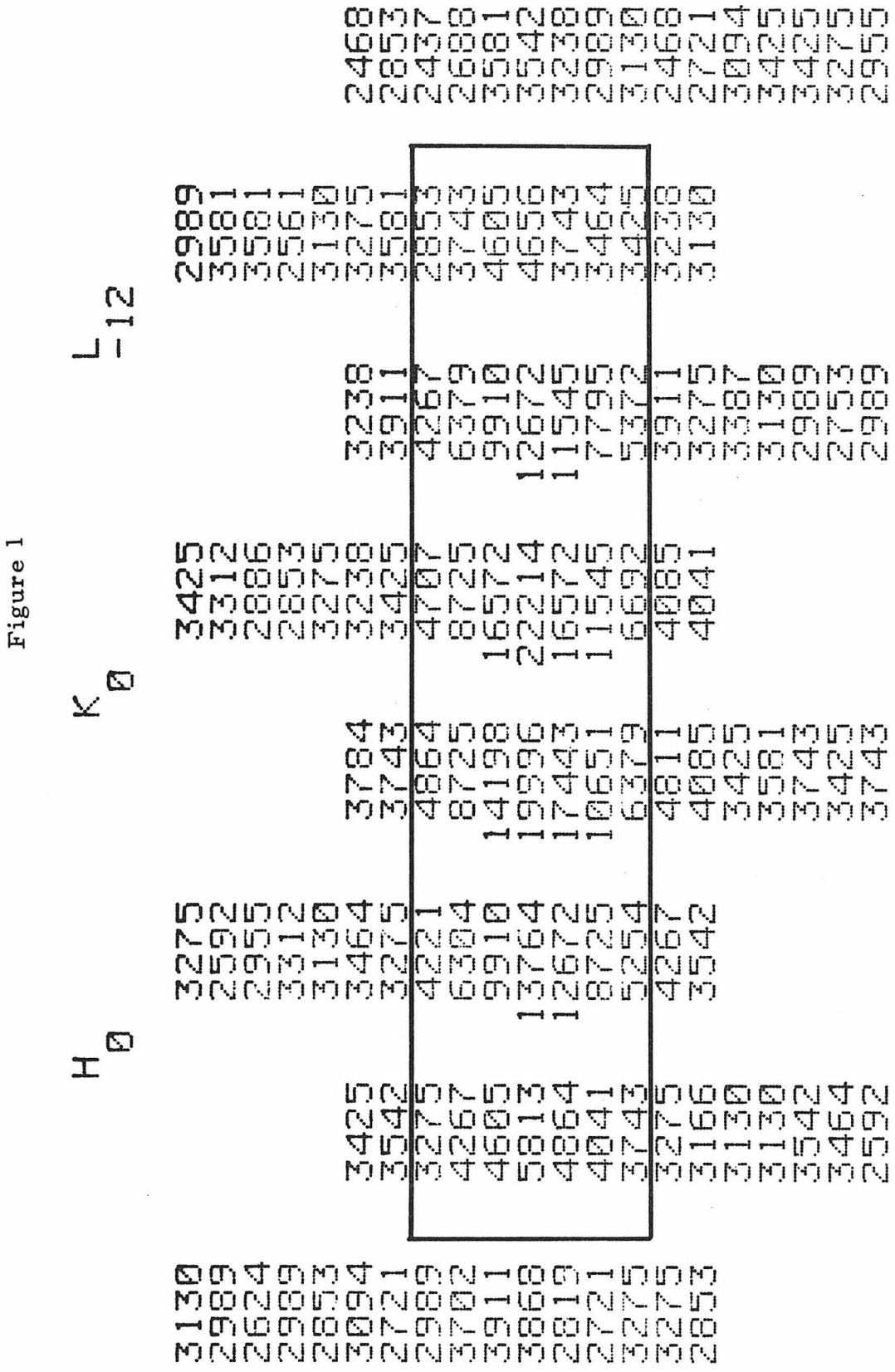

Figure 1

Figure 2

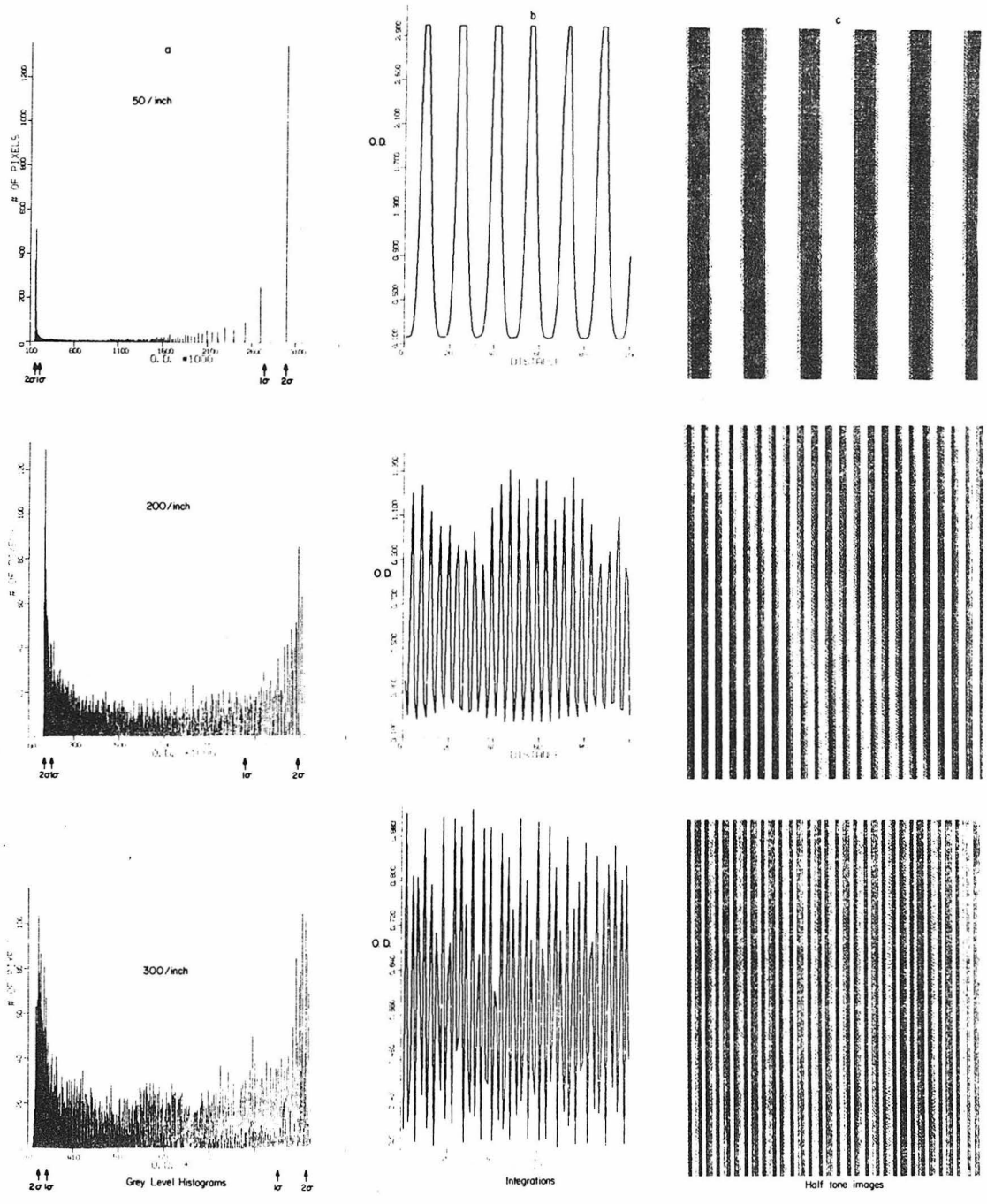
a
50 / inch
OF PIXELS
O.D. ×1000
2σ 1σ
1σ
2σ
b
O.D.
c
200/inch
300/inch
Grey Level Histograms
Integrations
Half tone images

Figure 3

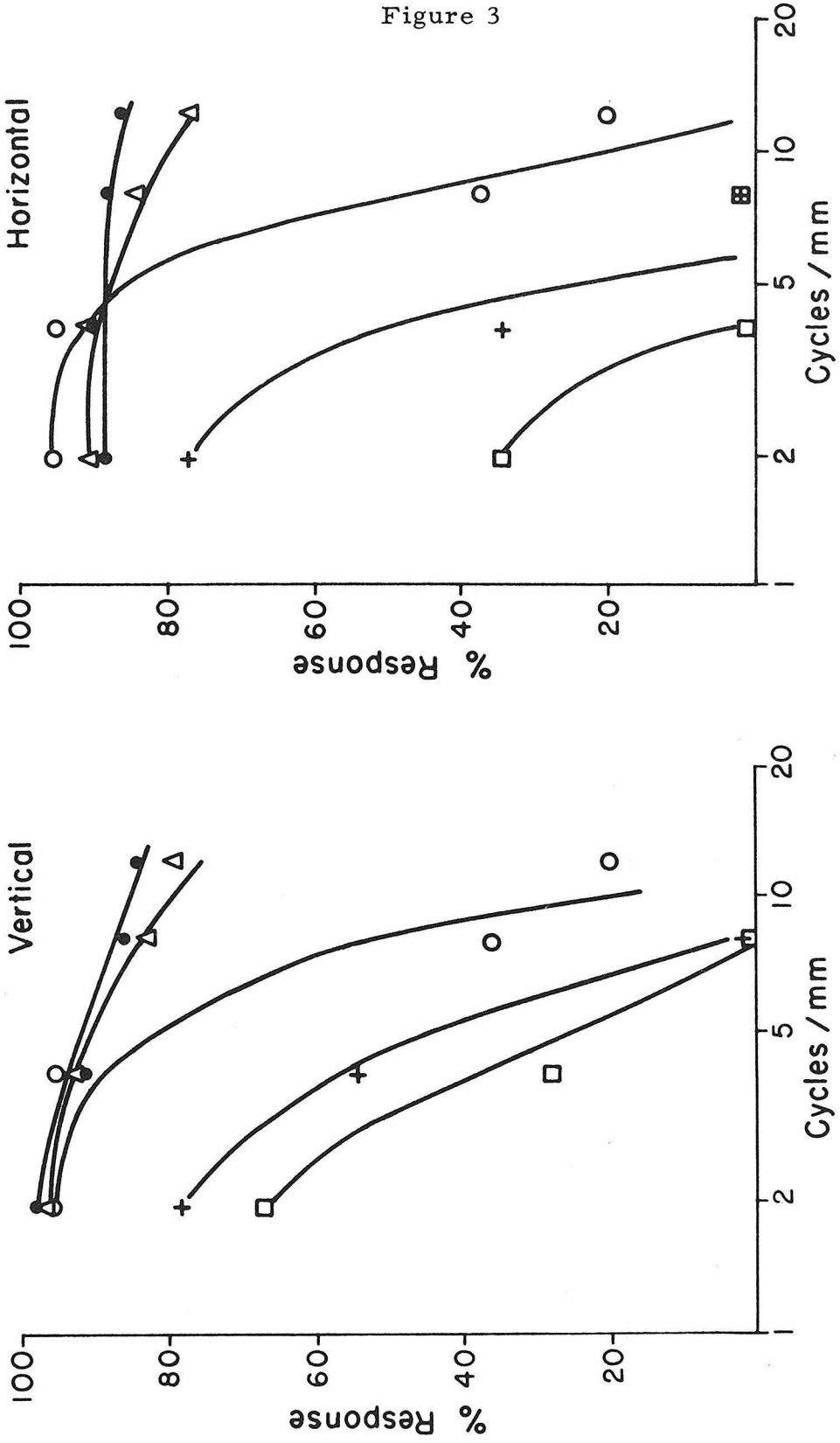
Horizontal
Vertical
% Response
Cycles / mm
100
80
60
40
20
1
2
5
10
20

Figure 4

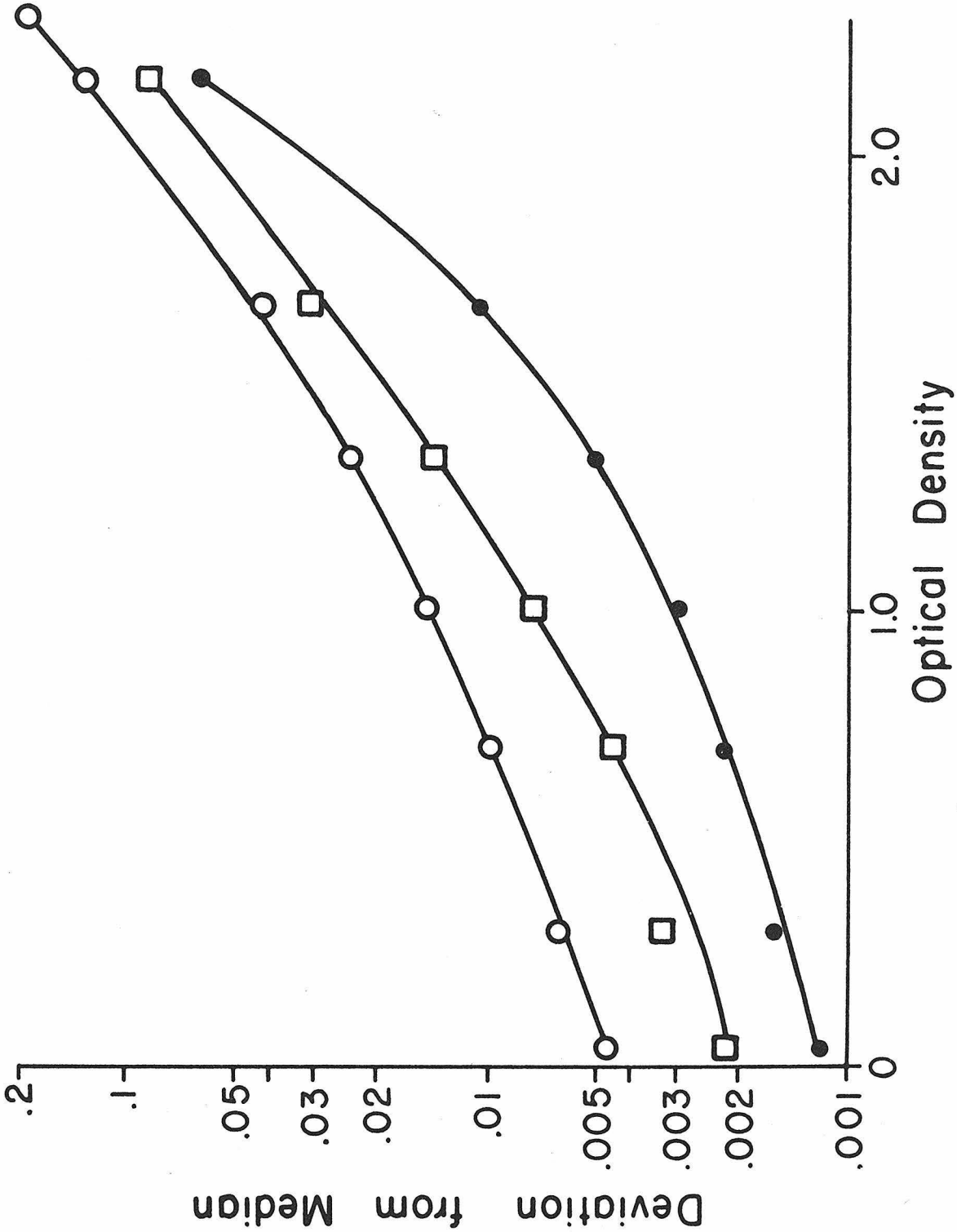
Deviation from Median
.2
.1
.05
.03
.02
.01
.005
.003
.002
.001
0
1.0
2.0
Optical Density

Figure 5

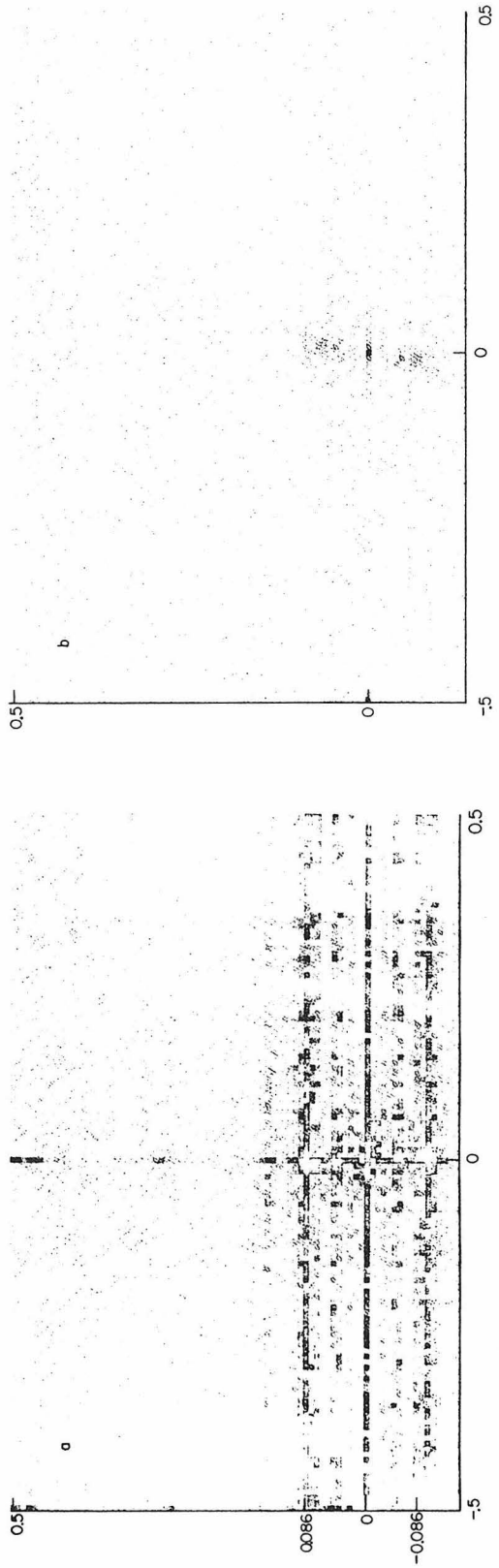

Figure 6

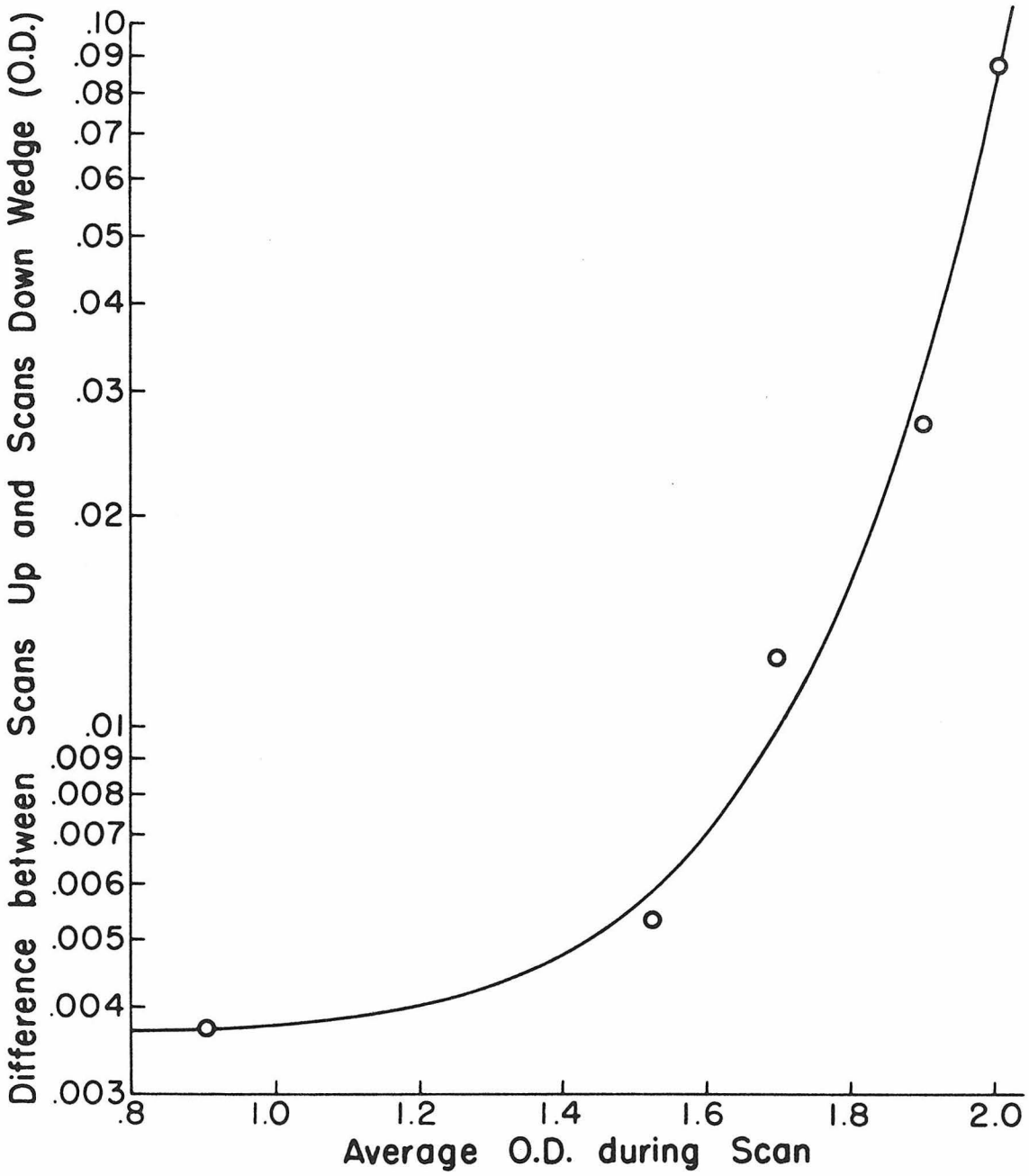
Difference between Scans Up and Scans Down Wedge (O.D.)
.10
.09
.08
.07
.06
.05
.04
.03
.02
.01
.009
.008
.007
.006
.005
.004
.003
.8
1.0
1.2
1.4
1.6
1.8
2.0
Average O.D. during Scan

Figure 7

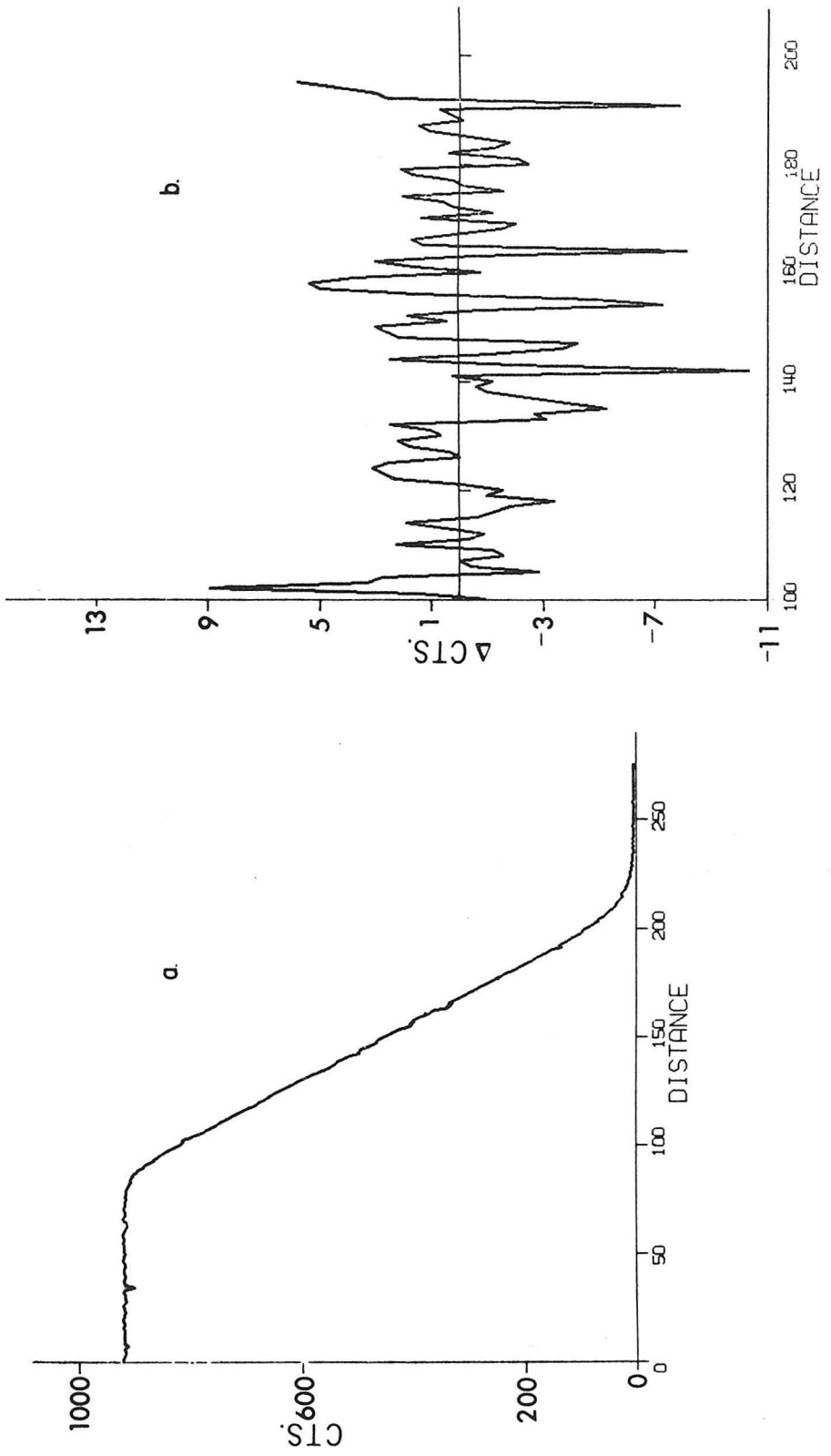
a.
CTS.
1000
600
200
0
0
50
100
150
200
250
DISTANCE
b.
ΔCTS.
13
9
5
1
-3
-7
-11
100
120
140
160
180
200
DISTANCE

Figure 8

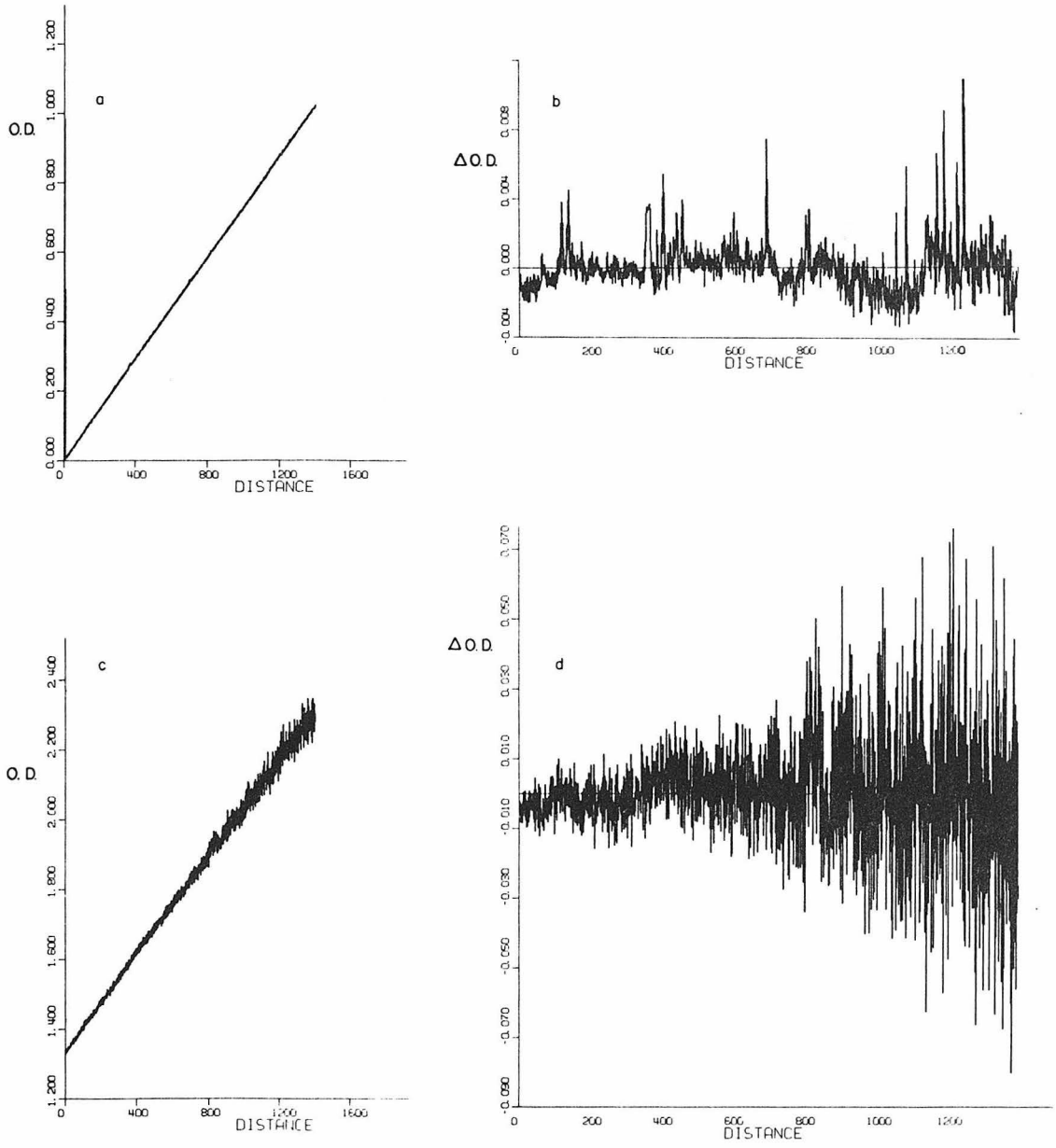
a
O.D.
1.200
1.000
0.800
0.600
0.400
0.200
0.000
0
400
800
1200
1600
DISTANCE
b
ΔO.D.
0.008
0.004
0.000
-0.004
0
200
400
600
800
1000
1200
DISTANCE
c
O. D.
2.400
2.200
2.000
1.800
1.600
1.400
1.200
0
400
800
1200
1600
DISTANCE
d
ΔO.D.
0.070
0.050
0.030
0.010
-0.010
-0.030
-0.050
-0.070
-0.090
0
200
400
600
800
1000
1200
DISTANCE

Figure 9

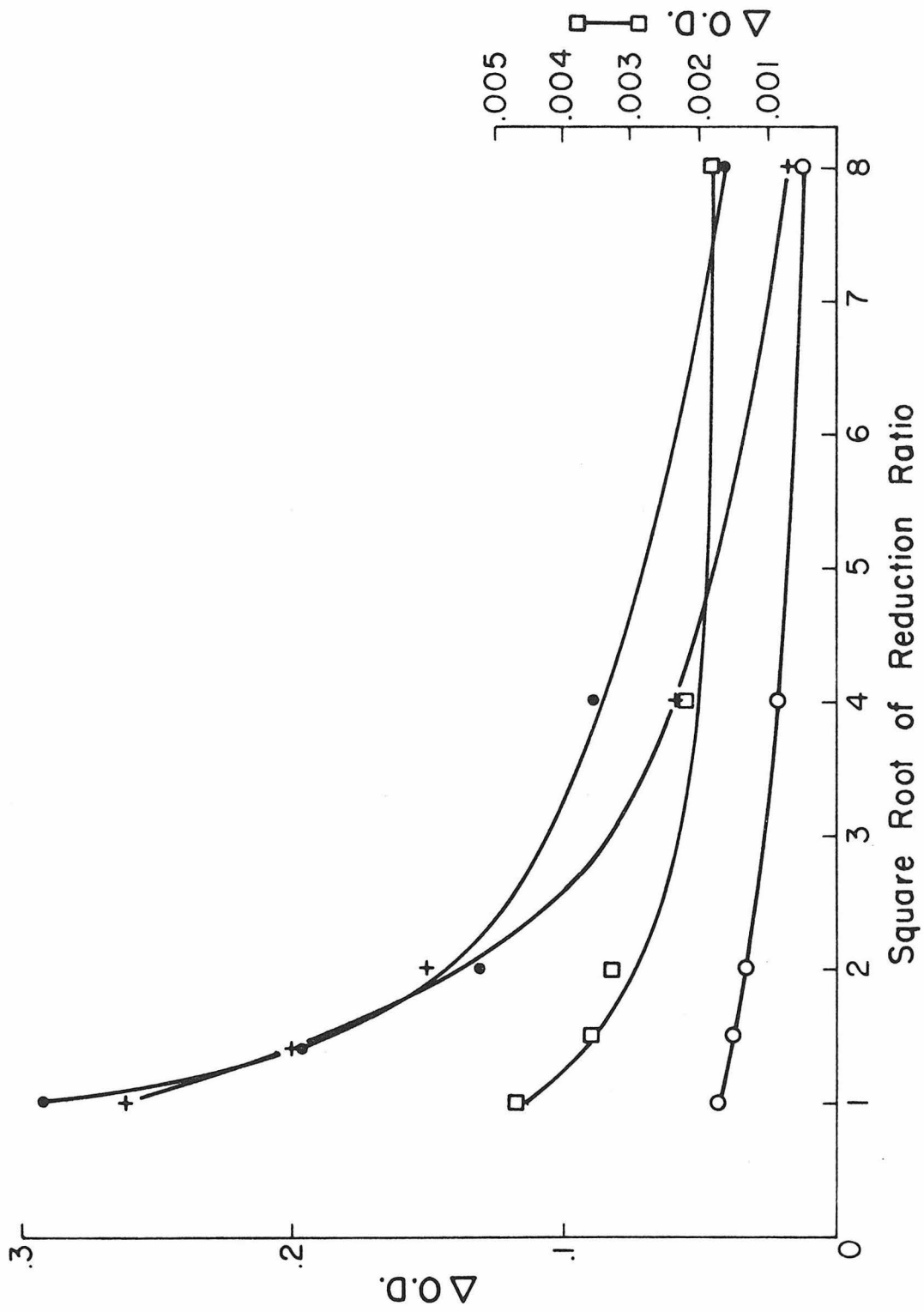
Δ O.D.
.3
.2
.1
0
1
2
3
4
5
6
7
8
Square Root of Reduction Ratio
Δ O.D.
.005
.004
.003
.002
.001

APPENDIX D

Observation of an Extended Lattice Structure in Membrane Fragments Rich in an Acetylcholine Receptor from Torpedo californica

M. W. Klymkowsky, M. J. Ross, and R. M. Stroud

Submitted to J. Mol. Biol

Observation of an Extended Lattice Structure in Membrane Fragments Rich in an Acetylcholine Receptor from Torpedo californica

MICHAEL W. KLYMKOWSKY, MICHAEL J. ROSS

AND ROBERT M. STROUD

Norman W. Church Laboratory of Chemical Biology
California Institute of Technology
Pasadena, California 91125, U.S.A.

J. Mol. Biol.

RUNNING TITLE: Lattice Structure of an Acetylcholine Receptor

Abstract

An extended lattice structure has been observed in membrane fragments rich in acetylcholine receptor from the electroplax organs of the species Torpedo californica and Narcine brasiliensis. The lattices were observed by electron microscopy of negatively stained samples. They were found only in membrane sheets, and not in vesicles, which contained closely packed receptor molecules instead. Membrane sheets containing arrays were always found in multilayered assemblies in which each layer contained a lattice structure. The lattice is oblique with cell dimensions of about $\underline{a} = 90.8 \pm 4.1$ Å, $\underline{b} = 91.3 \pm 4.3$ Å, $\gamma = 117.7° \pm 4.1°$ ($d = 93.9 \pm 2.7$ Å)[1] (calculated using the nominal magnification of the electron microscope).

---

[1] d refers to the diagonal of the unit cell ($\underline{d} = \underline{a} + \underline{b}$).

1. Introduction

Membranes containing acetylcholine receptor (AcChR) can be prepared from homogenates of the electric tissue of various species of the electric skates or eels: Torpedo, Narcine and Electrophorus (O'Brien and Gilmour, 1969). It has since been shown that membrane fragments highly enriched in AcChR can be separated from membranes containing acetylcholine esterase (Cohen et al. 1972; Duguid and Raftery, 1973), or ATPase activities (Duguid and Raftery, 1973) from the same source by sucrose gradient centrifugation. Since each of the three activities are localized at nerve synapses within the cells of the electric organ, their separability as membrane fragments has led to the suggestion that the different proteins are localized in different regions of the post-synaptic membrane (Cohen et al. 1972; Duguid and Raftery, 1973). Electron microscopy of the receptor-rich membrane fragments has shown them to contain particles of average diameter ~90 Å. The particles generally contain a central stain-filled pit (Cartaud et al., 1973; Nickel and Potter, 1973; Raftery et al., 1974). Limited regions of lattice structure have been observed in AcChr membrane fragments from Torpedo marmorata by freeze-etch electron microscopy (Cartaud et al., 1973); however, no

reports of extended lattice structures have appeared in the literature.

We have observed large ordered arrays of AcChR in membranes and attempted to define optimal conditions for their visualization. We have characterized the acetylcholine receptor arrays seen in negatively stained specimens by electron microscopy. The arrayed distribution of receptor molecules in membranes allows for use of image reconstruction methods (Ross et al., 1976).

2. Materials and Methods

a. Membrane preparation and preservation

Membrane fragments enriched in AcChR were prepared and biochemically characterized by M. A. Raftery, R. Vandlen and collaborators by the methods of Reed et al. (1975). Care was taken to minimize proteolytic degradation and lipid oxidation (Vandlen and Raftery, 1976). Samples received after homogenization and sucrose gradient separation had typical protein concentrations of 1-5 mg/ml (as determined by the methods of Lowry et al. 1951) and specific α-Bungarotoxin binding values (Q ≡ nmoles α-Bungarotoxin/mg protein) in the range of 10 to 70 (Schmidt and Raftery, 1973). Samples were prepared in either 10 mM sodium phosphate or Torpedo

Ringers (250 mM NaCl, 5 mM KCl, 4 mM $CaCl_2$, 2 mM $MgCl_2$, 5 mM Tris-HCl), both at pH 7.4.

b. Negative stains

The following electron dense negative stains were tested: uranyl acetate ($U(OAc)_2$), pH 4.8 to 6.5, uranyl oxylate, pH 5 to 6, uranyl formate, pH 6 to 7, phosphotungstic acid (PTA), pH 4 to 8, and ammonium molybdate, pH 5 to 7.

A 1% solution of uranyl acetate (pH 4.8) was prepared in deionized distilled water and stored in the dark until used. The $U(OAc)_2$ was filtered through a 0.45 μ millipore filter immediately before use. For use at pH's higher than 4.8, a plastic weighing dish was placed on ice and 0.5 ml each of 1% $U(OAc)_2$ and 0.1 M NH_4OH were placed in opposite corners of the dish. NH_4OH was slowly mixed into the $U(OAc)_2$ with a glass rod and the pH monitored with pH paper. When the pH reached 6.0 to 6.5, the stain was used within one minute (modification of the technique of J. P. Revel, personal communication). If the stain precipitated, the dish was discarded and the procedure repeated.

A 1-2% solution of phosphotungstic acid was made in deionized distilled water. The pH of the solution was brought to the desired value by adding dilute NaOH. PTA stain was used at pH 5.4, 6.5,

7.0, and 7.4.

c. Carbon-coated grids

Thin carbon films (100–200 Å thick) were made by evaporation onto freshly cleaved mica surfaces. To prepare grids, the carbon film was floated off onto a water surface. The surface had been previously cleaned by placing a drop of parlodion dissolved in amyl acetate on the water. The parlodion spread across the water surface and polymerized, providing a dust-free surface when removed. The water level was then lowered and the carbon film gently dropped onto 400-mesh copper electron microscope grids. After drying, the grids were stored until use. Immediately before use, the coated grids were cleaned by dipping into 100% ethanol, and dried by placing them, carbon side up, on filter paper. Ethanol cleaning removed contaminants from the carbon, and provided a surface of decreased hydrophobicity without the conventional electrostatic charging.

d. Microscopy

Electron microscopy was carried out on Phillips EM 201c, 300, and 301 transmission electron microscopes. All three were equipped with anti-contamination stages which were used routinely. Both the 300 and 301 have double-condenser illumination systems.

In addition, the 301 was equipped with a goniometer stage. The accelerating voltage was either 100 kV or 80 kV. Accurate measurement of magnification (e.g., by measurement of repeat spacings in catalase crystals) was not routinely carried out. Errors in estimates of magnification may be expected to be as large as ±5% (Phillips Electronic Instruments), although actual errors are probably smaller.

Micrographs were recorded on Kodak electron microscope film or Kodak electron image plates. Development was in Kodak D-19 (for film) or Kodak HRP (for plates) as per manufacturer's directions. Developing time was five minutes for each with continuous agitation.

Grids were initially scanned at low magnification (20,000x nominal). When a promising area was located the magnification was stepped up to 100,000x (nominal), the image focused to maximum contrast (~900 Å under focus) within one or two seconds, and immediately imaged on film. Minimum beam current consistent with efficient operation by a dark-adapted operator was used at all times in order to minimize beam exposure and stain migration (Unwin, 1974; 1975).

A major effort went into determining optimal conditions for observing AcChR membrane fragments by negative stain microscopy. A wide range of dilution buffers was tested, including; i) 10 mM

phosphate at pH 7.4; ii) Torpedo Ringers at pH 5-8; iii) 10 mM $CaCl_2$ and 5 mM $MgCl_2$ at pH 6 and 7; and iv) 10 mM EDTA at pH 7. The effect of 1% dextrose added to these buffers was examined, as it had been reported effective in preserving biological structures during dehydration (Unwin and Henderson, 1975). After dilution into buffer, the samples were stored for various lengths of time at both room temperature and 4°C. The effects of cholinergic agonists and antagonists (carbamylcholine, 10 mM, and curare, 10 mM) were also tested by addition to diluted samples.

For microscopy, a 20 µl drop of the sample solution was applied to a cleaned carbon grid, and allowed to stand for about 30 seconds. Sample was removed with a torn piece of filter paper touched to the edge of the grid. A 20 µl drop of negative stain solution was applied, allowed to stand for 30 seconds, removed as above, and allowed to dry completely in air. Grids were examined immediately after drying.

e. Image analysis

Micrograph negatives were densitometered and fast Fourier transformed using software developed by one of us (MJR) and described in the accompanying paper (Ross et al. 1976). Preliminary analysis was done with a laser optical diffractometer, and recorded

on Polaroid Type 55 P/N film. The optical diffractometer was built after the design of Markham (1968).

3. Results

a. Electron microscopy

When visualized in the electron microscope, the membrane fragments containing acetylcholine receptor typically occurred as vesicles several microns across (Plate I). The vesicles were often highly irregular in shape, puckered and folded (Plate Ib). Acetylcholine receptor molecules were reasonably close-packed within the "receptor-rich" fraction, and were generally scattered in random orientations throughout the vesicles. Similar observations were made by Reed et al. (1975) for AcChR membranes from the same source, and by Cartaud et al. (1973) and by Nickel and Potter (1973) for AcChR membranes isolated from Torpedo marmarota, and Electrophorus electricus. Each receptor appeared as an irregular "doughnut-like" structure of diameter about 80 - 90 Å. AcChR-rich membranes from the electric organ of the related species Narcine brasiliensis showed very similar structures (Plate Ic).

The stain density in the center of isolated molecules (as defined by densitometry of the images) was often about the same as that

immediately surrounding the isolated molecules; this suggests that the region in the center of the molecule, which is inaccessible to the stain, is about the same thickness as the phospholipid bilayer alone (see Plate Ic).

Electron micrographs of negatively stained preparations of isolated receptor molecules, obtained after solubilization by detergent, revealed a similar stain-filled depression in the surface (D. J. Kent and R. M. Stroud, 1974, unpublished results; Meunier et al., 1974).

The receptor molecules are readily identified in all preparations, and with all procedures outlined in the previous section. These structures are quite different in appearance from those seen in membrane fractions rich in acetylcholine esterase from the same source (Reed et al., 1975).

In some cases the membrane fragments were sheets rather than vesicles, and it was only in these sheets that large areas of organized lattice structure were observed (Plate II). These areas can extend for over 10,000 Å in each direction and contain as many as 10^4 molecules in a single array. The ordered arrays were always found in multilayers, although overlap of the layers was often incomplete, thereby allowing single arrayed sheets to be discerned (Plate IIIb).

The lattices in the Plates are best viewed by tilting the page to

look obliquely down rows of molecules. By rotating the page, the lattices in different layers can be resolved. The lattice lines were not always completely straight and had a tendency to bend slightly over long distances. In addition it was noted that ordering due to intermolecular association is generally somewhat better in one close contact direction than in the other two. In rare cases fragmented patches are seen, and isolated molecules can be seen alongside or in between the ordered domains (Plate IIIa).

b. Multilayered arrays

Each multilayered membrane area contains a region of moiré pattern of varying extent. Such patterns are caused by the superposition of different lattices (Plate IVa). The presence of the moiré patterns indicates that the negative stain penetrates the multilayered assembly, and is fixed on at least one side of each sheet. These lattices are easily separated by Fourier transformation (see Plate IVb).

In view of the rather low frequency with which lattices are seen, it was surprising to find that the multilayered arrays always contained ordered domains within each sheet rather than a statistically determined assembly of ordered and disordered layers.

This raises the question of whether one membrane sheet forms

a particularly favorable substrate for the buildup of subsequent layers. If this were the case, we might have expected to find some tendency toward orientation of the adjacent layers. This possibility was analyzed by inspection of optical diffraction patterns generated from regions of the micrographs, or by analysis of computed Fourier transforms of densitometered images.

The optical diffraction pattern generated from a part of the image shown in Plate Va (containing only a single sheet) is shown in Plate Vb, and schematized in Figure 1. The patterns indicate that the two-dimensional lattices are oblique, and fall into one of two possible two-dimensional space groups, p1 or p2. (Based on analysis of the phases of reflections, the lattice was identified as p1 (Ross et al., 1976).) The reflections in the diffraction pattern were indexed on a common scheme such that the (10) reflection was the largest first-order intensity. The (01) reflection was the second largest first-order intensity, and was chosen to make the included angle (γ^*) between the a* and b* axial directions acute. The same indexing scheme was applied to computed diffraction patterns generated by Fourier transformation of densitometered arrays (Ross et al., 1976).

When the moiré patterned areas were transformed there was no detectable correspondence between the angular orientation of one

lattice and its neighbor. This argues against any tendency for ordering in the third dimension, i. e. between one layer and the next.

The facts that; i) the lattice is oblique, and ii) relative intensities of the first-order maxima (10), (01) and $(1\bar{1})$ are quite different, allow definition of the relative sidedness of each layer. By these criteria there was no uniform correspondence between one layer and the next in terms of which "way up" they were in multilayers of arrayed sheets. Thus, it would seem that ordered membrane sheets have a tendency to stick together, but that interactions between one sheet and the next tend to be nonspecific.

c. Characterization of the lattices

Numerous images of arrayed structures were digitized and Fourier transformed; the computed transforms were inspected for maxima which lay on a two-dimensional lattice. The lattice parameters for each transform of a particular image were refined by a weighted least-squares minimization of the distance between calculated reciprocal lattice points, and the maxima in the transform of the image. Indexing of the reciprocal lattice was as described above.

Since the absolute magnification of each micrograph was not routinely calibrated at the time each image was recorded, there will be a somewhat different scale factor, k ($\simeq 0.95 - 1.05$), which should

be applied to the lattice dimensions from all regions of the same micrograph. Within one micrograph however, the magnification is assumed to be constant, and therefore lattice parameters for different sheets, or for different regions of each micrograph, give an estimate of the variation in lattice constants as well as nonlinearity in recording techniques.

Lattice constants were determined for a number of arrayed areas (Table I). The table also includes averaged values and standard deviations for different arrays taken from the same micrograph. As an example, the cell dimensions for four different regions (containing about 100 unit cells each) of the lattices shown in Plate V are described by: $a = 90.9 \pm 2.4$ Å, $b = 91.7 \pm 2.6$ Å, ($d = 93.0 \pm 0.6$ Å), $\gamma = 118.8 \pm 1.8°$. (Lattice parameters and intensities of first-order maxima in several specimens are included in Table I. Standard deviations were computed using

$$\sigma = \left(\frac{\Sigma_1^n (x - \bar{x})^2}{n - 1} \right) .$$

Thus there is a variation of 1-3% in these lattice parameters. The area of the two-dimensional cell was 7301 ± 216 Å^2, i.e. the standard deviation in calculated area was about 3.0%. Differences in the lattice parameters are presumed to be due to either; i) real

differences in the lattice structure observed, or ii) errors in the choice of weighted centers of the diffraction maxima due to the noise level, lattice distortion, or incomplete resolution of superimposed lattices in the transform. The calculated standard deviations in parameters from the least-squares matrix (due to ii) above) were typically 1-2½%.

The amplitudes $F_{(hk)}$ for each lattice were scaled by a constant factor to make $F_{(10)} + F_{(01)} + F_{(1\bar{1})} = 300$. After scaling, the consistency between one transform and the next was compared both by computing a crystallographic residual,

$$R = \frac{\Sigma F_{hk} - \overline{F}_{hk}}{\Sigma \overline{F}_{hk}} \quad \text{for } h = 0, 1;\ k = 0, 1$$

for n lattices from one micrograph, and by statistical analysis of the variation in each $F_{(hk)}$ amplitude. In some cases the residual indicated excellent agreement between transforms of different lattices. For example, R was 0.033 for the four lattices chosen from Plate Va and R was 0.005 for two superimposed images in one of the specimens treated with carbamylcholine (see Table I). In other cases, the agreement between equivalent reflections was poor (Table I).

We had wondered whether any possible change in lattice dimensions, lattice angles, or in the $F_{(hk)}$ amplitudes might be seen after

the membranes were treated with the cholinergic agonist, carbamylcholine, or the antagonist, curare. In view of the rather large deviations we observed in untreated specimens, this test is obviously insensitive. Nevertheless, the lattice parameters were not significantly different. The averaged cell dimensions for lattices from carbamylcholine-treated specimens were a = 90.7 ±5.3 Å, b = 91.8 ±5.6 Å, (d = 94.3 ± 3.5), and γ = 117.2 ±5.3°; and these are not significantly different from the lattice parameters for the four lattices (untreated with carbamylcholine) picked from Plate V (see above).

Likewise there was no significant change in amplitudes $|F_{hk}|$ between the agonist- or antagonist-treated and native membranes. The difference between one negatively stained specimen and the next, even after indexing based on the relative peak heights in the transform, was too great to allow for detection of anything short of a major reorganization of the structure.

d. Optimal conditions for observing lattice structures

Many different staining conditions were tried in an attempt to characterize an optimal system for imaging arrayed areas within samples from each preparation. Of the stains tested only 1% $U(OAc)_2$

(pH 4.8 and 6.5) and 1-2% PTA (pH 5.4 to 7.4) proved effective in visualizing the large arrays.

Pretreatment of the sample in different buffers or with dextrose as described in Materials and Methods, had no apparent effect on the frequency with which lattices were observed from a particular membrane preparation. Whether the organ had been freshly dissected or had been frozen and stored at -80°C prior to purification of membrane fragments seemed to have little effect if any on the number of arrayed areas which were seen.

The frequency with which lattice structures could be seen in different preparations varied from none to ten per 1000 membrane fragments. There was a high correlation between the number of lattices seen and the particular membrane preparation. Different samples from some preparations consistently had higher numbers of arrays, while samples from other preparations contained no arrayed structures at all.

For a particular preparation, the occurrence of lattice structures was highest immediately after isolation and declined with time after that, suggesting that arrayed structure was not induced by a process akin to crystallization, but tended to be inherent to the specimen. The number of ordered arrays also diminished rapidly as lipid oxidation increased. For this reason samples were routinely

stored under nitrogen or argon at 4°C.

4. Discussion

A lattice structure was observed in membrane fragments rich in acetylcholine receptor from two sources: Torpedo californica and Narcine brasiliensis. The lattices were always found in membrane sheets rather than vesicles, and indeed, the frequency with which they were found in membrane sheets was about one per five to ten membrane sheets examined. It may be that the curvature implied in a vesicle surface makes the lattice unstable, and that multilayer formation inhibits vesicle formation.

The presence of the lattice is important in that: i) It presents an assay for improvement in preparative conditions which favor the observation, preservation, or formation of arrayed structure. ii) The lattices permit analysis of the surface structure of the receptor molecules in the membrane by the use of image reconstruction methods (Ross et al., 1976). Structural changes induced by ligand binding or desensitization of the receptor for example, may be tested for although there are limitations implied in the use of these image reconstruction techniques at low resolution in a high noise environment. It may also be possible to localize the binding sites

for such macromolecular inhibitors as α-Bungarotoxin. iii) The lattices may permit structure analysis of the protein in unstained specimens at high resolution by use of the methods of Unwin and Henderson (1975). However, at present, the number of arrays found on any particular microscope grid is too small to permit analysis of unstained material using their methods.

Although the use of negative stain is extremely harsh treatment, it is currently the only way to develop enough contrast in the image for assay of the parameters affecting the lattice content of the samples.

The lattice is oblique, with one molecule per unit cell. This of itself implies that the receptor complex can have no more than two-fold symmetry. The two-dimensional lattice dimensions, when averaged by the above procedure,are not significantly different than those of a hexagonal lattice; however, the observed lattice angle was never 120°, and the intensities in the transform clearly indicate oblique symmetry. The lattice dimensions are not inconsistent with those found by freeze-etch microscopy (Cartaud et al. 1973) of AcChR membranes from Torpedo marmorata, although the lattice is not hexagonally symmetric as these authors suggested.

Similar methods were applied to electron micrographs taken by J. P. Revel of arrayed structures of gap junctions, isolated

from mouse liver cells. The lattices in this case were found to be of truly hexagonal or trigonal symmetry, as previously reported by Revel and Karnovsky (1967), and J. P. Revel, private communication.

It seems likely that the acetylcholine receptor may exist as an arrayed structure *in vivo*, since the rather harsh preparative conditions used are certainly not expected to be conducive to "crystallization" of the membrane-bound protein. This kind of organization *in vivo* might simply represent an energetically favorable system for concentrating receptor activity at the tips of post-synaptic membranes, or might be functionally important for molecule-molecule cooperativity (Levitski, 1974).

5. Acknowledgments

Initial preparation of membrane fragments from electric organs, through the initial sucrose density gradient separation step, was carried out by M. A. Raftery and his colleagues. We are particularly grateful to M. A. Raftery and R. Vandlen for help and advice, and also to J. P. Revel and P. F. Koen for advice and instruction in the use and applications of electron microscopy. We thank the Biology Division of the California Institute of Technology for use of electron microscopes and supporting facilities. This work was carried out

with the support of the National Institutes of Health grant No. GM-19984 and the National Science Foundation grant No. BMS75-04105 whose help is gratefully acknowledged. One of us (RMS) is the recipient of a National Institutes of Health Career Development Award, another (MJR) is the recipient of a National Institutes of Health Predoctoral Traineeship, and another (MWK) is the recipient of a California Foundation Fellowship for Biochemical Research. This is contribution No. 5355 from the Norman W. Church Laboratory of Chemical Biology, California Institute of Technology.

REFERENCES

Cartaud, J., Benedetti, E. L., Cohen, J. B., Meunier, J.-C., and Changeux, J.-P. (1973). FEBS Letters 33, 109-113.

Cohen, J. B., Weber, M., Huchet, M., and Changeux, J.-P. (1972). FEBS Letters 26, 43-47.

Duguid, J. R. and Raftery, M. A. (1973). Biochemistry 12, 3593-3597.

Levitski, A. (1974). J. Theor. Biol. 44, 367-372.

Lowry, O. B., Rosebrough, N. J., Farr, A. L., and Randall, R. J. (1951). J. Biol. Chem. 193, 265-275.

Markham, R. (1968). Meth. Virol. 4, 503-529.

Meunier, J.-C., Sealock, R., Olsen, R. and Changeux, J.-P. (1974). Eur. J. Bioch. 45, 371-394.

Nickel, E. and Potter, L. T. (1973). Brain Research 57, 508-517.

O'Brien, R. D. and Gilmour, L. P. (1969). Proc. Nat. Acad. Sci. USA 63, 496-503.

Raftery, M. A., Bode, J., Vandlen, R., Michaelson, D., Moody, T., Ross, M. J. and Stroud, R. M. (1974). FEBS Meeting [Proc.], 9th 24, 9-23.

Reed, K., Vandlen, R., Bode, J., Duguid, J., and Raftery, M. A. (1975). Arch. Biochem. Biophys. 167, 138-144.

Revel, J. P. and Karnovsky, M. J. (1967). J. Cell. Biol. 33, C7-C12.

Ross, M.J., Klymkowsky, M.W., Agard, D.A., and Stroud, R.M. (1976)--submitted to J. Mol. Biol.

Schmidt, J., and Raftery, M.A. (1973). Anal. Biochem. 52, 349-352.

Unwin, P.N.T. (1974). J. Mol. Biol. 87, 657-670.

Unwin, P.N.T. (1975). J. Mol. Biol. 98, 235-242.

Unwin, P.N.T. and Henderson, R. (1975). J. Mol. Biol. 94, 425-440.

Vandlen, R. and Raftery, M.A. (1976). Submitted to Biochemistry.

TABLE I. Lattice parameters[1] and amplitudes $F_{(hk)}$[2] for first-order diffraction maxima for several lattices.

Specimen	Stain	Form in Image[3]	$F_{(hk)}$ (10)	$F_{(hk)}$ (01)	$F_{(hk)}$ (1$\bar{1}$)	Cell Dimensions a (Å)	b (Å)	d (Å)[4]	γ (°)
Native	$U(OAc)_2$	M	116	105	79	90.4	91.5	92.3	119.0
			114	99	87	88.0	89.1	93.6	116.2
		M	110	103	87	91.5	95.2	93.3	120.1
			106	99	95	93.8	90.9	92.6	119.8
			111.5(4.4)	101.5(3.0)	87(6.5)	90.9(2.4)	91.7(2.6)	93.0(0.6)	118.8(1.8)
Native	PTA	S	125	105	74	90.7	90.1	94.4	117.1
Carbamyl-choline	PTA	M	124	96	80	90.5	101.5	92.9	122.7
			122	97	80	86.4	87.6	93.5	114.9
			123(1.4)	96.5(0.7)	80	88.5(2.9)	94.6(9.8)	93.2(0.4)	118.8(5.5)
Carbamyl-choline	PTA	S	126	92	83	90.1	87.6	98.8	112.3
Carbamyl-choline	PTA	S	110	104	86	88.7	85.8	93.3	115.3
			113	97	90	84.2	87.8	98.7	110.1
			109	103	88	100.0	95.3	94.5	122.3
			110.7(2.1)	101.3(3.8)	88(2.0)	91.0(8.1)	89.6(5.0)	95.5(2.8)	115.9(6.1)
Carbamyl-choline	PTA	S	120	92	88	94.8	90.1	88.6	122.8
						90.8(4.1)	91.0(4.3)	93.9(2.7)	117.7(4.1)

[1] Magnification of each micrograph was scaled so as to make the average unit cell areas for all transformed areas equal to the average value from the first micrograph listed. Corrections were all less than ± 7%.

[2] Amplitudes $F_{(hk)}$ were scaled so as to make $F_{(10)} + F_{(01)} + F_{(1\bar{1})} = 300$ for comparison.

[3] Single sheet (S) or paired components of a moire patterned image (M).

[4] d = diagonal of lattice.

Figure and Plate Captions

FIGURE 1. Schematic of the optical diffraction pattern shown in Plate Vb.

PLATE I. Electron micrographs of AcChR-rich membrane vesicles:

a) Specimen from Torpedo stained with 1% PTA at pH 7.4. Symbols (Λ) indicate regions of limited ordering.

b) Specimen from Torpedo stained with 2% PTA at pH 7.4.

c) Specimen from Narcine stained with 2% PTA at pH 7.0.

PLATE II. Membrane sheets containing large arrays often occur together as multilayered assemblies. The lattice organization can be traced across most of the Plate. Lattice lines can be identified by tilting the page and viewing it obliquely. Specimen from Torpedo stained with 2% PTA at pH 7.1.

PLATE III. Specimens from Torpedo stained with 2% PTA at pH 7.0.

a) Fragmented sheets containing partially ordered particles. Symbols (Λ) indicate areas of partial ordering.

b) Multilayered sheets in which separate lattices can be seen in all layers.

PLATE IV.

a) A pair of membrane sheets show some regions of single sheet, and multilayers which give rise to moiré patterns in the image. Specimen from Torpedo stained with 2% PTA at pH 7.0. 10 mM Carbamyl-choline was present in the dilution buffer.

b) Computed transform of the area of the moiré pattern between the symbols (Δ) in Plate IVa. The transform is displayed as the modulus of the amplitude in the continuous transform.

PLATE V.

a) Image showing a large array of particles organized into latticed domains. The arrays are contained in membrane sheets. In most areas there are at least two membrane sheets superposed in the image (sample from Torpedo stained with $UO(Ac)_2$, pH 6.5). The extent of ordering in the micrograph is best revealed if the moiré patterned images are viewed almost parallel to the page. This allows for a

crude optical filtering of one image from another.

b) The optical diffraction patterns are from areas of the image seen in Plate Va.

Figure 1

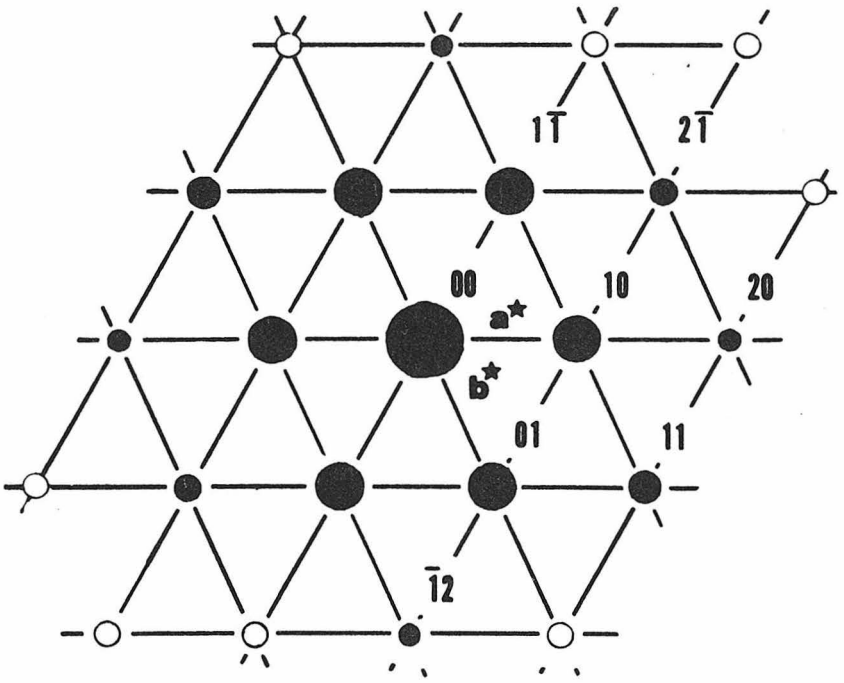

Plate I

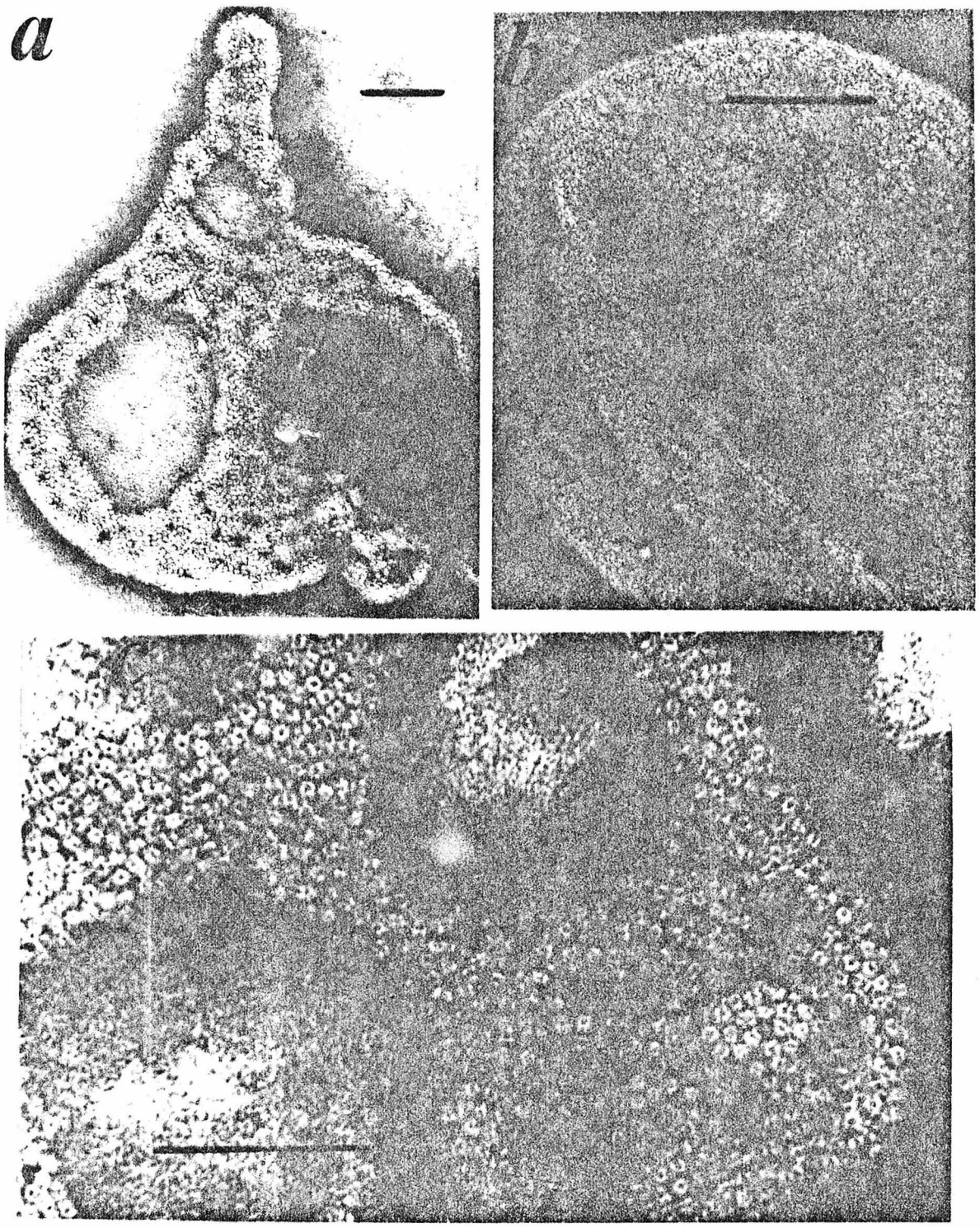

Plate II

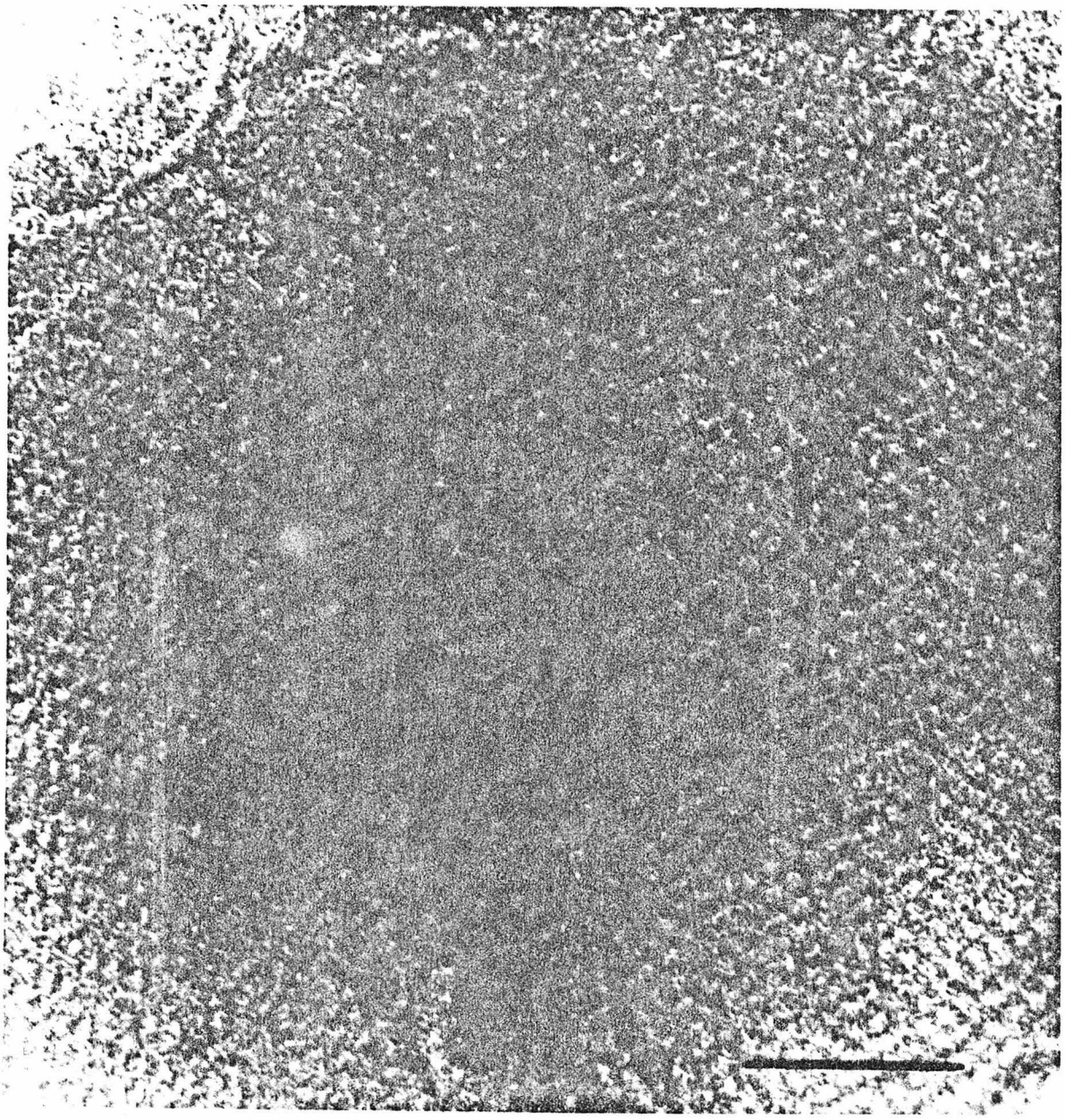

Plate III

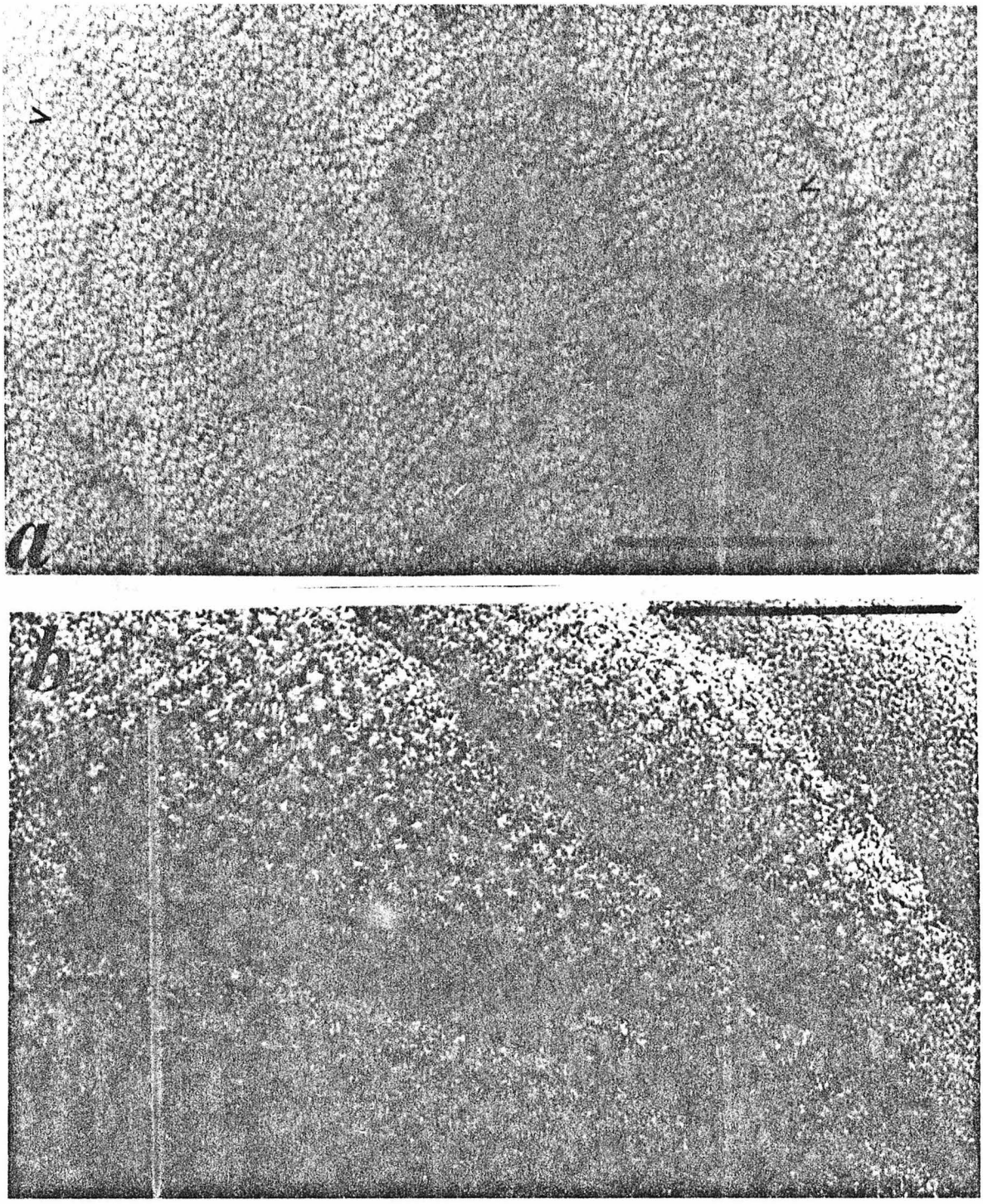

Plate IV

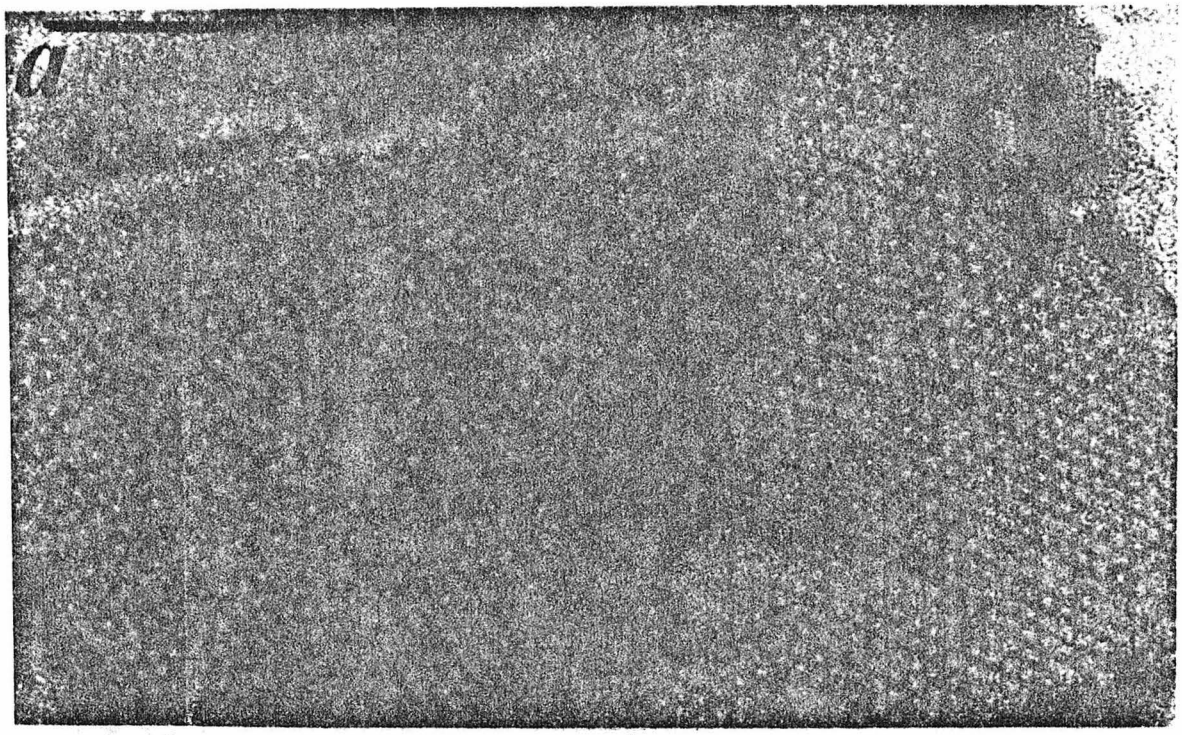

b

Plate V

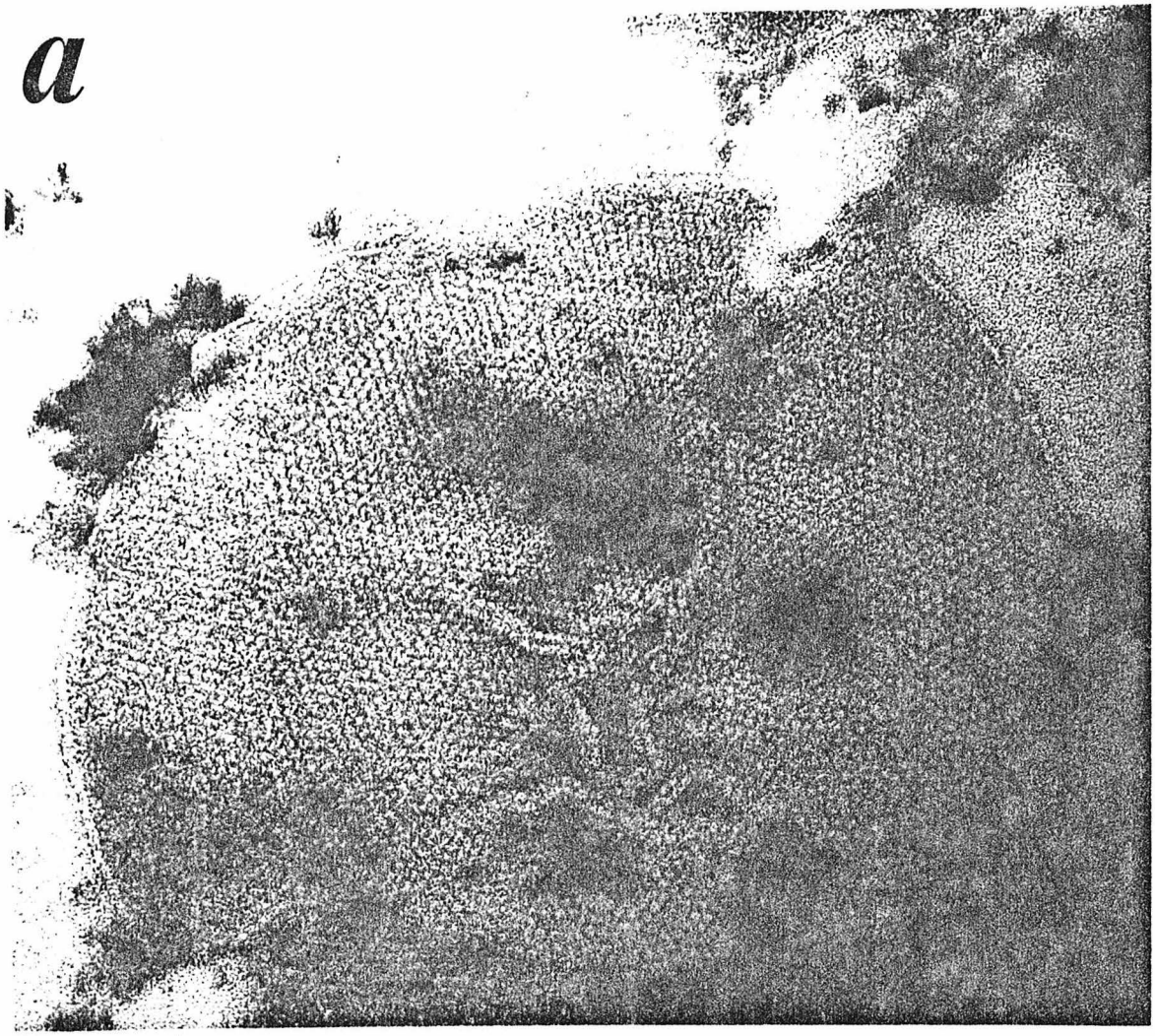

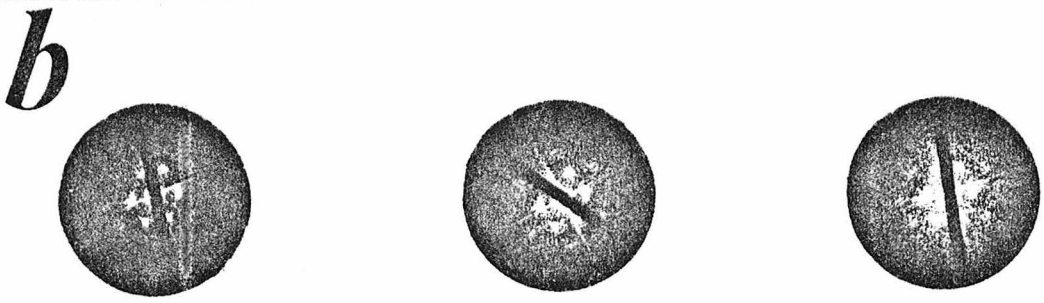

APPENDIX E

Structural Studies of a Membrane-Bound Acetylcholine Receptor from *Torpedo californica*

M. J. Ross, M. W. Klymkowsky, D. A. Agard, and R. M. Stroud

Submitted to J. Mol. Biol.

Structural Studies of a Membrane-Bound Acetylcholine Receptor from *Torpedo californica*

MICHAEL J. ROSS†, MICHAEL W. KLYMKOWSKY,

DAVID A. AGARD, AND ROBERT M. STROUD

Norman W. Church Laboratory of Chemical Biology

California Institute of Technology

Pasadena, California 91125, U.S.A.

(Received _____)

†Present Address: The Biological Laboratories, Harvard University, 12 Divinity Avenue, Cambridge, Massachusetts 02138.

J. Mol. Biol.

RUNNING TITLE: Structure of an Acetylcholine Receptor

1. Summary

Membranes prepared from Torpedo californica electroplax containing acetylcholine receptors have been studied by x-ray diffraction and electron microscopy. X-ray diffraction data suggest that acetylcholine receptor molecules traverse the endplate membrane, extending 15 ±5 Å on one side of the bilayer and some 55 ±5 Å on the other, with an overall length normal to the membrane of 110 Å.

Lattices of acetylcholine receptor have the symmetry of the crystallographic plane group p1, with one molecule per unit cell. A low resolution projection of the surface structure of receptor arrays was determined by reconstruction of images from electron micrographs. The resolution of the image is ~ 20 Å in the plane of the membrane. The electron density profile through the membrane, derived from x-ray diffraction of vesicle dispersions, has been analyzed to about the same resolution. The high-angle x-ray scattering pattern was observed to a resolution of 1.7 Å. Maxima in the scattering pattern were analyzed in terms of the state of the lipids and secondary structure in the membranes. Sharp maxima in the scattering pattern indicate that long stretches of secondary structure are present in the receptor-containing membranes. The receptor membranes contain repeating structural units of length 80 Å (5.2 Å

repeat) oriented perpendicular to the membrane plane, and uninterpreted components greater than 90 Å in length with a basic repeat of 6.3 Å.

2. Introduction

Nicotinic acetylcholine receptor (AcChR) molecules provide one of several mechanisms found in nature for neural transmission. AcChR-mediated synaptic transmission depends on pre-synaptic release of the low molecular weight transmitter, acetylcholine. After the transmitter diffuses across the synaptic space, it interacts with the membrane-bound receptor and effects depolarization.

The acetylcholine receptor has been shown to operate by increasing permeability to cations in the motor endplate (Takeuchi and Takeuchi, 1960). No permeability to anions was found. The ions are presumed to be conducted through a channel which spans the endplate membrane. The lifetime of this channel was estimated to be about one millisecond when excited by acetylcholine; during this time about 5×10^4 sodium ions can pass from one side of the membrane to the other (Katz and Miledi, 1972). The channel is presumably at least 5 Å across, since it has been shown to conduct cations as large as isopropyl ammonium (Furukawa and Furukawa, 1959).

Membrane fragments rich in AcChR have been purified from several species of electric eel and skate (Cohen et al., 1972; Duguid and Raftery, 1973). Further purification of AcChR isolated from membranes by detergent extraction has been accomplished and the molecular weight of these isolated molecules estimated at 330,000 daltons for AcChR from the species Torpedo marmarota and Torpedo californica by Edelstein et al. (1975) and 375,000 daltons for AcChR from T. californica by Vandlen and Raftery (1976).

Sodium dodecylsulfate (SDS) gel electrophoresis and cross-linking experiments have established a tentative subunit structure for AcChR; four different subunits have been identified (Weill et al., 1974; Vandlen and Raftery, 1976). The stoichiometry of these subunits is estimated as A_4B_2CD, where A has a molecular weight of 40,000 daltons, B, 45,000 daltons, C, 60,000 daltons, and D, 65,000 daltons (Vandlen and Raftery, 1976). α-Bungarotoxin, which blocks the action of the receptor, binds strongly to two of the 40,000 dalton subunits, competing with acetylcholine (Weber and Changeux, 1974). Weak binding sites for cholinergic agonists have been identified on the other two 40,000 dalton subunits (Michaelson et al., 1974).

Studies reported here are concerned with the structure and organization of a membrane-bound acetylcholine receptor from the electric skate T. californica. Three major questions are considered;

i) the distribution of protein relative to the lipid leaflet in AcChR membranes; ii) the secondary structure present within the subunits of the receptor and the thermodynamic state of the lipids; and iii) the three-dimensional structure of the molecules at low resolution.

3. Materials and Methods

a) Sample preparation

Samples of AcChR membranes were prepared by M.A. Raftery, R. Vandlen and collaborators as described by Reed et al. (1975). Argon or nitrogen saturated buffers, low temperatures and added anti-oxidants (e.g. 3,5-di-tert-butyl-4-hydroxy-benzyl alcohol) were used to minimize lipid oxidation; phenylmethane-sulfonyl fluoride (PMSF) (10^{-4} M) and EDTA (10^{-3} M) were added to inhibit proteolytic degradation (Vandlen and Raftery, 1976).

b) X-ray diffraction

The x-ray camera used for both low and high-angle pictures was designed by two of us (MJR and RMS). The source was a rotating anode generator (Elliott Neutron Division GX-6) run at either 1.6 kW with a 2.0 x 0.2 mm focus, or 0.6 kW with a 1.0 x 0.1 mm focus. The anode was viewed through a nickel filter at a takeoff angle of 3°

to 6° to provide an approximately square image of the target. The beam was focused onto the film plane by two perpendicular, elliptically bent silica mirrors (Franks, 1955), and passed through a 1-mm hole in the center of the film into the direct beam trap. The sample was kept at 2°C in an atmosphere of hydrated nitrogen (for wet samples) or dry helium (for dried samples). Two 0.001-inch Mylar ® windows were used to isolate the sample chamber from both the room atmosphere and the dry helium which filled the remainder of the camera length. The films (two per pack) were flat and oriented perpendicular to the beam; camera lengths from 1.0 to 19.7 cm were used; exposure times varied from four to 48 hours.

Several types of samples were used for diffraction analysis. These included dispersions of membrane vesicles, oriented membrane pellets of varying degrees of hydration, and dried pellets. Membranes were concentrated by centrifugation into specially designed polycarbonate sample holders contained in cellulose nitrate preparative ultracentrifuge tubes. Two types of membrane sample holders were used. In the first, the membranes were pelleted onto an acetate window, and in the second, membranes were pelleted onto a flat surface (1-mm wide) between two acetate windows. The first holder described allowed for collection of circularly averaged

in-plane (equatorial) diffraction from the membranes. The second type allowed for recording lamellar (meridional) and sectioned equatorial diffraction data.

If the sample had been oriented, care was taken to align the axis of orientation at approximately 45° to the vertical (or horizontal) to avoid the vertical and horizontal parasitic scatter flashes from the mirrors. Oriented samples were aligned such that the membrane planes were either parallel, or inclined at 30° to the incident x-ray beam.

In attempts to generate ordered pellets of membrane fragments, samples containing about 0.2 mg of protein were added to argon saturated buffer and were centrifuged at 120k to 300kg's for 2 to 48 hours in either Beckman SW-65L-Ti or SW-41-Ti rotors. Some samples were subjected to three freeze-thaw cycles (between -80°C and +5°C) immediately before centrifugation. This empirical procedure was found to assist in close packing the pellets by breaking up the vesicles in the dispersions. Excess buffer was removed from the pellet with absorbant paper. Omitting this step allowed the membrane pellet to swell, and the orientation of the bilayers was lost. This resulted in an unoriented membrane dispersion. Suspensions of vesicles which had not been concentrated by centrifugation contained so little sample that very little diffraction could be seen above the high background

from water scatter. Some samples of oriented membrane pellets were dried under a gentle stream of nitrogen at 4°C for about 24 hours.

c) Densitometry of x-ray films

Selected areas of each film, centered around the beam-stop, were digitized and recorded onto magnetic tape using either the 32 μ x 32 μ or 109 μ x 55 μ scanning spot (and step size) on a Syntex AD-1 flatbed autodensitometer. When the 109 μ x 55 μ spot was used, every two rows of data were averaged to give an effective 109 μ x 109 μ density reading.

During the process of data analysis, it proved necessary to locate the center of the film to within ±100 μ, and when sharp reflections were present to within ±20 μ. The center of the 1-mm beam-stop hole (punched before exposure) was found for each digitized area. By using a very short exposure of the direct beam, an approximate beam location could be determined to within 100 microns. The position of the film center was refined using iterative calculations based on the positions of pairs of equivalent reflections located on opposite sides of the film center.

Optical densities (OD's) measured on the film were corrected for film nonlinearity (grain coincidence) using parameters determined by Morimoto and Uyeda (1963). Film OD's above 2.2 were not

used to calculate membrane density profiles because the noise level of the densitometer and film nonlinearity became limiting. Signal-to-noise enhancements on the order of five to tenfold were achieved by use of radial integration techniques (Ross and Stroud, 1976).

d) X-ray data reduction

Continuous diffraction data were obtained from partially ordered membrane pellets (see above, Section b)) and from vesicle dispersions. The scattering from vesicle dispersions should represent the square of the transform of a single AcChR membrane, F(s), multiplied by the transform of the vesicle shape and distribution. The effects of vesicle size and curvature should be small perturbations only on the observed transform (Lesslauer et al., 1971; Moody, 1975). Meridional scattering (i.e. perpendicular to the membrane sheets) from partially ordered membrane sheets was corrected for background scatter by subtracting the equatorial from the meridional scattering. Observed intensities were then corrected for finite beam size, beam divergence and degree of orientation in the sample. The amount of orientation present in the sample was estimated from the angular width at half maximum of peaks in the meridional scattering pattern. This angular width was typically $\pm 12°$ to $\pm 40°$.

The background function for the unoriented vesicle data was more difficult to obtain and required a separate, shorter exposure from a much lower sample concentration. The scattering pattern from a more dilute vesicle dispersion should contain a smaller component of F(s) in proportion to the background scatter B(s), and the presumption is that the background scatter should be of the same form. In order to obtain a measure of $I(s)[= F^2(s)]$, the two scattering patterns $I_1(s)$ from the concentrated solutions and $I_2(s)$ from the dilute dispersions were scaled together. First, the constant density level on the films at high angles ($s^{-1} > 10$ Å) was subtracted both from $I_1(s)$ and from $I_2(s)$, on the assumption that such scattering contains little or no component from F(s). After this background was subtracted, the scattering from the more dilute sample $I_2(s)$ was scaled up by a constant multiplicative factor (c) such that $I_1(s) \geq I'_2(s)$ for all s. $I'_2(s)$ equalled $I_1(s)$ at only one s value, $s^{-1} = 22.7$ Å, where F(s) had its lowest minimum. The transform F(s) was then approximated as $F(s) = \sin\theta\ (I_1(s) - cI_2(s))$. The appropriate geometric factor of $\sin\theta$ was derived by Levine and Wilkins (1971).

Fourier refinement of electron density profiles against F(s) was carried out by the method of Stroud and Agard (1976).

e) Electron microscopy

Negatively stained samples were prepared and imaged as described by Klymkowsky et al. (1976). Images were also recorded on a tilting stage in a Phillips EM301 electron microscope. This allowed for recording views of up to 60° from the normal to the membrane surface.

Thin sections of pellets used for x-ray diffraction were embedded, stained and analyzed by electron microscopy as follows: The pellets were glutaraldehyde-formaldehyde fixed (4% formaldehyde, 5% glutaraldehyde in 0.05 M sodium/potassium phosphate buffer, pH 7.4) for two hours and washed overnight in phosphate buffer. The pellets were further fixed in 1% osmium tetraoxide also buffered in 0.05 M phosphate buffer, pH 7.4 for two hours, dehydrated and embedded in Epon 812 epoxy resin (Luft, 1961). Thin (silver gray) sections were cut parallel to the direction of sedimentation using a freshly made glass knife, and lead citrate post-stained before viewing (Reynolds, 1963). No change in pellet thickness occurred during the fixation or embedding. Micrographs were taken on a Phillips EM 301 at 80 kV.

f) Image reconstruction

Areas of electron micrographs of negatively stained samples containing an ordered array were digitized using a Syntex AD-1 flat-bed scanner. Data were collected using a 32 μ square illuminating aperture, a round (approximately 90 μ) receiving aperture and a 32 μ step size. The step size of 32 μ corresponds to a spacing of 2 - 4 Å in the electron micrographs of arrays that were analyzed. Well-ordered areas on the micrographs were identified by visual inspection and assayed for degree of perfection by optical diffraction or by computer transform (see below). Optical diffraction was carried out on an optical diffractometer (Markham, 1968) using He-Ne laser illumination (Hughes, Model No. 3599H) and an oil-filled film gate.

Selected areas were densitometered, recorded on magnetic tape and Fourier transformed using a two-dimensional fast Fourier algorithm (Cooley and Tukey, 1965)*. When data were to be used for image reconstructions, the mean OD of the area was subtracted from all picture elements, and the digitized image was "floated" in

*All calculations were done on a Data General NOVA 800 computer with 32k words of core, a Syntex Analytical Instruments floating point processor, a 2.5 M byte disk, and two 800 BPI 9-track tape units. Times for transform calculations using the program written by one of us (MJR) are: 128 x 128 transform, 3 minutes; 256 x 256 transform, 13 minutes; 512 x 512 transform, 1 hour 10 minutes. If a real -- hermite transform is calculated instead of a complex -- complex transform, these times are halved.

borders equal to or greater than half of the original image size in all directions (DeRosier and Moore, 1970). These procedures greatly diminished the effects due to first order mask diffraction, and edge discontinuity. After Fourier transformation, the reciprocal lattice parameters were refined (Klymkowsky et al., 1976).

The internal consistency of each lattice chosen for reconstruction was checked by examining the deviation of the positions of the observed maxima in the Fourier transform from their expected positions. Any lattice with an overall standard deviation of greater than $\pm 0.75\,[\text{scan area}]^{-1}$ was rejected. The magnitudes of the Fourier coefficients at each diffraction maximum were examined and those lattices containing split peaks (indicative of a distorted lattice (Klymkowsky et al., 1976)) were also rejected.

Phases of the stronger reflections were examined for discontinuities within the region of a diffraction maximum. If phase incoherence was found, the lattice was rejected. This latter test proved useful when searching the electron micrograph for a region suitable for reconstruction.

Two courses of action were taken with respect to the reconstruction of the final image. A digital process, formally identical to the optical filtering techniques developed by Klug and Berger (1964), was used to take the masked Fourier transform and back transform

it into real space. The second method involved an averaging procedure where amplitudes $F_{(hk)}$ for each reflection were generated by integration of the peaks. Phases $\varphi_{(hk)}$ were calculated as the weighted average across the peak. Weighting was according to the square of the amplitude at points in a 3 x 3 or 5 x 5 array surrounding the lattice points, thus

$$\varphi_{(hk)} = \tan^{-1} \left(\frac{\sum_{ij} F_{ij}^2 \sin(\varphi_{ij})}{\sum_{ij} F_{ij}^2 \cos(\varphi_{ij})} \right)_{(hk)}$$

The averaged structure factors were placed at the refined reciprocal lattice points prior to Fourier transformation.

As a quantitative measure of the quality of each reconstruction, the weighted average phase for each reflection was compared to each of the individual phases that went into calculating this average. The weighted mean phase angle discrepancy and the weighted mean cosine of this angle ("figure of merit") were calculated for each reflection according to

$$\Delta\varphi_{(hk)} = \left(\frac{\sum_{ij} F_{ij}^2 (\varphi_{ij} - \bar{\varphi})}{\sum_{ij} F_{ij}^2} \right)_{(hk)}$$

$$m_{(hk)} = \left(\frac{\sum_{ij} F_{ij}^{2} \cos (\varphi_{ij} - \bar{\varphi})}{\sum_{ij} F_{ij}^{2}} \right)_{(hk)}$$

An overall figure of merit was also calculated for the entire diffraction pattern:

$$\bar{m} = \frac{\sum_{hk} F_{(hk)}^{2} \, m_{(hk)}}{\sum_{hk} F^{2}_{(hk)}}$$

4. Results

a) Membrane profile analysis

When visualized by negative staining in the electron microscope, AcChR membrane fragments generally appeared as vesicles which contained a dense population of AcChR molecules of diameter 80 - 90 Å (Klymkowsky et al., 1976). In an attempt to characterize the distribution of protein and lipid in the membranes, pelletted samples were analyzed by x-ray diffraction. The x-ray scattering pattern shown in Plate Ia was typical of those generated from partially oriented pellets. There is little indication of regular order in the plane of the membranes. Such order would give rise to equatorial diffraction (horizontal in Plate I). This is consistent with our

observation that most of the sample does not contain arrayed structures (Klymkowsky et al., 1976).

The meridional scattering pattern showed a continuous scattering profile. The first minimum in the pattern from hydrated pellets occurred at d = 110 Å, and maxima were seen at d spacings of about 76 Å and 37 Å. Meridional scattering from oriented dried pellets showed a broad maximum centered at d = 59 Å, presumably due to the scattering function of the denatured membranes (see Figure 1).

Oriented patterns provided a means of separating the meridional scattering pattern from the equatorial scattering. The meridional scattering function F(s) was calculated. Electron density profiles through the membrane were calculated by the Fourier method described by Stroud and Agard (1976).

In view of the possibility that the oriented patterns such as those shown in Plate Ia contain sampling due to close packing within the pellet, similar methods were applied to the x-ray scattering function F(s) derived from vesicle dispersions.

To apply the Fourier refinement method it is important to obtain an estimate of the thickness of the membrane leaflet. Several different lines of evidence indicated a boundary thickness of about 110 Å:

i) Membrane fragments subjected to freeze-thaw cycles (see Materials and Methods Section) were pelletted for 48 hours at 200,000 g's, and the x-ray scattering patterns from these samples showed weak maxima superposed on a broad pillar of continuous meridional diffraction (Plate Ib). The first of these maxima occurred at a d-spacing of 110 Å (Figure 2). The second order maximum at d = 55 Å was weak, and there was a peak at the position expected for the third order (d = 37 Å). The continuous pillar of meridional scatter was assumed to be due to statistically random stacking of asymmetric membranes (Stroud and Agard, 1976). Therefore, the close-packed sheets which by chance do form a truly repeating block (3 - 5 layers thick) were responsible for the 110 Å peak, indicating a thickness of 110 Å for the membranes themselves.

ii) The Patterson function $P(r) = \int F^2(s)\cos(2\pi rs)\,ds$ calculated from either the partially oriented, or the vesicle dispersion data, gave an indication of the largest vectors across the membrane leaflet. In both cases the Patterson function indicated a minimum membrane thickness of about 110 Å.

iii) Pellets used for x-ray diffraction were sectioned and analyzed by electron microscopy (see Plate II). The thickness of a single leaflet was estimated to be about 100 Å ± 25 Å.

iv) Isolated AcChR molecules prepared by M. A. Raftery and

collaborators according to the procedures of Michaelson et al. (1974) were shadowed at 15° and at 45° with platinum (Kent and Stroud, unpublished results, 1974). Particles seen in the electron microscope were equidimensional with diameters of ca. 85 - 125 Å.

The corrected scattering function |F(s)| from vesicle dispersions (Figure 3a) and the corrected meridional scattering from partially oriented samples (Figure 3d) were used as a basis for one-dimensional electron density refinement. After 40 cycles of refinement from several different starting models, the structures shown in Figures 3b and 3e were obtained. A boundary thickness of 115 Å was used to refine the electron density profile obtained from the vesicle data. Narrower boundaries did not allow convergence to a solution.

Application of the Fourier refinement method to the diffraction data from the partially oriented sample indicated that these data are also inconsistent with a structure narrower than 110 Å. Using a boundary width of 120 Å, the agreement between observed and calculated |F(s)|, and the Patterson and autocorrelation functions was considerably worse than found for the vesicle data. However, if the boundary was relaxed to 300 Å, agreement was radically improved and the results shown in Figure 3d, e, and f were obtained. It is important to note that the membrane profile itself did not change significantly.

The agreement between observed and calculated scattering functions after refinement are indicated in Figure 3a (R = 2.3 %) and 3d (R = 1.25 %). The Patterson and autocorrelation functions in the two cases, as shown in Figures 3c and 3f, are also in excellent agreement.

The two structures shown in Figures 3b and 3e are surprisingly similar in general features, although they differ in resolution (the resolution was 22 Å for vesicle data; 13 Å for oriented patterns). Both profiles have characteristics of a bilayer structure in that the distance between highest peaks on either side of the negative density region were 40 ±3Å. The negative density relative to solvent is interpreted as the center of a bilayer. Both profiles also indicate an extension of density on one side of the bilayer by some 55 ±5 Å. The height of the peak for phosphatidyl head groups on the other side is lower than expected, and may be due to insertion of some lower density material--protein or solvent. It therefore seems that protein spans the entire structure and extends mostly on one side of the membrane (~ 55 Å) and very little (~ 5 Å) on the other.

It must be noted that there is a difference between the oriented and vesicle scattering profiles and Patterson syntheses. This is primarily reflected in the peak at d = 76 Å, which is no more than a shoulder in the vesicle profile (see Figure 3a, 3d). The difference

may be due to the lower intensity, and therefore lower accuracy, of the radially smeared vesicle scattering function, or may be due to a stacking disorder in the oriented pattern. The second explanation does not seem unreasonable since the refined electron density function from oriented sample seems to contain a second membrane profile of much weaker amplitude.

A thin section of partially ordered membrane pellet shows a degree of ordering in the pellet qualitatively consistent with the small angle x-ray results (Plate II). The average intermembrane distance (in the pelleting direction) is ~ 800 Å; however, the membranes occasionally appear as pairs with much closer spacings between the two sheets in a pair. The bilayers in each pair of membranes are an average of 225 Å apart (center to center) with a standard deviation of ± 90 Å, and approach as close as ~ 105 Å. These data could account for the small amount of sampling observed in the x-ray pattern of partially ordered pellets.

b) Images and image enhancement

The nature of negative staining makes interpretation of stained images less than straightforward. According to current models (Huxley and Zubay, 1960), the heavy metals form an amorphous glass over the specimen, filling in uneven features on the surface of the membrane. Stain density should therefore be inversely proportional to the surface relief of the membrane-bound components. One or both sides of the membrane may contribute to the image creating ambiguities.

Some membrane fragments contain areas of extended lattice organization (Klymkowsky et al., 1976). Ordering in these lattices, although often perturbed by the effects of desiccation and negative staining, allowed the application of image enhancement techniques to certain areas. Image enhancement techniques used here fall into two related types: 1) pseudo-optical masking, and ii) phase averaging. Areas of micrographs showing good, extended ordering were processed using both techniques.

Pseudo-optical masking suffers from two disadvantages when applied to AcChR membrane lattices in that; i) low frequency components of the noise, belonging to a family of repeats greater than the inverse of the mask aperture used around each diffraction spot, are not removed (Erickson, 1974), and ii) whatever lack of phase

coherence exists across each reflection remains. These low frequency terms are sometimes quite large and are mainly due to stain variations on the sample. Compared with stained three-dimensional crystals (e. g., catalase) these problems were about five times worse for AcChR membranes.

As noted by Klug and DeRosier (1966) and by Gibbs and Rowe (1973), the pseudo-optical process leads to an ordered image even when applied to an area of incoherent noise in the Fourier transform, although the reconstructed image is correspondingly weaker. There is perhaps an even greater possibility of reinforcing such errors in the averaging procedure since the reconstructed image in that case is perfectly repeating by definition. The overall figure of merit (see Materials and Methods Section) for a lattice applied to a wrong area, or to an unordered electron micrograph, varied from about .2 to .8 with individual figures of merit for reflections as low as 0.05 to .30. A good AcChR reconstruction gave an overall figure of merit of .95 to .99 with no reflection below .80.

The stained images usually contained multiple layers which gave rise to moiré patterns. Many reconstructions were carried out on different areas, each containing no more than two superposed lattices, and components of the two lattices were separated in the Fourier transform. Reconstructed images from uranyl acetate

stained membranes consistently gave either of two different views of the receptor (a, b, in Plates III, IV, and Figure 4). One of these views indicated that the stain penetrated a well in the center of the molecule. The reconstructed molecule looked very much like the isolated particles seen in vesicles (Klymkowsky et al., 1976) (a in Plates III, IV, and Figure 4). The alternate view consistently showed a groove part of the way across the molecule, with a shallow central well (b in Plates III, IV, and Figure 4). The presence of these two views from alternate layers of moiré-patterned images suggests a different distribution of stain in the two layers.

The contrast transfer function (Erickson and Klug, 1971) was evaluated from the image transforms. All images were underfocused by about 900 Å to achieve maximum contrast. The first phase change in the transfer function occurred at about 15 - 18 Å resolution. All maxima in transforms used for reconstruction were of lower resolution than the first node in the transfer function, thereby eliminating the need for phase correction.

The transform to 20 Å resolution contained thirty-two independent (hk) reflections out to the fourth order (h = 4). Typically 18 - 23 reflections had enough significant intensity and phase coherence for inclusion in the reconstruction.

Reconstructed images of PTA-stained lattices rarely showed any evidence for a central well in the molecule (c in Plate III, IV, and Figure 4); however, images stained with PTA consistently gave relatively lower maxima at higher resolution in the transform than those stained with uranyl acetate.

It is possible that the central hole becomes positively stained by the (positively charged) uranyl ions, while the negative charge of the phosphotungstate ion, or the larger grain size of the polymerized stain inhibit staining of the central hole. The particles seen in reconstructed images are not centrosymmetric, even at lower resolution (90 Å), indicating that the phases are inconsistent with the oblique plane lattice p2. The lattice therefore has p1 symmetry.

c) Secondary structure

High-angle x-ray diffraction photographs of AcChR-rich membrane vesicles reveal several broad maxima characteristic of lipid or water spacings (Plate Va, b). A broad band centered at a d-spacing of 4.6 Å is characteristic of the interhydrocarbon chain spacings in lipids above the fluid/crystalline phase transition (Luzzati et al., 1960). A sharper maximum at d = 4.2 Å is expected for the crystalline lipid phase (Dervichian, 1964). High-angle vesicle patterns recorded at either 2°C or at 20°C (relative humidity

100%) indicate that a small proportion of the lipids are in the crystalline phase. The phase transition is broad, and this is not surprising in view of the heterogeneous nature of the Torpedo lipids (Michaelson and Raftery, 1974) or the temperatures of the natural habitat of Torpedo.

As a quantitative assay for the orientation of these rings, a difference plot of the equatorial pattern subtracted from the meridional pattern was calculated (Figure 5). 4.2 Å diffraction appeared in both meridional and equatorial scans, the diffraction from fluid phase lipids at 4.6 Å was, however, strongly equatorially oriented. This would suggest that most of the lipids contained in the oriented vesicles are above their phase transition temperature (at 4°C), but that crystalline lipids exist in some of the impurities in the preparation. These are presumably not in vesicles or sheets and thus do not orient during pelleting.

There is a broad peak centered at d = 3.3 Å characteristic of water scattering. The degree of hydration of the sample can be estimated from the height of the water peak. There are two sharp reflections at spacings d = 5.2 Å and d = 6.3 Å in the high-angle pattern of hydrated AcChR membranes. In addition there is a maximum at d = 4.06 Å (Figure 5) and a broad maximum at d = 2.2 Å (Plate Vb).

The maximum at d = 5.2 Å is highly oriented toward the meridion, while the 6.3 Å reflection is slightly oriented toward the equator. Both the 5.2 Å and the 6.3 Å reflections are extremely sharp. The ratio of the width of these rings at half-height to their radial position from the film center can be used as an index to the length of the structural feature giving rise to the diffraction. These ratios are one-eighteenth for the 5.2 Å reflection, and one-seventeenth for the 6.3 Å reflection. This indicates that the 5.2 Å reflection is caused by a stretch of secondary structure ~80 Å in length running perpendicular to the membrane, and that the 6.3 Å reflection is caused by structures of ~ 90 Å in length. The angular reflection width of the 5.2 Å reflection was analyzed and compared to the angular width of the small-angle diffraction maxima in the same pattern; the 5.2 Å reflection had an angular peak width about twice that of the low-angle maxima.

5. Discussion

a) Contents of the unit cell

Taking the unit cell parameters in the membrane plane as a = 90.8 Å, c = 91.3 Å and $\beta = 118°$, the area of one unit cell in the membrane plane is calculated to be 7320 $Å^2$ (Klymkowsky et al.,

1976). Each cell contains one molecule of AcChR oligomer, of estimated molecular weight 350,000. The volume occupied by a protein molecule of this molecular weight may be estimated from the data summarized by Matthews (1968). We chose a value of 1.3 for the volume (in $Å^3$) per dalton of protein (calculated for trypsin crystals after subtraction of the solvent content volume in the crystal (Stroud et al., 1974)). Thus, the protein volume is estimated as about 457,000 $Å^3$. If this amount of protein were totally close-packed into a cell of area 7320 $Å^2$, it would account for a cell thickness of 62.5 Å (about 57% of a 110 Å unit cell).

The measured density of the bulk membrane samples was 1.17 gm/ml, and the weight ratio of protein to lipid was ~ 50% protein:50% lipid (Michaelson et al., 1974). The bulk sample is nonetheless much less concentrated in protein than are the sheets used for image analysis which contained close-packed two-dimensional lattices of protein. Thus, the estimate of 50% protein is a lower limit to the amount of receptor in each unit cell.

Based on the image analyses (see Figure 4), we estimate that no more than half of the area of each unit cell may be lipid. The number of lipid molecules present in such an area can be obtained by dividing the lipid area of each unit cell (less than 3700 $Å^2$) by the estimated area per lipid molecule. Assuming a value of 62.7 $Å^2$ per

lipid molecule (obtained by Levine and Wilkins (1971) for lecithin bilayers at 100% relative humidity), 60 x 2 lipid molecules would be contained in bilayer structure per unit cell. The volume occupied by the lipids would be 3700 x 40 = 148,000 $Å^3$ (taking 40 Å as the bilayer thickness in hydrated lecithin bilayers (Levine and Wilkins, 1971)).

The estimated volume occupied by protein and lipid thus totals 605,000 $Å^3$. If no other components were present, this volume would account for an 83 Å thickness of a close-packed unit cell of area 7320 $Å^2$. The third dimension of the unit cell from the x-ray results is 110 Å, therefore protein and lipid alone would account for 75% of the unit cell volume.

If the remaining volume of the cell, not filled by lipid and protein, is assumed to be filled by solvent (200,000 $Å^3$ or about 25% of the unit cell), then the value of V_m for the protein plus solvent volume (657,000 $Å^3$) would be 1.87 $Å^3$ per dalton of protein. This is at the lower end of the reasonable V_m for protein molecules in crystals (Matthews, 1968).

It must be emphasized that the three unit cell parameters, a, b, and c are never observed simultaneously, since no estimate of the thickness of one layer b is obtained from the microscopy of single or multilayered arrays used to define a and c. Conversely, since the bulk of the sample contains membranes with close-packed, but

not highly ordered arrays of molecules, the x-ray diffraction studies used to define the b dimension do not allow for an estimate of the in-plane lattice dimensions.

b) Distribution of lipid and protein

The electron density profile perpendicular to the membrane surface indicates that the protein molecules extend through the bilayer. The AcChR is therefore an integral membrane protein. From the solutions indicated in Figure 3, we presume that the main minimum in the function lies at the center of a lipid bilayer. It appears that the protein spans the bilayer and extends considerably on one side, ~ 55 Å, and little on the other, ~ 15 Å. The two maxima in the electron density profile on either side of the lowest minimum are ~ 40 Å apart, i. e. about equal to the separation between the electron dense phosphatidyl head groups in artificial lipid bilayers (Levine and Wilkins, 1971; Lesslauer et al., 1972). The conclusion that the protein extends out on one side much more than on the other seems inescapable. More symmetric models were found to be incompatible with the continuous scattering profiles.

c) The state of close-packed membrane pellets

The x-ray pattern shown in Plate Ib is evidence for some three-dimensional ordering in the sample. The off-axial reflections with a d spacing of 37 Å do not seem to correspond to any of the lipid phases characterized by Gulik-Krzywicki et al. (1967), and the observation of this feature of the x-ray pattern has not been repeated. Nevertheless, it deserves some consideration. The distribution of 37 Å reflections is hexagonal, and suggests that a hexagonal phase may have been formed in the specimen. The radial widths of the off-axial reflections indicate a paracrystalline domain size of about 500 Å in each direction. If the components of structure were in a hexagonal phase, the symmetry axis must be parallel to the plane of the membrane. It is attractive to place the lipids in such a phase, however, any further attempt at interpretation of this feature of the pattern would be mere speculation.

d) Secondary structure

Henderson (1975) observed that bacterial rhodopsin in the purple membrane of Halobacterium halobium contained α-helices, all oriented perpendicular to the membrane. Henderson also presented and discussed strong evidence for α-helical structure in other transmembrane proteins, and argued that the α-helix neatly satisfies the

hydrogen-bonding requirements of a polypeptide chain in a hydrophobic environment. It is notable that AcChR membranes give rise to a sharp reflection at d = 5.2 Å. This spacing is one diagnostic test for α-helices in the coiled coil conformation.. If this reflection arises from α-helices, then they are of average length ~ 80 Å, and oriented perpendicular to the membrane surface.

Two other structures which may represent an energetically acceptable way to define a channel of dimensions ~ 5 - 10 Å would be i)a large diameter coil of polypeptide, cross-linked as a parallel β-sheet structure, and ii) a barrel formed by twisted antiparallel β-sheet. This latter structure has been found in several proteins. Either of these two structures might account for the 6.3 Å reflection.

The antiparallel-pleated sheet gives rise to a chain repeat of 7 Å, with 4.75 Å between chains running in alternate directions (as found for silk (Marsh et al., 1955)). A twisted pleated sheet might reduce the chain repeat perpendicular to the membrane to 6.3 Å.

The parallel β-sheet arrangement was suggested by β-keratin (Pauling and Corey, 1951), and gives rise to a 6.5 Å chain repeat, with 4.85 Å separation between chains. The sharpness of the 6.3 Å reflection is nevertheless surprising, and it is difficult to see how a coiled chain could account for the apparently large number of repetitions. The 6.3 Å reflection was observed in the x-ray patterns of

other membranes prepared from Torpedo and Electrophorus electricus including those enriched in acetylcholine esterase, or ATPase. Therefore, there is at least the possibility in this case that the reflection arises from regular lipid phase in the membranes.

6. Conclusion

The acetylcholine receptor from T. californica is an integral membrane protein, which traverses the endplate membrane. Evidence presented indicates that the protein extends some 55 Å on one side of the lipid bilayer. This receptor frequently occurs in an ordered lattice which is presumably maintained by protein-protein interactions. The center of each molecule is more accessible to uranyl stain than other parts of the molecule, and this well is tentatively identified as the ionophoretic channel. Further low resolution studies are aimed at i) locating binding sites for macromolecular toxins such as α-Bungarotoxin which bind tightly to the receptor, and ii) assaying for ligand-induced conformational change. The single crystal structure analysis of α-Bungarotoxin is nearing completion in our laboratory, and it is hoped that details of toxin binding may be obtained from the high resolution structure of the α-toxin.

7. Acknowledgments

This work was carried out with the support of the National Institutes of Health grant No. GM-19984 and the National Science Foundation grant No. BMS75-04105, whose help is gratefully acknowledged. One of us (RMS) is the recipient of a National Institutes of Health Career Development Award, another (MJR) is the recipient of a National Institutes of Health Predoctoral Traineeship, another (DAA) is the recipient of a National Science Foundation Predoctoral Fellowship, and another (MWK) is the recipient of a California Foundation Fellowship for Biochemical Research. This is contribution No. 5370 from the Norman W. Church Laboratory of Chemical Biology, California Institute of Technology.

8. References

Cohen, J. B., Weber, M., Huchet, M., and Changeux, J.-P. (1972). FEBS Letters 26, 43-47.

Cooley, J. W., and Tukey, J. W. (1965). Math. of Comput. 19, 297-301.

Dervichian, D. G. (1964). Prog. Biophys. and Mol. Biol. 14, 263-342.

DeRosier, D. J. and Moore, P. B. (1970). J. Mol. Biol. 52, 355-369.

Duguid, J. R. and Raftery, M. A. (1973). Biochemistry 12, 3593-3597.

Edelstein, S. J., Beyer, W. B., Edelfrawi, A. T., and Edelfrawi, M. E. (1975). J. Biol. Chem. 250, 6101-6106.

Erickson, H. P. (1974). Eighth International Congress on Electron Microscopy, Canberra, 310-311.

Erickson, H. P. and Klug, A. (1971). Phil. Trans. Roy. Soc. London B261, 105-118.

Franks, A. (1955). Proc. Phys. Soc. (Lond.) B68, 1054-1064.

Furukawa, T. and Furukawa, A. (1959). Jap. J. Physiol. 9, 130-142.

Gibbs, A. J., and Rowe, A. J. (1973). Nature 246, 509-511.

Gulik-Krzywicki, T., Rivas, E., and Luzzati, V. (1967). J. Mol. Biol. 27, 303-322.

Henderson, R. (1975). J. Mol. Biol. 93, 123-138.

Huxley, H. E. and Zubay, G. (1960). J. Mol. Biol. 2, 10-18.

Katz, B. and Miledi, R. (1972). J. Physiol (Lond) 224, 665-699.

Klug, A. and Berger, J. E. (1964). J. Mol. Biol. 10, 565-569.

Klug, A. and DeRosier, D. J. (1966). Nature 212, 29-32.

Klymkowsky, M. W., Ross, M. J., and Stroud, R. M. (1976). Submitted to J. Mol. Biol.

Lesslauer, W., Cain, J., and Blasie, J. K. (1971). Biochim. Biophys. Acta 241, 547-566.

Lesslauer, W., Cain, J. E., and Blasie, J. K. (1972). Proc. Nat. Acad. Sci. USA 69, 1499-1503.

Levine, Y. K. and Wilkins, M. H. F. (1971). Nature New Biol. 230, 69-72.

Luft, J. H. (1961). J. Biophys. Biochem. Cytol. 9, 409-414.

Luzzati, V., Mustacchi, H., Skoulos, A., and Husson, F. (1960). Acta Crystallogr. 13, 660-667.

Markham, R. (1968). Meth. Virol. 4, 503-529.

Marsh, R. E., Corey, R. B. and Pauling, L. (1955). Biochim. Biophys. Acta 16, 1-34.

Matthews, B. W. (1968). J. Mol. Biol. 33, 491-497.

Michaelson, D. M. and Raftery, M. A. (1974). Proc. Nat. Acad. Sci. USA 71, 4768-4772.

Michaelson, D., Vandlen, R., Bode, J., Moody, T., Schmidt, J., and Raftery, M. A. (1974). Arch. Bioch. Bioph. 165, 796-804.

Moody, M. F. (1975). Acta Crystallogr. A31, 8-15.

Morimoto, H. and Uyeda, R. (1963). Acta Crystallogr. 16, 1107-1119.

Pauling, L. and Corey, R. B. (1951). Proc. Nat. Acad. Sci. USA 37, 729-740.

Reed, K., Vandlen, R., Bode, J., Duguid, J., and Raftery, M. A. (1975). Arch. Bioch. Bioph. 167, 138-144.

Reynolds, E. S. (1963). J. Cell. Biol. 17, 208-212.

Ross, M. J. and Stroud, R. M. (1976). Submitted to Acta Crystallogr.

Stroud, R. M. and Agard, D. A. (1976). Submitted to J. Mol. Biol.

Stroud, R. M., Kay, L. M., and Dickerson, R. E. (1974). J. Mol. Biol. 83, 185-208.

Takeuchi, A., and Takeuchi, N. (1960). J. Physiol. (Lond.) 154, 52-67.

Vandlen, R. and Raftery, M. A. (1976). Submitted to Biochemistry.

Weber, M. and Changeux, J.-P. (1974). Mol. Pharm. 10, 15-34.

Weill, C. L., McNamee, M. G., and Karlin, A. (1974). Biochem. Biophys. Res. Commun. 61, 997-1003.

Figure Captions

FIGURE 1. Densitometer tracings of low-angle x-ray films of partially oriented pellets of AcChR membranes. The data are computed from radial integrations within an angular spread of ±20° of the meridian. The x-ray camera length was 19.67 cm.

a) Data derived from a two-hour exposure of a dried pellet using the .2 mm x 2 mm focus.

b) Integrated data from the film shown in Plate Ia.

FIGURE 2. Densitometer tracing of the scattering pattern shown in Plate Ib for highly pelletted AcChR membranes. Equatorial and meridional data were integrated with an angle of acceptance of ±12°. Although the equatorial scattering is far stronger here than in less oriented pellets which had not been subjected to freeze-thaw cycles, it is considerably weaker than the meridional scatter.

Inset (upper right) is a polar integration of a circular shell centered on the 37 Å reflection. The angular widths of the meridional and off-axis reflections are both ±12° half-height.

FIGURE 3. Results of Fourier refinement of diffraction data from vesicle dispersions (a, b, c)(to a resolution of 22 Å) and

partially oriented pellets (d, e, f)(resolution 13 Å). Starting models included two rectangular box functions, a delta function, and a linear ramp. All gave essentially the same results. Calculated and observed continuous scattering patterns for each of these data sets are shown superimposed in (a) and (d). The electron density profiles computed from these x-ray data are seen in (b) and (e). Panels (c) and (f) each contain superimpositions of the autocorrelation and Patterson functions (R_P = 2.3% and R_P = 1.1%, respectively).

FIGURE 4. Contoured plots of phase averaged images. The images shown in Plate IVa, b, c, were contoured at isodensity levels to indicate the overall molecular shape and lattice contacts present in AcChR membranes.

a) and b) Uranyl acetate stained.

c) Phosphotungstate stained.

FIGURE 5. Densitometer tracings of high-angle scattering from AcChR-rich membranes. Equatorial and meridional integrations from the film shown in Plate Va were carried out with angular acceptance limits of ±50°. Insets on the equatorial and meridional figures are expansions which show the sharp 6.3 Å and 5.2 Å reflections. A difference curve displaying the meridional minus equatorial

density is shown on the right. Peaks with meridional orientation are positive; those with equatorial are negative on this plot.

Plate Captions

PLATE I. Small-angle scattering patterns from AcChR-rich membrane pellets. The x-ray camera length was 19.67 cm. The x-ray focus was .2 mm x 2.0 mm. The patterns are oriented such that the merional (lamellar spacing) reflections are vertical. Densitometer tracings of these films are shown in Figures 1 and 2. Specimens were: a) Partially oriented pellet. This pattern shows meridional diffraction with maxima at 76 Å and 37 Å. The angular widths of these maxima are ±22°. The pellet was exposed at a relative humidity (r.h.) of 100% for 35 hours. b) Close-packed pellet (r.h. = 92%). The pellet was prepared by centrifugation at 200 kg's for 48 hours after three freeze-thaw cycles. Exposure time was ten hours. The meridional pattern contains a strong pillar of continuous diffraction with peaks at 110 Å and 37 Å. Prominent off-axial reflections occur on a 74 Å layer line with a d spacing of 37 Å.

PLATE II. Thin section of a partially oriented pellet of AcChR membrane vesicles. The direction of sedimentation in the pellet is indicated by the arrow. Membranes appear as dark lines with an average thickness of ~100 Å.

PLATE III. Pseudo-optically enhanced images. Stain is dark.

a, b) Uranyl acetate-stained images from a double sheet of AcChR membrane. Separate reconstructions were carried out on each of the moiréd lattices. 32 independent reflections from each lattice were masked (resolution 20 Å).

c) Phosphotungstate-stained image of one sheet of AcChR membrane. twenty-three independent reflections were masked and used in the reconstruction (resolution 20 Å).

PLATE IV. Phase averaged enhanced images. Stain is dark. Areas corresponding to Plate IIIa, b (uranyl acetate stained) and c) phosphotungstate stained).

a) Eighteen independent reflections phase averaged. Average overall error in $x = .57$, $y = .41\ [\text{scan area}]^{-1}$ from calculated lattice positions. Overall figure of merit = .96.

b) Twenty-two independent reflections used. Averaged overall error in $x = .47$, $y = .43\ [\text{scan area}]^{-1}$ from calculated lattice positions. Overall figure of merit = .9 .

c) Eighteen independent reflections used. Average overall error $x = .54$, $y = .60\ [\text{scan area}]^{-1}$. Overall figure of merit = .96.

PLATE V. High-angle x-ray diffraction from partially oriented membrane samples (meridion vertical)

a) Camera length was 4.66 cm. Exposure time was fifteen hours. X-ray focus .2 mm x 2 mm.

b) Camera length was 2.0 cm. Exposure time was twenty hours. X-ray focus .1 x 1 mm.

Figure 1

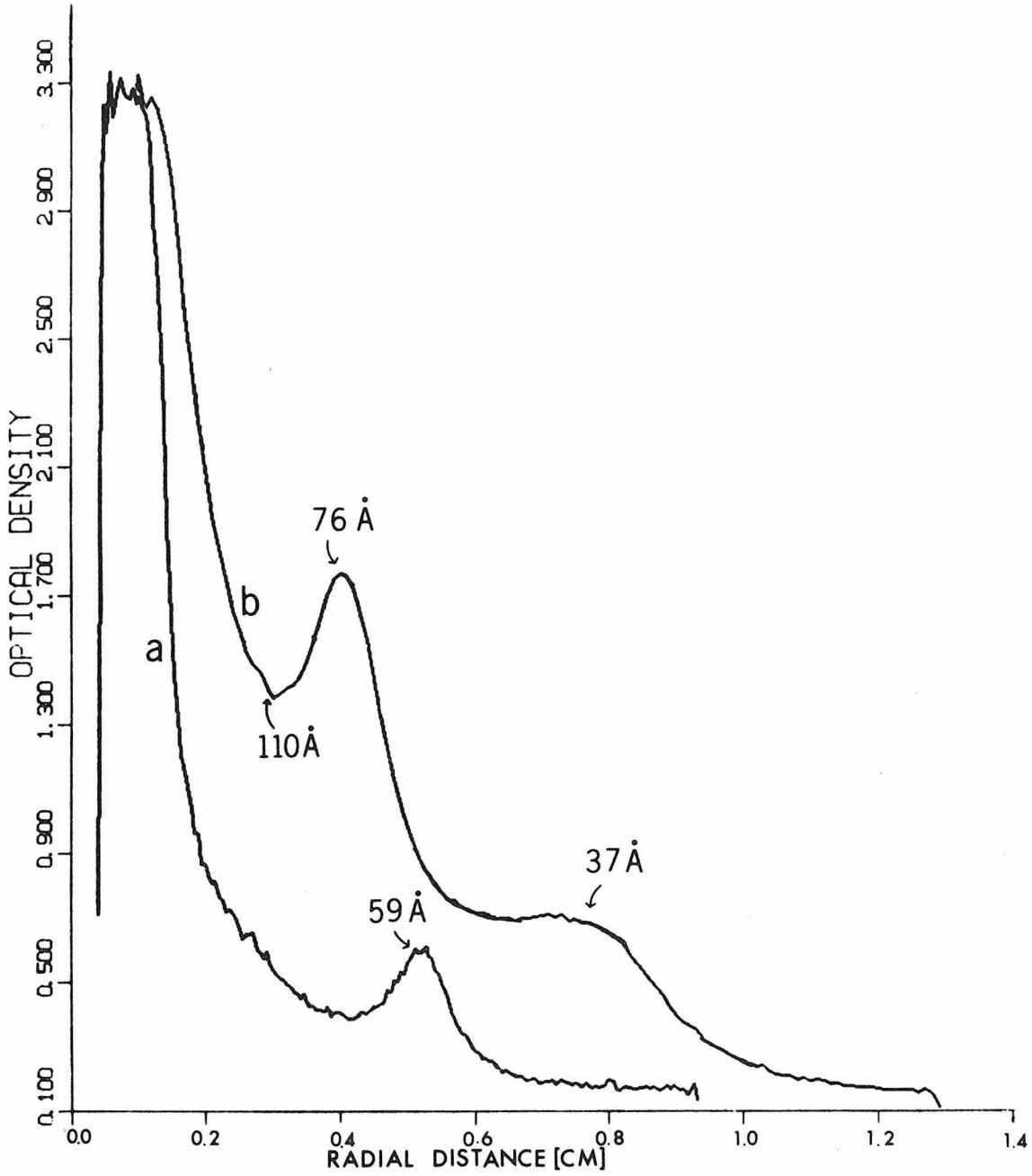
OPTICAL DENSITY
0.100
0.500
0.900
1.300
1.700
2.100
2.500
2.900
3.300
0.0
0.2
0.4
0.6
0.8
1.0
1.2
1.4
RADIAL DISTANCE [CM]
a
b
76 Å
110Å
59 Å
37 Å

Figure 2

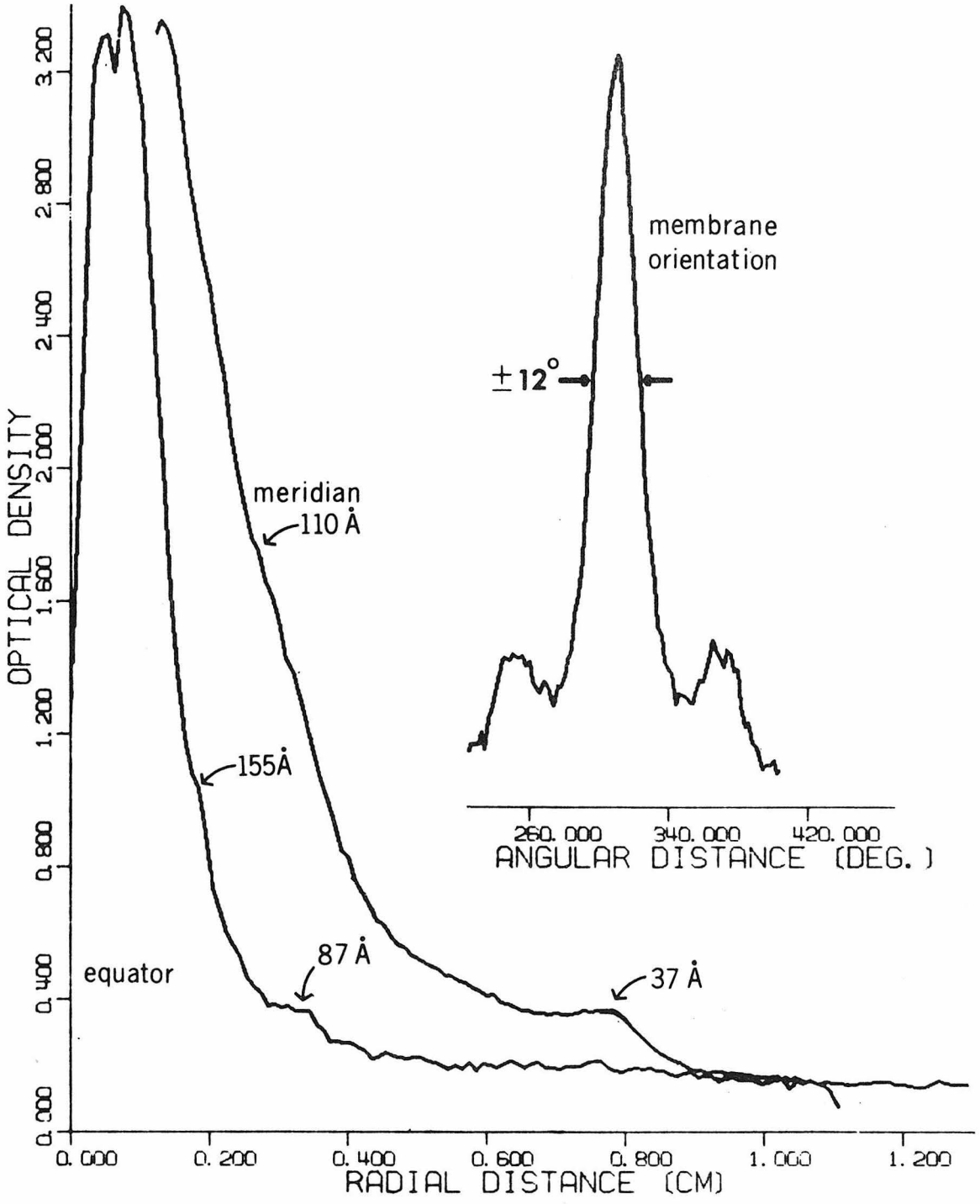
OPTICAL DENSITY
0.000
0.400
0.800
1.200
1.600
2.000
2.400
2.800
3.200
meridian
110 Å
155Å
equator
87 Å
37 Å
0.000
0.200
0.400
0.600
0.800
1.000
1.200
RADIAL DISTANCE (CM)
membrane
orientation
±12°
260.000
340.000
420.000
ANGULAR DISTANCE (DEG.)

Figure 3

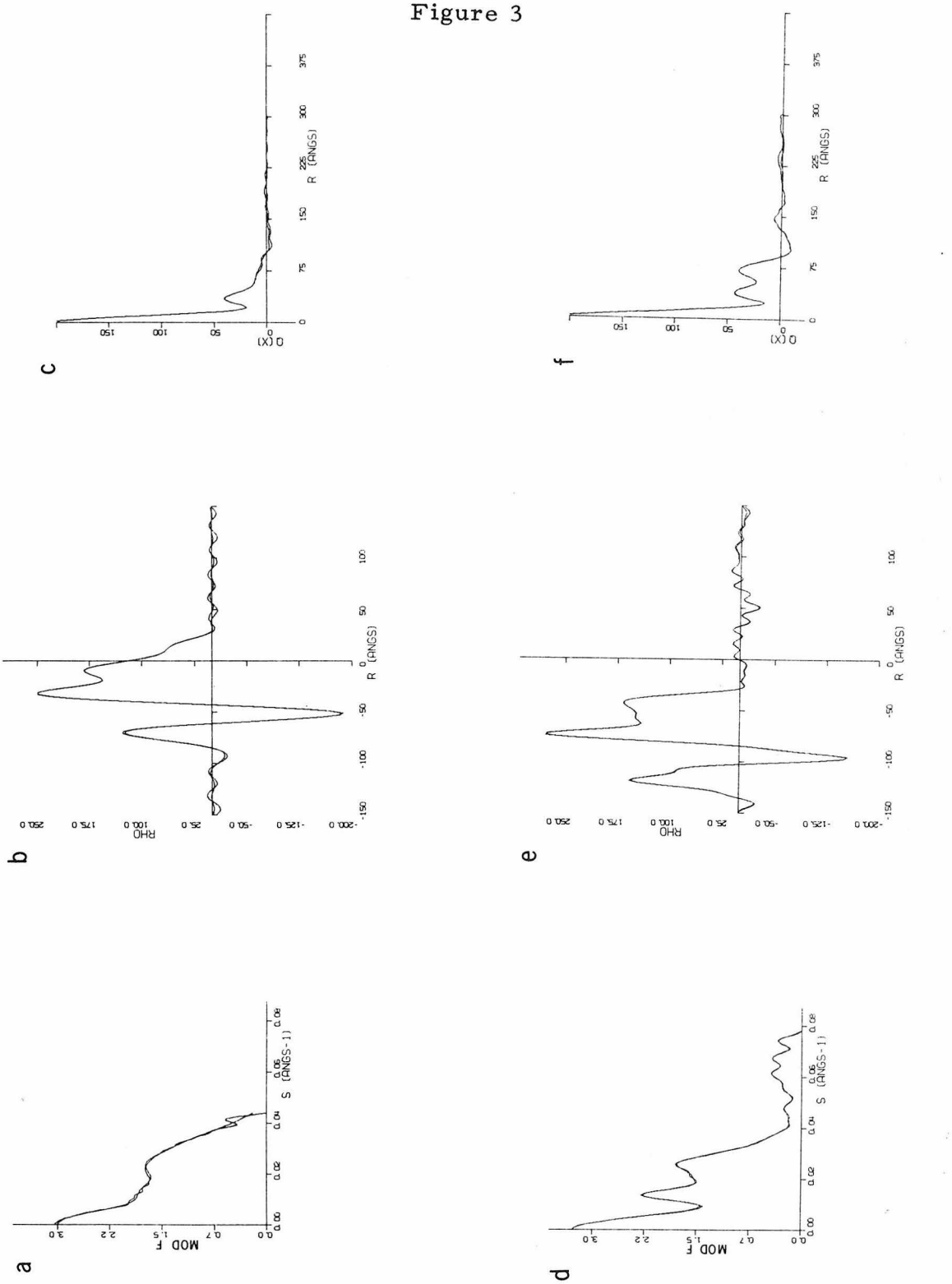
a
MOD F
S (ANGS-1)
b
RHO
R (ANGS)
c
G(X)
R (ANGS)
d
MOD F
S (ANGS-1)
e
RHO
R (ANGS)
f
G(X)
R (ANGS)

Figure 4a

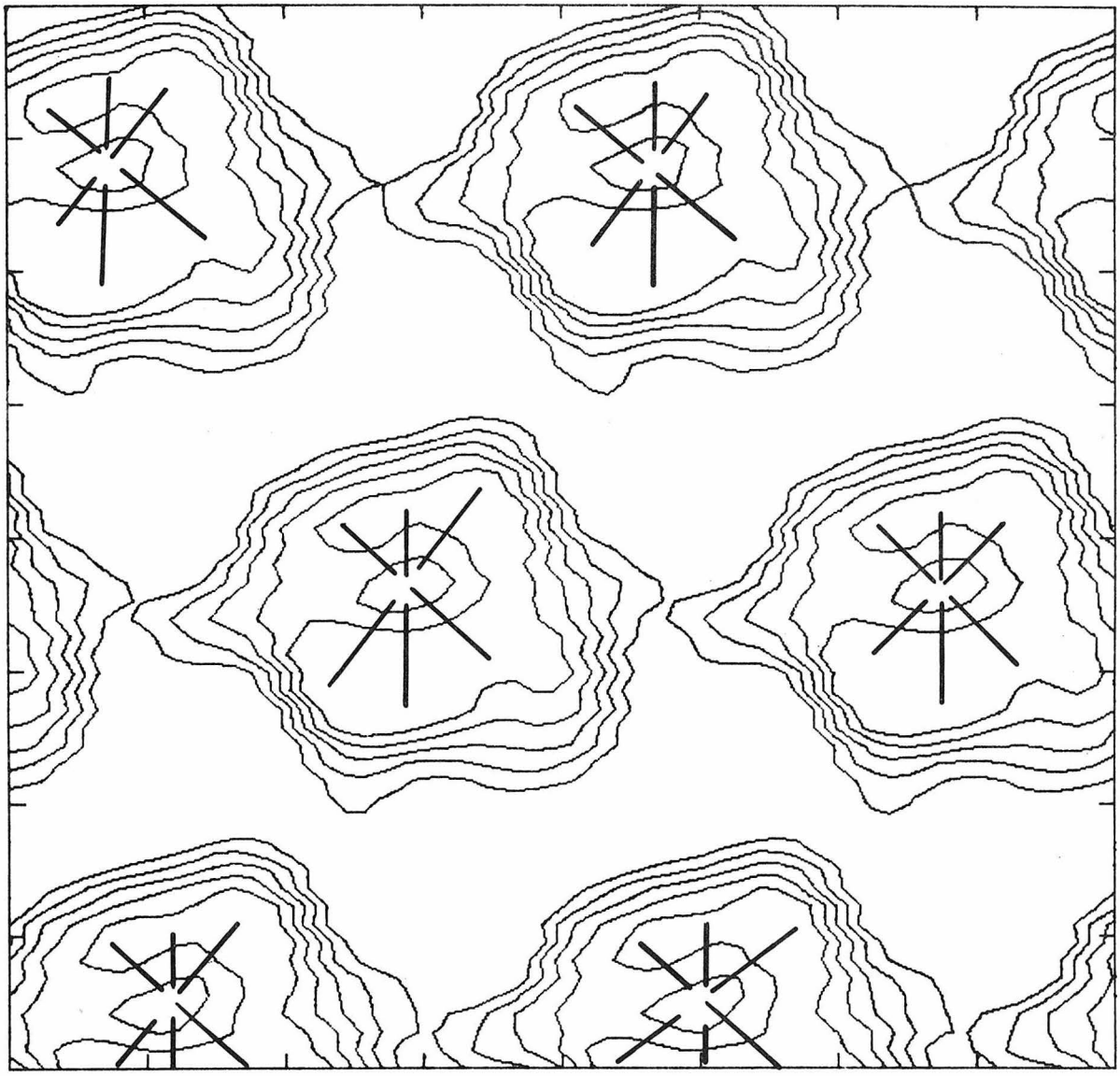

Figure 4b

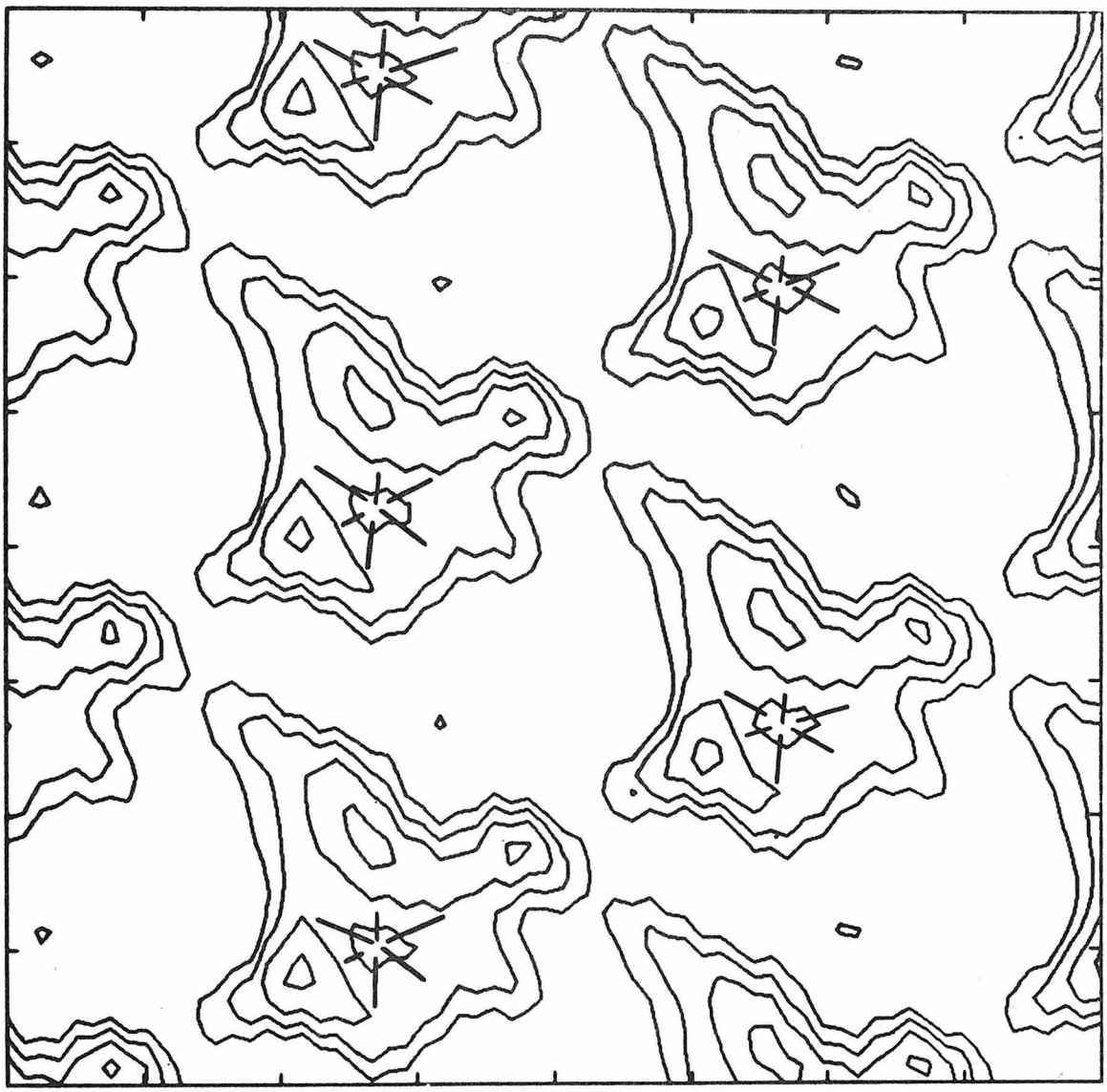

Figure 4c

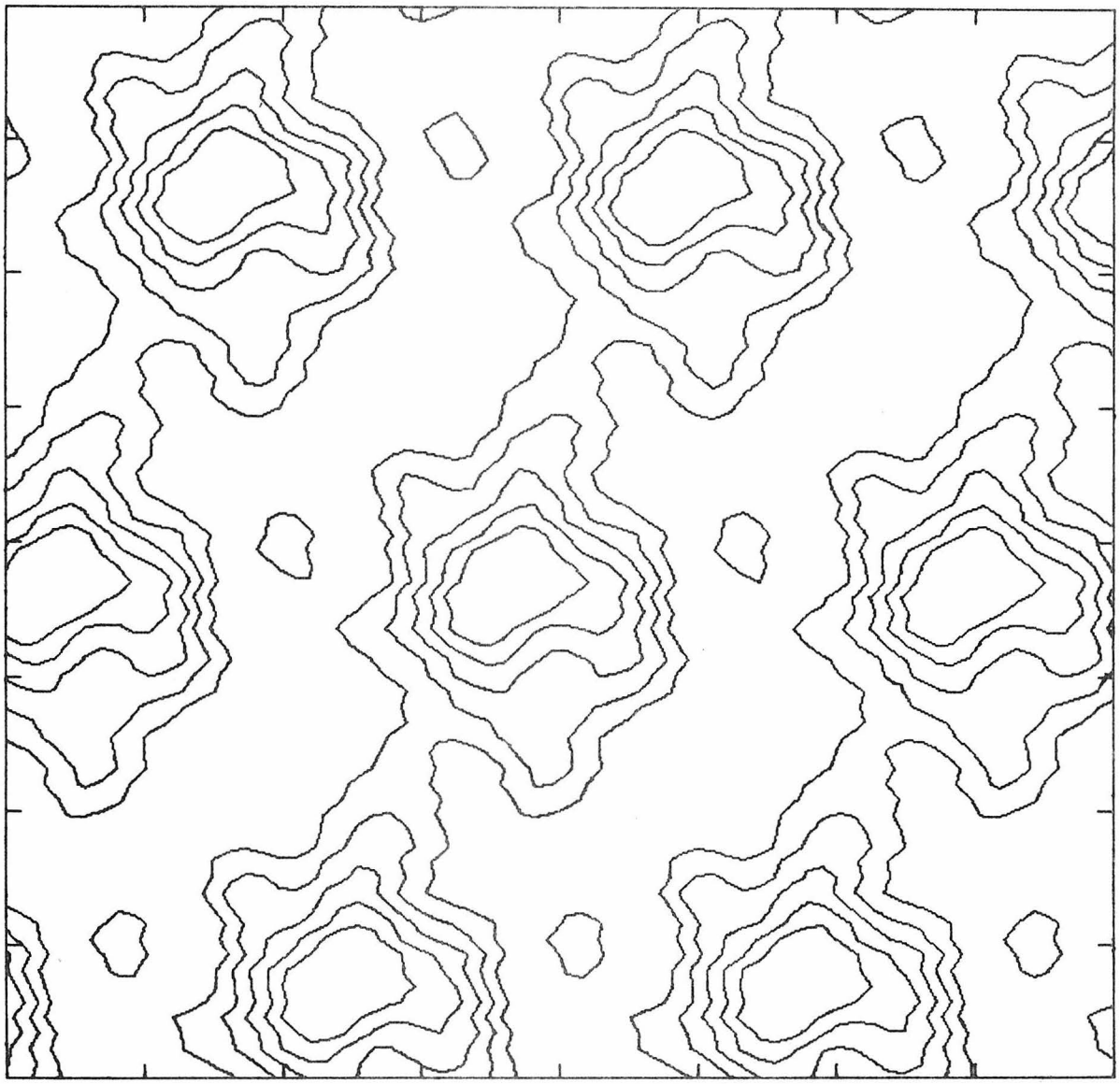

Figure 5

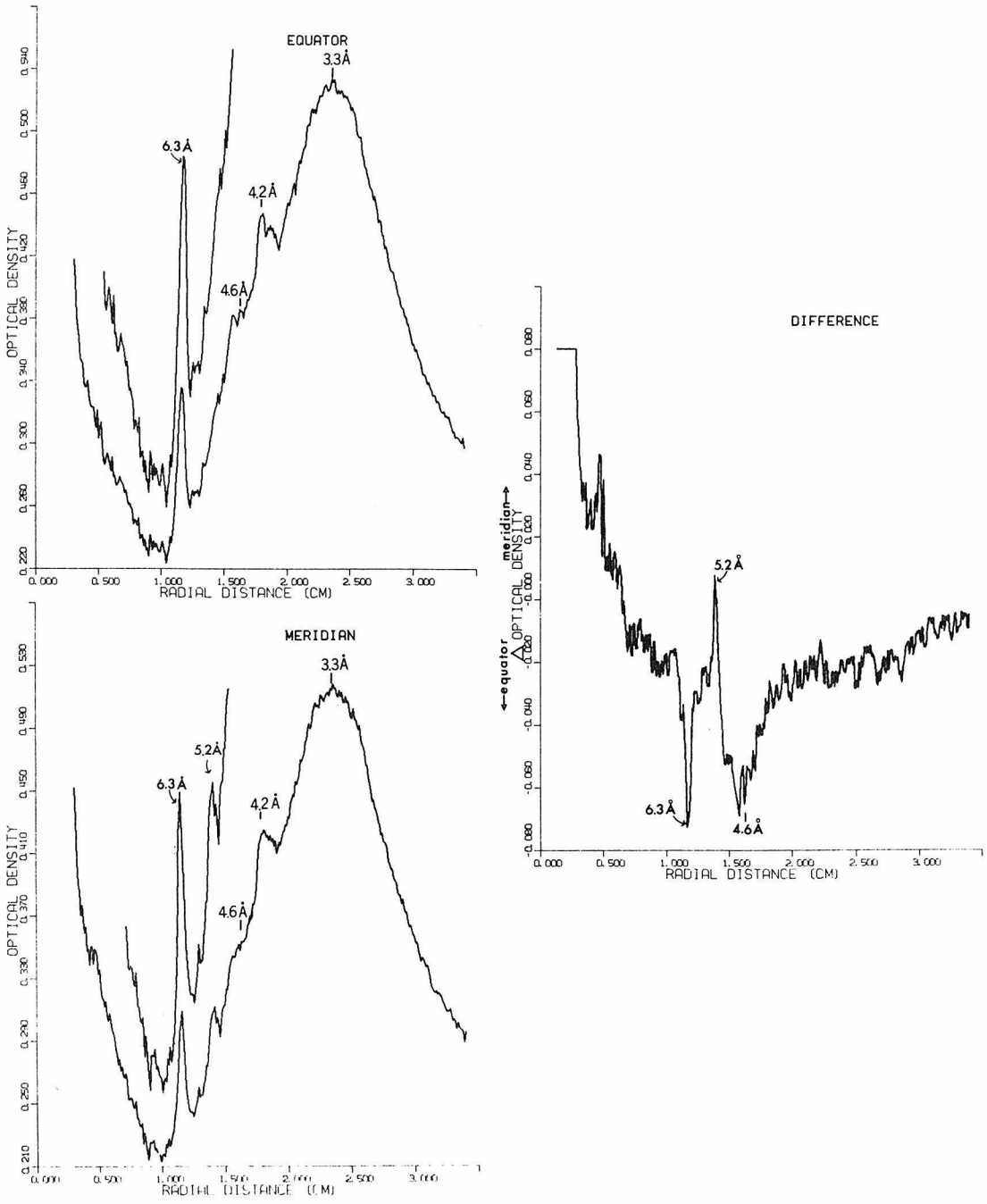
EQUATOR
3.3Å
6.3Å
4.2Å
4.6Å
OPTICAL DENSITY
RADIAL DISTANCE (CM)
MERIDIAN
3.3Å
5.2Å
6.3Å
4.2Å
4.6Å
OPTICAL DENSITY
RADIAL DISTANCE (CM)
DIFFERENCE
←equator
meridian→
OPTICAL DENSITY
5.2Å
6.3Å
4.6Å
RADIAL DISTANCE (CM)

Plate I

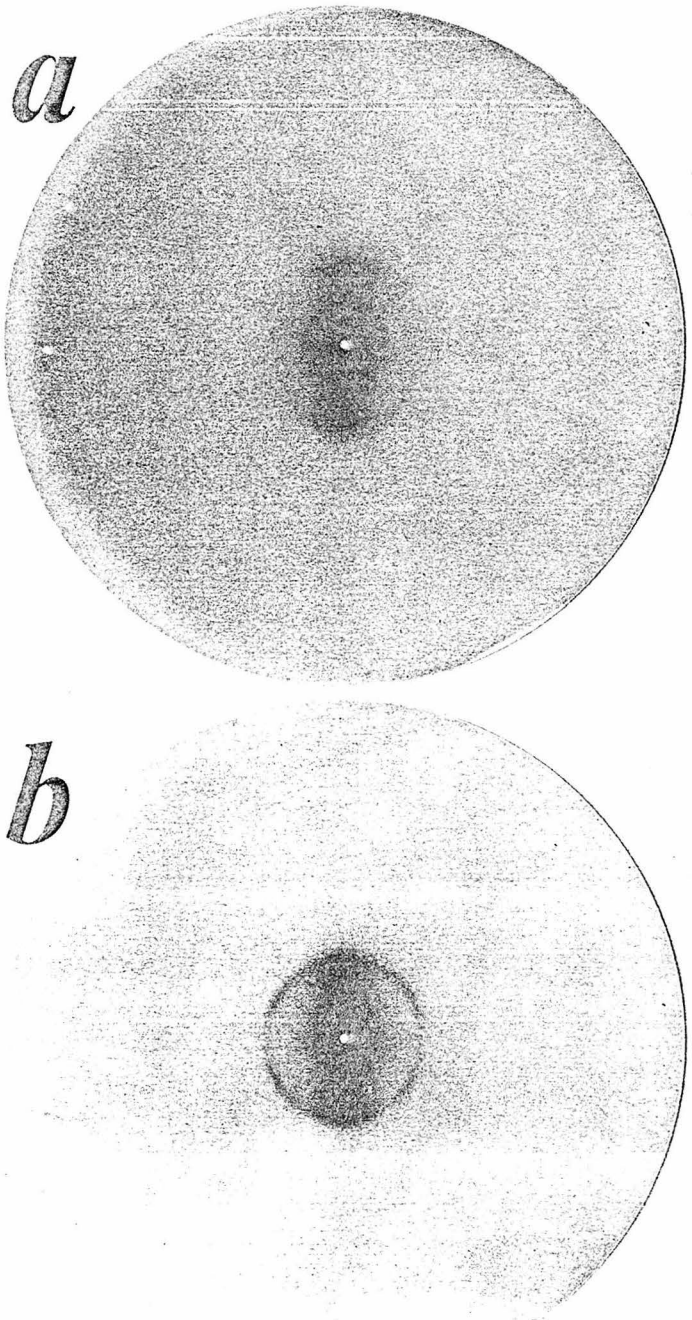

Plate II

Plate III

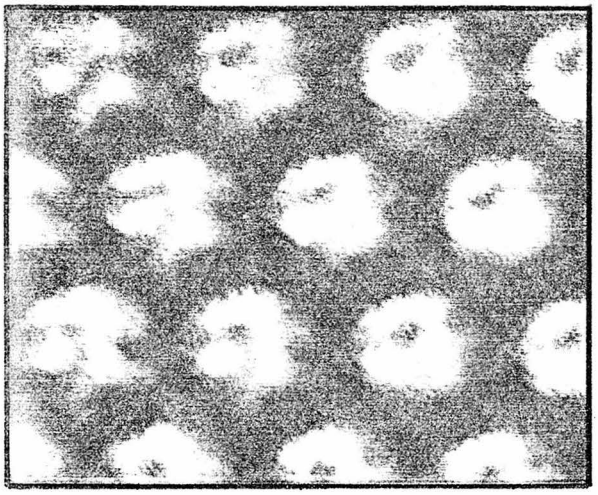

a

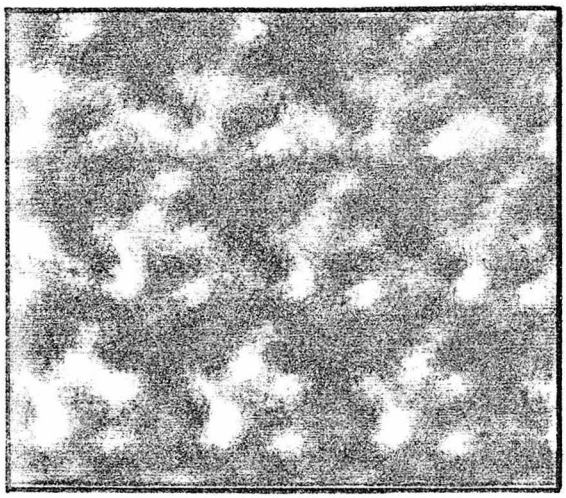

b

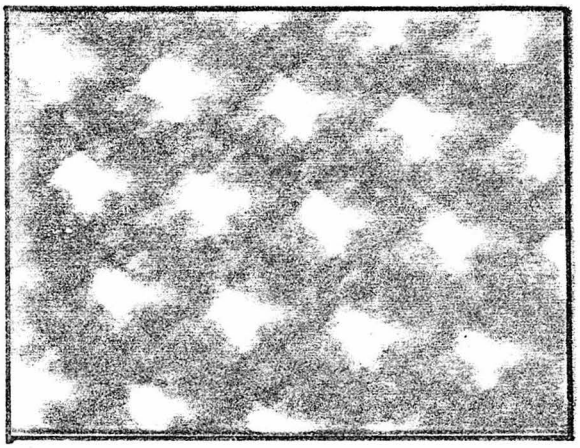

c

Plate IV

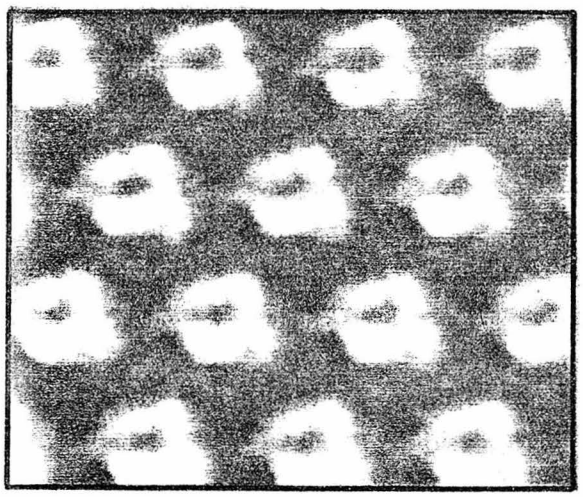

a

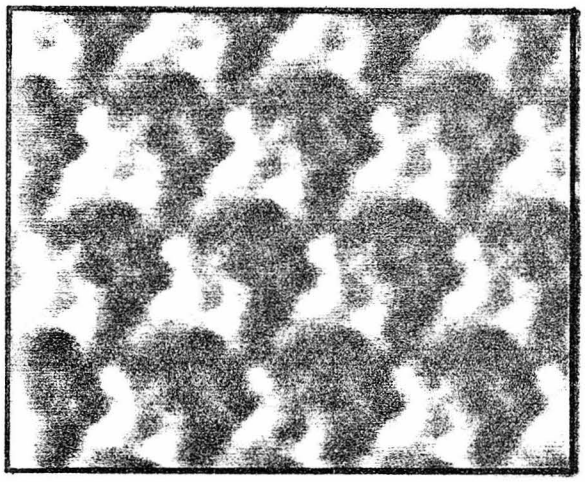

b

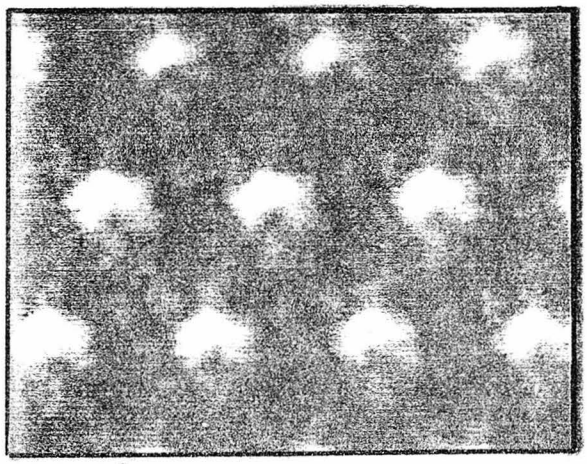

c

Plate V